1-1-2005

A finite element analysis approach to predicting intramedullary pressure during the insertion of prosthetic implants

Paul Saadetian
Ryerson University

A FINITE ELEMENT ANALYSIS APPROACH TO PREDICTING INTRAMEDULLARY PRESSURE DURING THE INSERTION OF PROSTHETIC IMPLANTS

By

Paul Saadetian, B.Eng

Ryerson University, 2003

A thesis presented to Ryerson University

in partial fulfillment of the requirements for the degree of

Master of Applied Science

in the Program of

Mechanical Engineering

Toronto, Ontario, Canada, 2005

AUTHOR'S DECLARATION

I hereby declare that I am the sole author of this thesis.

I authorize Ryerson University to lend this thesis to other institutions or individuals for the purpose of scholarly research.

I further authorize Ryerson University to reproduce this thesis by photocopying or by other means, in total or in part, at the request of other institutions or individuals for the purpose of scholarly research.

BORROWER'S PAGE

Ryerson University requires the signatures of all persons using or photocopying this thesis. Please sign below, and give address and date.

ABSTRACT

A Finite Element Analysis Approach to Predicting Intramedullary Pressure during the Insertion of Prosthetic Implants, M.A.Sc, 2005.

Paul Saadetian, Department of Mechanical and Industrial Engineering, Ryerson University.

Fat embolism syndrome is a serious post-operative complication of orthopaedic procedures such as fracture fixation and total joint replacement. Fat embolism syndrome can be a result of increased intramedullary pressure during the insertion of prosthetic implants in long bones. A macro was developed that automates the creation of finite element models representing a simplified bone/fluid/implant system and a hammering event. The finite element models were validated by computing the peak stresses at various locations in the bone and comparing them to pressures measured at similar locations in experimental tests. Finite element models were used to test the effect of using hollow implants on intramedullary pressure in the bone, in some cases yielding an average reduction of 19.1%. It has been shown that it is acceptable to use finite element models for such parametric studies and that hollow implants have the potential to decrease intramedullary pressure during insertion.

ACKNOWLEDGMENTS

First I would like to thank my supervisor, Dr. Kamran Behdinan for the time and effort he has dedicated to this thesis. I would also like to thank my co-supervisors, Dr. Marcello Papini and Dr. Ziad Saghir for their help and guidance over the course of this project. I would further like to thank the medical contributors, Dr. Paul Zalzal and Dr. Justin DeBeer for sharing their practical experience with orthopaedic procedures.

I would like to thank my father Haig for his advice and engineering knowledge, and my mother Deborah for her encouragement. Without the moral support of my parents, the completion of this thesis would have been impossible. I would also like to thank my research colleagues and friends Daniel Dobrjanski and Omar Gaber for their assistance and for making the project more enjoyable.

Finally, I would like to thank the Natural Sciences and Engineering Research Council of Canada for their financial support of this project.

TABLE OF CONTENTS

LIST OF TABLES

LIST OF FIGURES

CHAPTER 1

INTRODUCTION

1.1 Motivation

Intramedullary implants are very popular in the world of orthopaedics. Intramedullary nailing is the most commonly used and accepted method of bone fracture fixation because it greatly reduces the problems associated with casting a fractured bone, such as limb shortening, misalignment and muscle wastage [1]. Intramedullary implants are used in all total hip and total knee replacements to position and fix the new prosthetic joint. However, despite their popularity, there is a serious post-operative complication associated with the use of intramedullary implants known as fat embolism syndrome. The most commonly recognized cause of fat embolism syndrome is the increase in intramedullary pressure created during the preparation of the intramedullary canal and when the implant is inserted into the bone [2]. There were close to a half-million total joint replacements in North America for the year 2001, and, with an ever-growing population, that number is bound to increase [3]. With a 5% to 15% mortality rate for fat embolism syndrome, the potential loss of life is significant and the need for improving surgical procedures to reduce the incidence of fat embolism syndrome is clear [4].

1.2 Thesis Objectives

The main objective of this research is to investigate the phase of an orthopaedic procedure that involves the hammering of a prosthetic implant into the intramedullary canal of a bone. Computational modeling and experimental tests will be used to look at aspects of the hammering event that lead to increased intramedullary pressure and suggest improvements that may reduce the risk of fat embolism syndrome. This thesis will involve computational modeling, specifically, finite element analysis, and will aim to meet the objective through the following three steps: (i) Developing an automated macro that creates a parametric finite element model of the bone/fluid/implant system that can be used to test changes of the various aspects of the hammering event. (ii) Validating the use of a finite element model to represent the bone/fluid/implant system and the hammering event by comparison to experimental tests performed by another member of the research group. (iii) Using finite element models to perform a parametric study on a potential intramedullary implant design feature in an attempt to help reduce the build-up of pressure in the intramedullary canal during the hammering event.

1.3 Thesis Organization

This thesis is organized into six chapters representing the two year research project. Chapter one outlines the motivations and objectives of the research. Chapter two presents a literature review of past work conducted on the research and prevention of fat embolism syndrome. Chapter three discusses the structure of the macro that was

developed and presents a detailed description of how the macro is used to create the finite element models. Chapter four describes the methods used to validate the finite element models and presents the results of the validation, in collaboration with another member of the research group who was responsible for the experimental testing. Chapter five describes a parametric study that was conducted related to the implant design and discusses the effects on the build-up of intramedullary pressure in the bone. Finally, chapter six discusses the implications of the current work and presents suggestions for future work.

CHAPTER 2

LITERATURE REVIEW

2.1 History of Fat Embolism Syndrome

Fat embolism refers to the phenomenon of fat droplets being released into the venous system, most commonly as a result of trauma to long bones and orthopaedic procedures. Fat embolism syndrome is a potentially fatal complication of fat embolism as a result of the emboli being deposited in the lungs, brain and other organs. The presence of fat embolism does not guarantee the occurrence of fat embolism syndrome.

Fat embolism was first noted by the German physician, Zenker, in 1861 who observed fat droplets in the lung capillaries of a railroad worker who suffered a severe chest injury [5]. The first clinical diagnosis of fat embolism was in 1873 by the Latvian surgeon, Bergmann, in a patient with a fractured femur [6]. Early investigation into fat embolism syndrome came in 1875 when the Czech surgeon, Czerny, looked into the cerebral symptoms that sometimes occurred in cases of fat embolism [7].

In the early nineties, studies by Wartin [8] and Gauss [9] demonstrated that fat emboli present in the bloodstream originated from fracture sites in cases of trauma to long bones. Studies in the mid nineties by Maatz [10] and Peltier [11] suggested that intramedullary nailing could also be a factor that leads to the release of fat emboli into the venous system. More recently, investigations by Modig et al. [12] and Lachiewicz et al. [13] have shown that fat embolism and fat embolism syndrome can also be caused by the insertion of hip and knee prosthesis.

2.2 Etiology of Fat Embolism Syndrome

There is little argument over the cause of fat embolism. It is generally accepted that fat embolism originates at the fracture site in cases of bone trauma and as a result of increased intramedullary pressure caused by compression of the intramedullary canal during orthopaedic procedures [2]. This has been demonstrated in studies using transesophageal echocardiography that have shown showers of fat emboli in the pulmonary arterial circulation following fractures and orthopaedic surgeries [14]. However, despite being observed for over a century, the etiology of how fat emboli lead to fat embolism syndrome is still not widely agreed on. There are two main theories of how fat embolism leads to fat embolism syndrome: the chemical theory and the mechanical theory.

The chemical theory states that the fat emboli become trapped in the microvasculature of the lung, and the lung responds by secreting lipase. The lipase

hydrolyzes the fat into free fatty acids and glycerol, both of which have been shown to be toxic to the lung parenchyma [15]. The free fatty acids then cause a severe inflammatory reaction, which leads to an aggregation of leukocytes that in turn release chemotoxins. This causes a series of problems including endothelial damage, alveolar architecture injury, increased capillary permeability and damaged lung surfactant leading to fat embolism syndrome [16]. It is thought that the time it takes for fat embolism to develop into fat embolism syndrome is related to the time it takes for fat to metabolize to free fatty acids [17].

The mechanical theory of fat embolism syndrome involves the fat emboli becoming lodged in the lungs and the right atrium of the heart [18]. The fat emboli physically block pulmonary capillaries, resulting in a number of consequences. The obstructed pulmonary circulation can cause respiratory insufficiency and a variety of associated complications. Further, the blockage can cause an increase in pulmonary artery pressure that may lead to right heart strain or failure. Another less common occurrence of fat embolism syndrome involves fat emboli being deposited in other vital organs such as the brain and kidneys.

The pathways of the theories explaining the etiology of fat embolism syndrome are illustrated in Figure 1. It is clear that no matter what theory behind the etiology of fat embolism syndrome is subscribed to, the key to reducing its occurrence is to curb the degree of fat embolism.

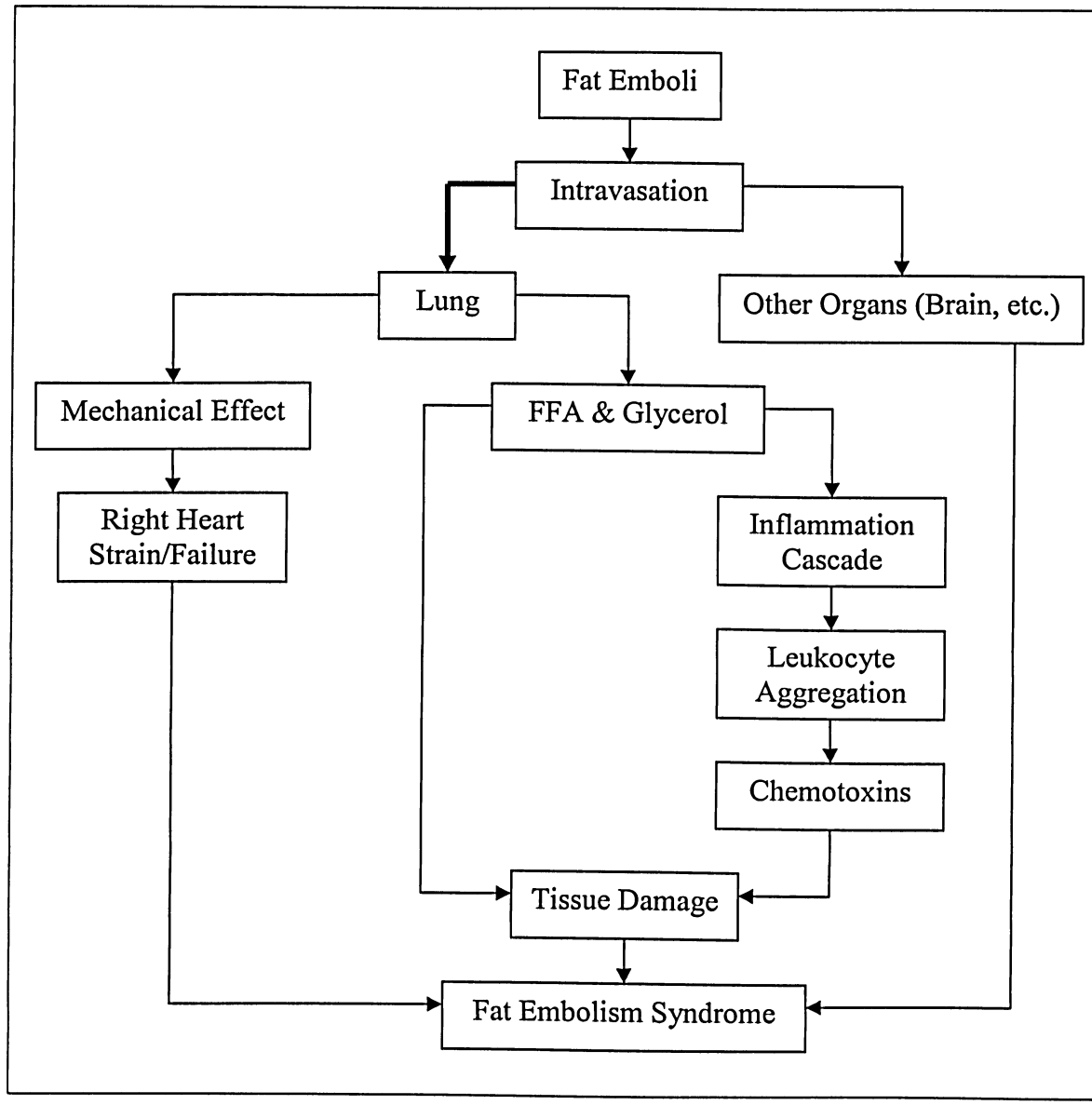

Figure 1: Pathophysiology of Fat Embolism Syndrome [19]

2.3 Diagnosis and Occurrence of Fat Embolism Syndrome

Although the symptoms of fat embolism syndrome can occur immediately or up to 3 days after trauma causing fat embolism, 85% of clinically apparent cases occur within 48 hours [20]. The most common symptoms of fat embolism syndrome are

respiratory problems, neurological changes, and petechial rash. The first guidelines for positively diagnosing fat embolism syndrome came from Gurd et al. [21]. Based on a number of major and minor signs, known as the Gurd fat embolism syndrome criteria (Table 1), the diagnosis of fat embolism syndrome would be accepted if one of the major signs and four of the minor signs were identified. Lindeque et al. argued that the Gurd fat embolism syndrome criteria are too restrictive and makes it difficult to differentiate patients with fat embolism syndrome from patients with other types of pulmonary disorders [22]. They believed that the diagnosis of fat embolism syndrome should be based solely on blood-gas levels of less than 60 mmHg of PaO_2 and greater than 55 mmHg of $PaCO_2$ and a respiratory rate of greater than 35 respirations per minute. In any case, there is no clear-cut laboratory test for fat embolism syndrome, and a diagnosis must be made based on the patient's history and clinical symptoms.

Major criteria	Cerebral changes
	Hypoxemia
	Axillary or subconjuctival petechia
	Pulmonary edema
Minor criteria	Tachycardia
	Pyrexia
	Emboli present in retina on fundoscopic examination
	Fat present in urine
	Sudden unexplainable drop in haematocrit or platelet values
	Increasing erythrocyte sedimentation rate or plasma volume
	Fat globules present in sputum

Table 1: Gurd Fat Embolism Syndrome Criteria

There are numerous reports in the literature that indicate the occurrence of fat embolism is greater than 90% after bone trauma and orthopaedic procedures [23,24]. The occurrence of fat embolism syndrome is not as frequent. For bone trauma, fat embolism syndrome incidence rates from 0.9% to 2.2% have been reported, and several examples are given in Table 2. The severity of the trauma has an effect on the degree of fat embolism and is a contributing factor to the variation in incidence rates in the literature. For orthopaedic procedures, such as total hip arthroplasty, total knee arthroplasty and intramedullary nailing, incidence rates of fat embolism syndrome are higher than for bone trauma. Some examples of fat embolism syndrome incidence rates for orthopaedic procedures are given in Table 2. Defining the mortality rate of fat embolism syndrome is difficult because of the injuries and complications that are associated with it, but it is thought to have a mortality rate of 5% to 15% [4]. In addition to trauma to bones and associated surgical procedures, fat embolism syndrome has been observed in a number of other settings. Table 3 lists some of the traumatic events, non-traumatic events and surgical procedures that have led to the occurrence of fat embolism syndrome.

Investigator	Incidence of Fat Embolism Syndrome
Magerl et al. [25]	0.9% of 4197 bone fractures
Peltier [26]	1.25% of 7701 bone fractures
Pelzl [27]	1.3% of 3650 bone fractures
Peltier et al. [29]	1.0% to 2.2% for tibia and femur fractures
Kim [29]	6% of 100 total knee arthroplasties
Dorr et al. [30]	12.3% of 65 total knee arthroplasties
Pell et al. [31]	12.5% of 24 tibial and femoral nailings

Table 2: Occurrence Rates of Fat Embolism Syndrome

Traumatic events	Lower extremity long-bone fracture
	Pelvic fractures
	Child abuse without fractures
	Blast concussion
	Liver trauma
	Severe burns
	Massive soft tissue injury
Non-traumatic events	External cardiac massage
	Carbon tetrachloride poisoning
	Fatty liver secondary to alcohol
	Prolonged corticosteroid therapy
	Epilepsy
	High-altitude flights
	Bone infection secondary to sickle-cell disease
Surgical procedures	Total joint replacement
	Intramedullary nailing of femoral shaft
	Femoral elongation
	Spinal fusion
	Liposuction
	Bone marrow transplantation
	Renal transplantation

Table 3: Clinical Settings for Fat Embolism Syndrome [19]

2.4 Increased Intramedullary Pressure in Orthopaedic Procedures

There have been a number of studies in the literature that investigate the change in intramedullary pressure at various phases of orthopaedic procedures. As mentioned previously, fat embolism resulting from orthopaedic procedures is credited to an increase

intramedullary pressure. These studies provide valuable information about what aspects of the procedure are the most responsible for the increase in intramedullary pressure and where improvements can be made.

In a study on animals by Sturmer et al. [32], reaming of the intramedullary canal in preparation for an intramedullary nail resulted in intramedullary pressure increases from 444 mmHg to 1520 mmHg. The insertion of the intramedullary nail after the reaming resulted in intramedullary pressure increases from 90 mmHg to 160 mmHg.

In a clinical femoral nailing study on 20 patients by Wenda et al. [33], reaming of the intramedullary canal was found to increase the intramedullary pressure by an average of 835 mmHg. Insertion of the intramedullary nails after reaming caused intramedullary pressure rises of approximately 70 mmHg. By using transesophageal echocardiography, two important observations were noted. First, higher intramedullary pressures led to greater amounts of fat embolism. Second, the critical intramedullary pressure that led to fat embolism in the venous system was determined to be 200 mmHg.

In a study of femoral nailings on male baboons, Kropfl et al. [34] investigated the difference in intramedullary pressure build-up between reamed and unreamed femoral nailing. In the unreamed group, the intramedullary pressure was found to increase by an average of 76 mmHg during the insertion of the intramedullary nail. In the reamed group, the intramedullary pressure was found to increase an average of 879 mmHg during the reaming of the intramedullary canal and an average of 254 mmHg during the insertion of

the intramedullary nail. These results follow the same trend noted by Wenda et al. and Sturmer et al. of a higher intramedullary pressure during reaming compared to insertion of the intramedullary nail. Further, the degree of fat embolism was ranked using a modified Gurd test on a blood sample taken at the vena cava inferior. In the unreamed group, the fat embolism during the insertion of the intramedullary nail was given a score of 2.9. In the reamed group, the fat embolism during the reaming of the intramedullary canal was given a score of 4.6 and during the insertion of the intramedullary nail was given a score of 3.5. This too supports the findings of Wenda et al. that higher intramedullary pressure results in a greater extent of fat embolism.

In a study on sheep femora, Wozasek et al. [35] made an observation that was contrary to previous findings. Similar to the studies mentioned previously, the intramedullary pressure was found to increase an average of 753 mmHg during reaming and less during insertion of the intramedullary nail. However, using transesophageal echocardiography it was shown that the greater amount of fat embolism occurred during the insertion of the intramedullary nail, despite the lower intramedullary pressure.

In a study on cadaver femora, Hopf et al. [36] also made observations that are in contrast to other reports in the literature. In this study, the intramedullary pressure was found to increase an average of 260 mmHg during the reaming of the femoral shaft. During the insertion of slotted intramedullary nails following reaming, the intramedullary pressure was found to increase an average of 628 mmHg. These results show an opposite

trend to the in vivo studies mentioned previously, where the intramedullary pressure during reaming was higher than during the insertion of the intramedullary nail.

Tronzo et al. [37] demonstrated an increase in intramedullary pressure exceeding 300 mmHg during the insertion of a cemented prosthesis in total hip arthroplasty. Inadome et al. [2] measured intramedullary pressures of 3190.6 mmHg during the insertion of a femoral stem with cement and 125.8 mmHg during the insertion of a femoral stem without cement in total hip arthroplasty. Beck et al. [38] reported intramedullary pressures of over 4200 mmHg during implantation of cemented femoral stems in total hip arthroplasty.

With all the reports in the literature of significant increases in intramedullary pressure during various orthopaedic procedures, and positive correlations between an increase in intramedullary pressure and fat embolism, it is clear that reducing intramedullary pressure through improved surgical procedures or equipment is important.

2.5 Reducing Intramedullary Pressure in Orthopaedic Procedures

A number of investigators have looked into modification of the orthopaedic surgical procedure in an attempt to find techniques to reduce the degree of fat embolism. The relative success of the modification is gauged by looking at the effect on the build-up of intramedullary pressure or, more directly, by monitoring the amount of fat embolism in the bloodstream.

Beck et al. [38] conducted a study to determine what effect the design of the femoral stem prosthesis can have on intramedullary pressure. Two different brands of femoral stems (Muller and Option 3000) were implanted into patients undergoing total hip arthroplasty. The intramedullary pressure was found to be an average of 1293 mmHg when using the Muller prosthesis and 289 mmHg when using the Option 3000 prosthesis. This study clearly demonstrated that prosthesis design can have a significant impact on the build-up of intramedullary pressure.

Schmidt et al. [39] looked at a modification to the preparation phase where the intramedullary canal is prepared for the prosthesis. For patients undergoing total hip arthroplasty, the effect of using hollow awls and rasps to prepare the intramedullary canal was compared to using solid awls and rasps. For the patients where solid awls and rasps were used, the average increase in intramedullary pressure was 246 mmHg. Further, macro-emboli and embolic showers were demonstrated for all the patients via transesophageal echocardiography. For the patients where hollow awls and rasps were used, no macro-emboli were detected and mild embolic showers were observed in only 3 of 5 patients. This study shows again how modifications to the surgical equipment can help to reduce the risk of increased intramedullary pressure and fat embolism.

Martin et al. [40] investigated the effect of creating a vent hole in the bone on the build-up of intramedullary pressure. For 78 embalmed femurs and tibias, a 4.5mm vent hole was drilled and the intramedullary pressures during awl, guide rod, reamer and nail insertion were compared to specimens without a vent hole. For proximal venting, the use

of a vent hole showed intramedullary pressure reductions of up to 90% in the tibia and up to 70% in the femur. For distal venting, the use of a vent hole showed intramedullary pressure reductions of up to 90% in both the tibia and femur.

A similar study conducted by Pitto et al. [41] investigated the effect of proximal drainage on intramedullary pressure in 40 patients undergoing total hip arthroplasty. For the patients without a venting hole, severe embolic events were observed in 85% of the cases via transesophageal echocardiography. For the patients with a venting hole, severe embolic events were observed in only 20% of the cases.

Another study by Pitto et al. [42] looked at the effect of creating a vacuum in the intramedullary canal during cemented total hip arthroplasty. This was achieved by placing 800 millibars of suction at the linea aspera and the diaphysis of the femur. For the patients on whom the conventional cementing technique was used, using transesophageal echocardiography, it was demonstrated that 85% suffered severe fat embolism. For the patients on whom the modified vacuum cementing technique was used, only 5% showed signs of severe fat embolism.

Muller et al. [43] looked at the effect of blunt and sharp reamers on the temperature in the bone and the intramedullary pressure. The tests were conducted on cadaveric human femurs submerged in a water bath at 37°C to simulate normal body conditions. It was found that the maximum temperature in the bone using the blunt reamer was 46.3°C while the maximum temperature using the sharp reamer was 40.1°C.

Further, compared to the sharp reamer, the intramedullary pressure using the blunt reamer was 2.1 times higher in the diaphyseal region of the bone and 1.7 times higher in the metaphyseal region of the bone.

Muller et al. [44] also investigated the effect of the force applied by the surgeon to the reamer on intramedullary pressure when a femur is being prepared. When a 107 N force was applied to the reamer, the intramedullary pressure was measured to be 970 mmHg in the diaphyseal region of the bone and 1152 mmHg in the metaphyseal region of the bone. When a 59 N force was applied to the reamer, the intramedullary pressure was measured to be 206 mmHg in the diaphyseal region of the bone and 367 mmHg in the metaphyseal region of the bone. However, in contrast, Johnson et al. [45] demonstrated no correlation between intramedullary pressure and the force applied to the reamer.

Yet another study by Muller et al. [46] looked at the effect of the diameter of flexible drive shafts and using hollow reamers on intramedullary pressure. Compared to a conventional reamer, using a hollow reamer resulted in an intramedullary pressure decrease of 19% in the diaphyseal region of the bone and 21% in the metaphyseal region of the bone. Compared to a 9 mm flexible drive shaft, using a 7 mm flexible drive shaft resulted in an intramedullary pressure decrease of 61% in the diaphyseal region of the bone and 66% in the metaphyseal region of the bone. Further, the study also revealed that different reamer designs had little effect on the intramedullary pressure.

Some of the modifications to the surgical procedure found in the literature are not practical. For example, the use of venting holes has been shown to be impractical in clinical settings because they become clogged with bone debris and fatty marrow [47]. However, the studies show the potential of simple modifications to the surgical procedure to reduce the occurrence of fat embolism. Considering the conflicting information in the literature and the lack of guidelines for orthopaedic procedures, any surgical techniques that reduce intramedullary pressure will be of benefit to patients.

CHAPTER 3

FINITE ELEMENT MODEL DEVELOPMENT

3.1 Macro Overview

One of the goals of the research is to do a parametric study on a potential design feature for an intramedullary implant that will involve a number of finite element models. Building a finite element model from scratch for each iteration to be tested in this project and for future work would be a time consuming process. To make the process more efficient, a macro was developed that allows quick creation of finite element models that represent a bone/fluid/implant system and the hammering event. The macro was written using the ANSYS Parametric Design Language (APDL). The macro prompts the user to input the necessary parameters of the bone/fluid/implant system and the hammering event and builds a corresponding finite element model in ANSYS. This finite element model is translated into a LS-DYNA input file that is then analyzed with the LS-DYNA solver. The results of the analysis can be reviewed in either LS-PREPOST or ANSYS to determine the effect of the changes that were tested. This sequence of events is summarized in Figure 2.

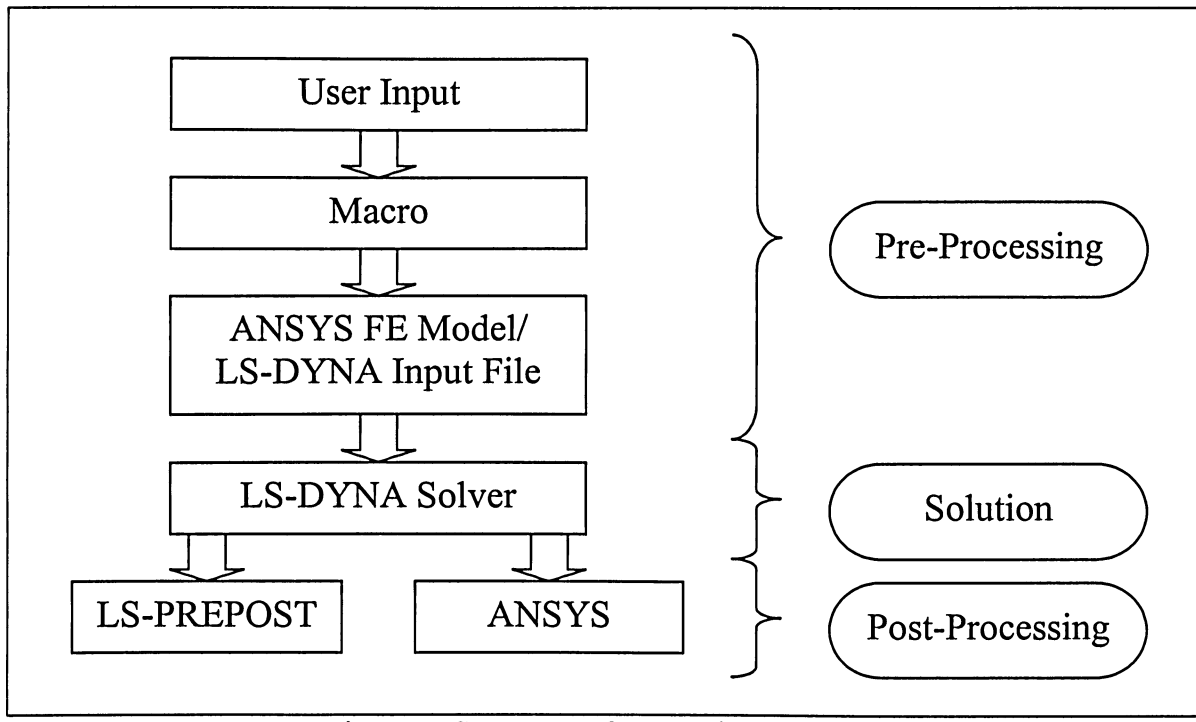

Figure 2: Sequence of Events in Macro Use

The macro itself is a text file that should be placed in a dedicated directory, and this directory should be specified as the working directory when starting ANSYS. The macro is executed by starting ANSYS and following these steps:

- Under the 'File' menu, select 'Read Input from ...'
- Highlight the name of the macro file, and enter 'OK'

The bone/fluid/implant system created by the macro is a simplified model of the real situation. The bone is modeled as a tube that is closed at one end and open at the other end where the implant is inserted. The inner cavity of the bone is filled with the fluid. The system was created this way to make finite element modeling easier and to correspond with an experimental apparatus created by another member of the research group. The simplified system is shown in Figure 3.

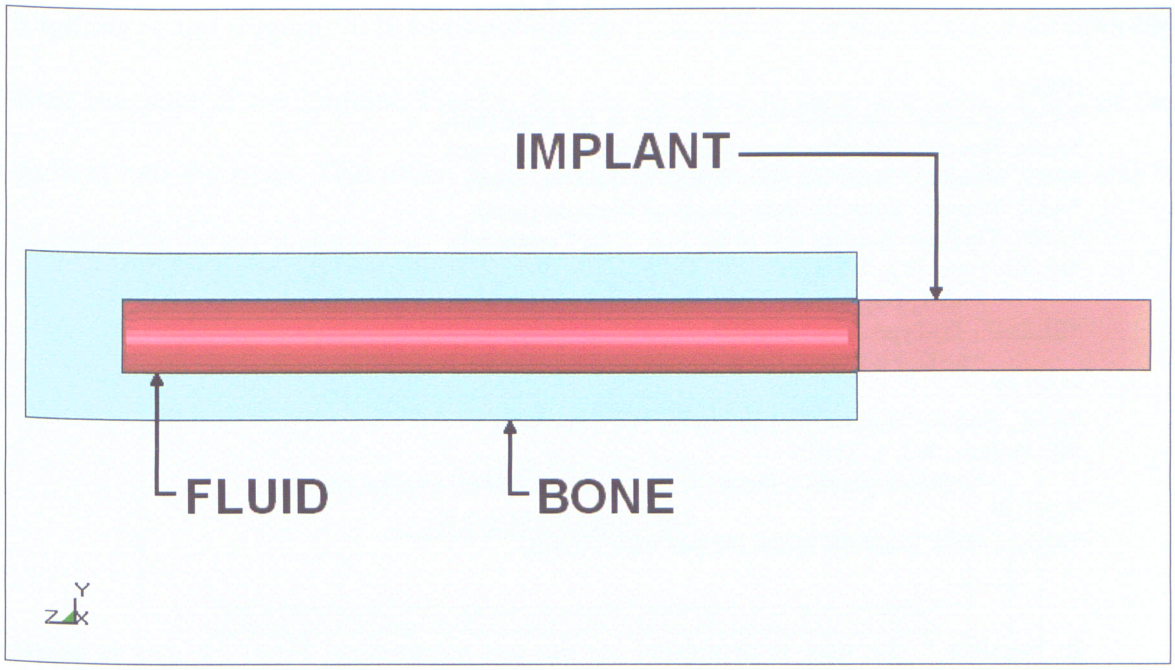

Figure 3: Cross-Section of Simplified Bone/Fluid/Implant System

3.2 Modeling Details

A complete listing of the macro can be found in Appendix A. It should be noted that there is no error checking for the user input. As such, care must be taken to ensure the information entered is exactly as specified in the following summaries of each section of the macro. The purpose of these summaries is not to provide a line-by-line explanation of the ANSYS commands used in the macro. Some APDL knowledge is assumed for individuals who may use and/or update the macro in the future. Rather, the summaries are provided to describe functionality of each section of the macro so that updates by future users can be made more easily.

SECTION 1

```
/PREP7
*ASK, BoneOD, Enter the outer diameter of the bone (mm),
*ASK, BoneID, Enter the inner diameter of the bone (mm),
*ASK, BoneOL, Enter the outer length of the bone (mm),
*ASK, BoneIL, Enter the inner length of the bone (mm),
*ASK, TipType, Implant tip? (0 for Flat, 1 for Contoured),
*IF, TipType, EQ, 0, THEN
        *ASK, ImplantOD, Enter the outer diameter of the implant (mm),
*ELSEIF, TipType, EQ, 1, THEN
        *ASK, FileName, Enter the name of the implant profile file,
*ENDIF
*ASK, Hollow, Hollow implant? (0 for No, 1 for Yes),
*IF, Hollow, EQ, 1, THEN
        *ASK, ImplantID, Enter the inner diameter of the implant (mm),
*ENDIF
*ASK, Offset, Enter the initial implant offset (mm),
```

In Section 1, the user is prompted for the test parameters. First, the user is asked to input the dimensions of the bone which include the outer diameter, inner diameter, outer length and inner length (Figure 4). Next, the user is asked to specify what type of tip the implant will have. The implant can have either a flat tip or a contoured tip of any shape (Figure 5). If a flat tip is specified for the implant, the user is asked to input the outer diameter of the implant. If a contoured tip is specified for the implant, the user is asked to input the name of a text file that contains the points of a spline that defines the desired contour. This name must be enclosed in single quotes when entered. For example, if the file with the desired implant contour is called RoundTip.txt, the user would input 'RoundTip'. Details of how the text file is defined and examples can be found in Appendix B. When a contoured tip is specified, the outer diameter of the implant is based on the Y coordinate of the last point defined in the spline. The text containing the spline points must be located in the same working directory that the macro text file is in. Care must be taken to ensure that the profile of the implant tip is such that it can be meshed without producing badly shaped elements. Next, the user is asked to specify if the implant

is hollow or not (Figure 6). If a hollow implant is specified, the user is asked to input the inner diameter of the implant. Finally, the user is asked to input the initial offset of the implant into the bone. This offset is defined relative to the open end of the bone and is described in greater detail below.

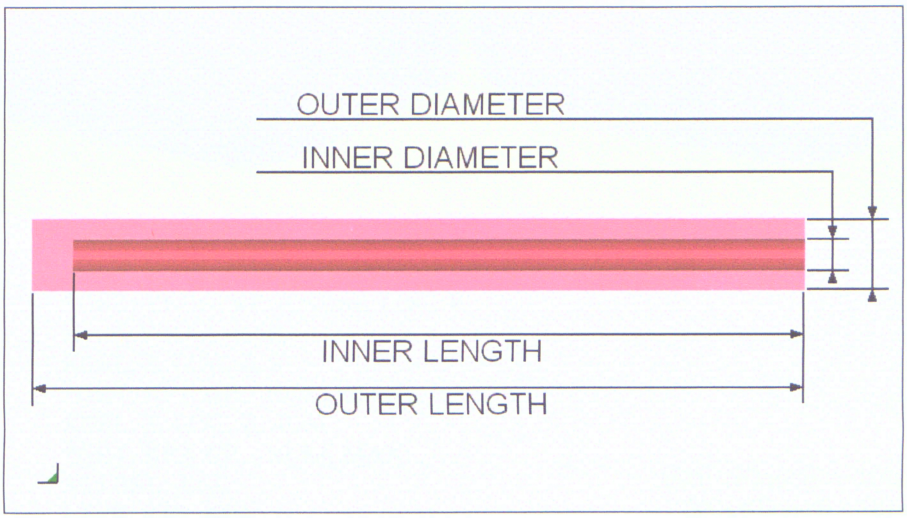

Figure 4: Parameters of Bone Geometry

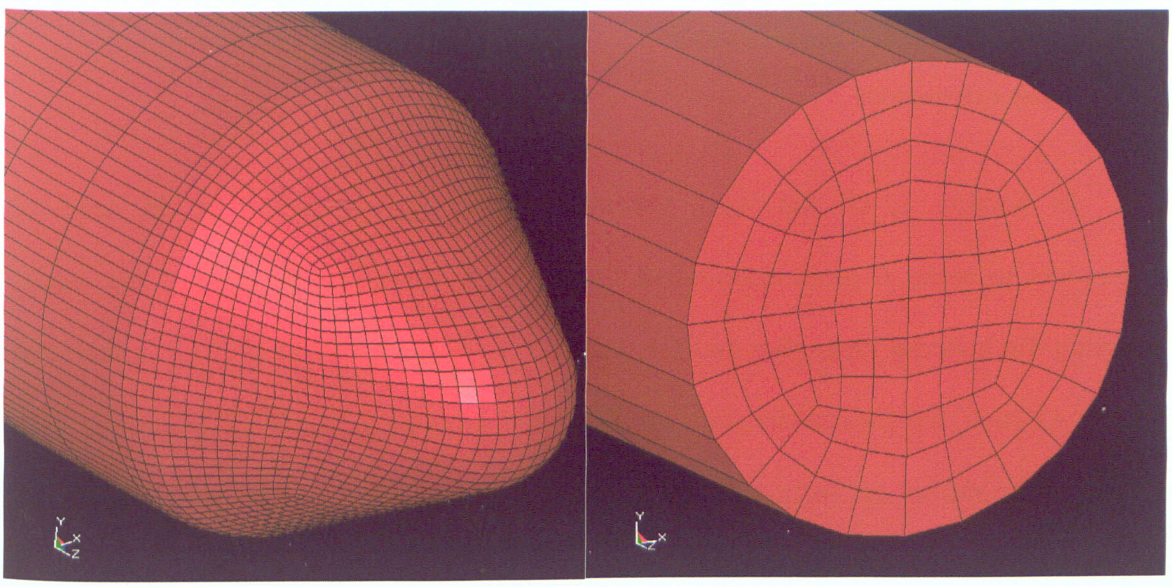

Figure 5: Contoured and Flat-Tipped Implants

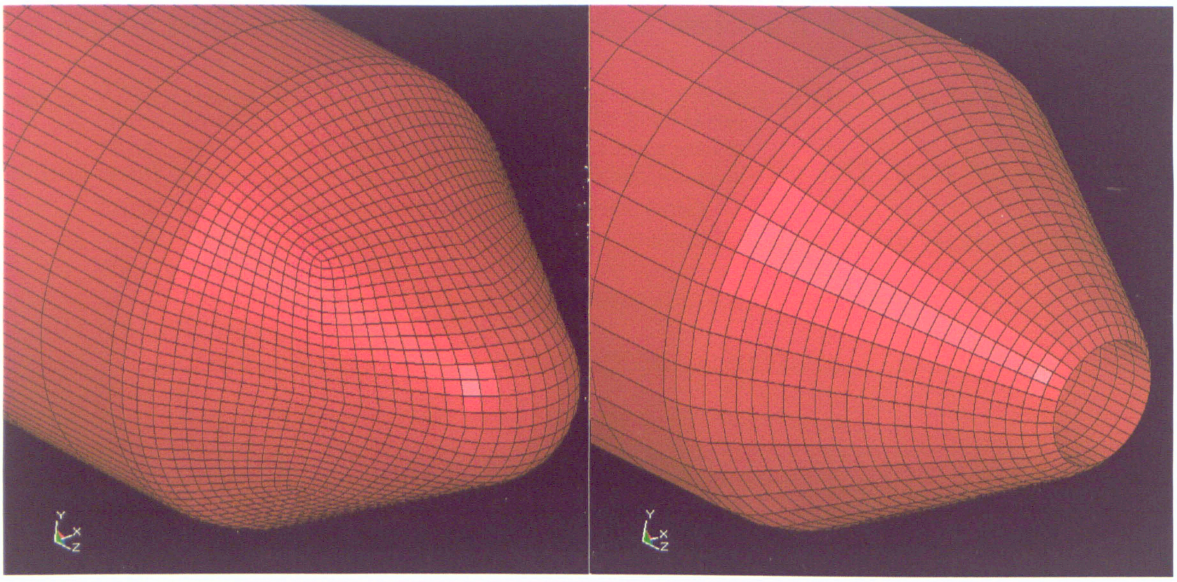

Figure 6: Solid and Hollow Implants

SECTION 2

```
BoneOD = BoneOD/1000
BoneID = BoneID/1000
BoneOL = BoneOL/1000
BoneIL = BoneIL/1000
*IF, TipType, EQ, 0, THEN
        ImplantOD = ImplantOD/1000
*ENDIF
*IF, Hollow, EQ, 1, THEN
        ImplantID = ImplantID/1000
*ENDIF
Offset = Offset/1000
```

In Section 1, all the input parameters involving geometry are in units of millimeters to make it more convenient for the user. However, the rest of the model including the material properties and the force on the implant will be defined in terms of meters. As such, the parameters from the Section 1 must be scaled to be consistent with the rest of the model. In Section 2, all the parameters involving geometry are divided by 1000 to scale them to units of meters.

```
*IF, TipType, EQ, 0, THEN
        CYL4, 0, 0, (ImplantOD/2), 90, , , -0.06
        *IF, Hollow, EQ, 1, THEN
                CYL4, 0, 0, (ImplantID/2), 90, , , -0.06
                VSBV, 1, 2
                NUMCMP, KP
                NUMCMP, LINE
                NUMCMP, AREA
                NUMCMP, VOLU
        *ENDIF
        VGEN, ,ALL, , , , ,Offset, , ,1
*ELSEIF, TipType, EQ, 1, THEN
        /UIS, MSGPOP, 3
        NREAD, FileName, txt,
        KNODE, 0, ALL
        BSPLIN, ALL,
        NDELE, ALL
        KSEL, S, LOC, Z, 0
        *GET, KPNum, KP, , NUM, MAX, ,
        *GET, YLOC, KP, KPNum, LOC, Y
        K, , 0, YLOC, -0.06,
        KSEL, S, LOC, Z, 0
        *GET, KP1, KP, , NUM, MAX, ,
        KSEL, S, LOC, Z, -0.06
        *GET, KP2, KP, , NUM, MAX, ,
        ALLSEL, ALL
        LSTR, KP1, KP2
        K, , 0, 0, -0.06,
        KSEL, S, LOC, Y, 0
        KSEL, U, LOC, Z, -0.06
        *GET, KP1, KP, , NUM, MAX, ,
        KSEL, S, LOC, Y, 0
        KSEL, R, LOC, Z, -0.06
        *GET, KP2, KP, , NUM, MAX, ,
        ALLSEL, ALL
        AROTAT, 1, 2, , , , , KP1, KP2, 90, ,
        LSTR, KP1, KP2
        KSEL, S, LOC, Z, -0.06
        KSEL, R, LOC, X, YLOC
        *GET, KP1, KP, , NUM, MAX, ,
        ALLSEL, ALL
        LSTR, KP1, KP2
        KSEL, S, LOC, Z, -0.06
        KSEL, R, LOC, Y, YLOC
        *GET, KP1, KP, , NUM, MAX, ,
        ALLSEL, ALL
        LSTR, KP1, KP2
        LSEL, S, LOC, Z, -0.06
        AL, ALL
        LSEL, S, LOC, X, 0
        AL, ALL
        LSEL, S, LOC, Y, 0
        AL, ALL
```

```
        ALLSEL, ALL
        VA, ALL
        *IF, Hollow, EQ, 1, THEN
                WPOFFS, 0, 0, (-0.06+(Offset))
                CYL4, 0, 0, (ImplantID/2), 90, 0, 0, 0.1
                VSBV, 1, 2
                WPCSYS,-1,0
                NUMCMP, VOLU
        *ENDIF
        VSBW, 1
        NUMCMP, KP
        NUMCMP, LINE
        NUMCMP, AREA
        NUMCMP, VOLU
        VGEN, ,ALL, , , , ,Offset, , ,1
        /UIS, MSGPOP, 2
*ENDIF
```

In Section 3, the geometry for the implant is created based on the input specified by the user. For simplicity, the implant is always given a length of 60 mm in the finite element model. However, actual intramedullary implants, in general, are much longer than 60 mm. For the analysis to be valid, it is important that the implant in the finite element model has the same mass as an actual implant that is being considered. To ensure that this is the case, an adjusted density of the implant in the finite element model is calculated, based on its volume and desired mass, further in the macro. If a flat tip is specified by the user, the stem ends at the open end of the bone. Because there is no tip, the implant does not extend into the bone unless there is an initial offset specified. If a contoured tip is specified by the user, the stem of the implant ends at the open end of the bone and the tip extends into the bone. If an initial offset is specified, the stem extends into the bone and the tip moves into the bone even further. Figure 7 shows flat and contoured-tipped implants with and without initial offsets. The implant is initially created as a quarter volume and is revolved during the meshing phase to create a complete part.

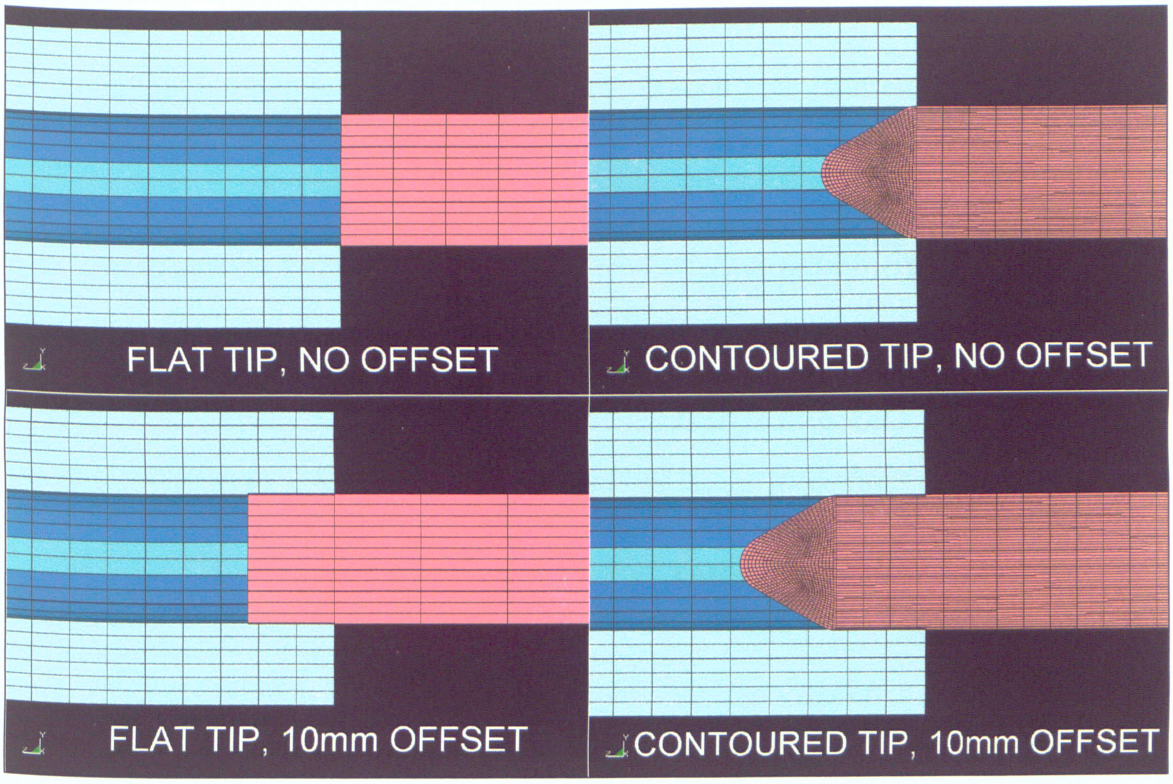

Figure 7: Offsets with Flat and Contoured-Tipped Implants

SECTION 4

```
*IF, TipType, EQ, 0, THEN
        VSUM, DEFAULT
        *GET, ImplantVolume, VOLU, 1, VOLU, , ,
        ImplantVolume = (ImplantVolume*4)
*ELSEIF, TipType, EQ, 1, THEN
        VSUM, DEFAULT
        *GET, V1, VOLU, 1, VOLU, , ,
        *GET, V2, VOLU, 2, VOLU, , ,
        ImplantVolume = V1+V2
        ImplantVolume = (ImplantVolume*4)
*ENDIF
```

In Section 4, the volume of the quarter implant is calculated and multiplied by four to give the total volume of a full implant. This value is saved as a parameter and used later in the macro to calculate the adjusted density value to be assigned to the implant.

```
CYL4, 0, 0, (BoneOD/2), 90, , , BoneOL
CYL4, 0, 0, (BoneID/2), 90, , , BoneIL
*GET, V2, VOLU, 0, NUM, MAX
V1 = V2-1
VSBV, V1, V2, , ,DELETE
WPOFFS, 0, 0, BoneIL
*GET, V1, VOLU, 0, NUM, MAX
VSBW, V1
WPCSYS, -1, 0
LSEL, S, LOC, Z, BoneIL
LSEL, R, RADIUS, , (BoneID/2)
*GET, LNum1, LINE, 0, NUM, MAX
ALLSEL, ALL
LSEL, S, LOC, Z, (((BoneOL-BoneIL)/2)+BoneIL)
LSEL, R, LOC, X, 0
LSEL, R, LOC, Y, 0
*GET, LNum2, LINE, 0, NUM, MAX
ALLSEL, ALL
ADRAG, LNum1, , , , , , LNum2
ALLSEL, ALL
LSEL, S, LOC, Z, BoneIL
LSEL, A, LOC, Z, BoneOL
LSEL, R, RADIUS, , (BoneID/2)
LSEL, A, LOC, Z, (((BoneOL-BoneIL)/2)+BoneIL)
LSEL, U, LOC, X, (BoneOD/2)
LSEL, U, LOC, Y, (BoneOD/2)
ASLL, S, 1
*GET, ANum, AREA, 0, NUM, MAX
ALLSEL, ALL
ASEL, S, LOC, Z, BoneOL
VSLA, S, 0
*GET, VNum, VOLU, 0, NUM, MAX
ALLSEL, ALL
VSBA, VNum, ANum, , , KEEP
ALLSEL, ALL
NUMCMP, KP
NUMCMP, LINE
NUMCMP, AREA
NUMCMP, VOLU
```

In Section 5, the geometry for the bone is created based on the input specified by the user. The geometry of the bone is created as three separate volumes, making it possible to create a clean mesh with control of the mesh density compared to meshing the bone as a single volume. As with the implant, the volume for the bone is initially created as a quarter volume and is revolved during the meshing phase to create a complete part.

SECTION 6

```
WPOFFS, 0, 0, -0.06
CYL4, 0, 0, ((((BoneOD/2)-(BoneID/2))/2)+(BoneID/2)), 90, , , (0.06+BoneOL)
WPCSYS, -1, 0
```

In Section 6, a cylindrical geometry is created in which the fluid will occupy. The cylindrical geometry spans the combined length of the implant and the bone and has a diameter halfway between the inner and outer diameter of the bone. The actual volume the fluid will occupy within this cylindrical geometry is defined further in the macro.

SECTION 7

```
KEYW, LSDYNA, 1
ET, 1, SOLID164
ET, 2, SOLID164
ET, 3, SOLID164
EDMP, RIGID, 1
KEYOPT, 2, 1, 2
*ASK, ImplantMass, Enter the mass of the implant (g),
*ASK, ImplantEX, Enter the elastic modulus of the implant (Pa),
*ASK, ImplantNUXY, Enter the Poisson's ratio of the implant (),
ImplantMass = ImplantMass/1000
ImplantDens = ImplantMass/ImplantVolume
MP, DENS, 1, ImplantDens
MP, EX, 1, ImplantEX
MP, NUXY, 1, ImplantNUXY
*ASK, Isotropic, Bone material isotropic? (0 for No, 1 for Yes),
*IF, Isotropic, EQ, 0, THEN
        *ASK, BoneDens, Enter the density of the bone (kg/m3),
        *ASK, BoneEX, Enter the transverse elastic modulus of the bone (Pa),
        *ASK, BoneEZ, Enter the longitudinal elastic modulus of the bone (Pa),
        *ASK, BoneGXY, Enter the transverse shear modulus of the bone (Pa),
        *ASK, BoneGXZ, Enter the longitudinal shear modulus of the bone (Pa),
        *ASK, BoneNUXY, Enter the transverse Poisson's ratio of the bone,
        *ASK, BoneNUXZ, Enter the longitudinal Poisson's ratio of the bone,
*ELSEIF, Isotropic, EQ, 1, THEN
        *ASK, BoneDens, Enter the density of the bone (kg/m3),
        *ASK, BoneEX, Enter the elastic modulus of the bone (Pa),
        *ASK, BoneNUXY, Enter the Poisson's ratio of the bone (),
*ENDIF
*IF, Isotropic, EQ, 0, THEN
        EDMP, ORTHO, 2, 100
        MP, DENS, 2, BoneDens
        MP, EX, 2, BoneEX
        MP, EY, 2, BoneEX
        MP, EZ, 2, BoneEZ
```

```
        MP, GXY, 2, BoneGXY
        MP, GYZ, 2, BoneGXY
        MP, GXZ, 2, BoneGXZ
        MP, NUXY, 2, BoneNUXY
        MP, NUYZ, 2, BoneNUXY
        MP, NUXZ, 2, BoneNUXZ
*ELSEIF, Isotropic, EQ, 1, THEN
        MP, DENS, 2, BoneDens
        MP, EX, 2, BoneEX
        MP, NUXY, 2, BoneNUXY
*ENDIF
*ASK, FluidDens, Enter the mass density of the fluid (kg/m3),
*ASK, FluidVisc, Enter the viscosity coefficient of the fluid (Ns/m2),
*ASK, FluidC, Enter the C parameter of the fluid EOS (m/s),
*ASK, FluidS1, Enter the S1 parameter of the fluid EOS,
*ASK, FluidS2, Enter the S2 parameter of the fluid EOS,
*ASK, FluidS3, Enter the S3 parameter of the fluid EOS,
*ASK, FluidGamma, Enter the Gamma parameter of the fluid EOS,
*ASK, FluidA, Enter the A parameter of the fluid EOS,
MP, DENS, 3, FluidDens
MP, EX, 3, 0
MP, NUXY, 3, 0
TB, EOS, 3, , , 2, 2
TBDATA, 2, FluidVisc
TBDATA, 16, FluidC
TBDATA, 17, FluidS1
TBDATA, 18, FluidS2
TBDATA, 19, FluidS3
TBDATA, 20, FluidGamma
TBDATA, 21, FluidA
```

In Section 7, the user is prompted for the material properties of the implant, bone and fluid. First, the user is asked to input the desired mass of the implant, as well as the elastic modulus and Poisson's ratio of the implant material. With the input mass of the implant and the volume of the implant calculated earlier in the macro, the required density of the implant is calculated. All the material properties are then assigned to the material model of the implant. The implant is modeled as a rigid body, for which stresses are not calculated. The result that is of most interest is the mechanical response of the bone to the hammer strike, not the implant. The added benefit of modeling the implant as a rigid body is a reduction in computation time, since implants with contoured tips can introduce a lot of elements to the model, as will be discussed later.

Next, the user is asked to specify if the bone material is isotropic. If an artificial bone material is being considered, the material properties are likely isotropic. If real bone is being considered, the properties will most likely be specified as orthotropic. If an isotropic bone material is specified, the user is asked to input the density, elastic modulus, and Poisson's ratio of the bone material. If an orthotropic bone material is specified, the user is asked to input the density, transverse elastic modulus, longitudinal elastic modulus, transverse shear modulus, longitudinal shear modulus, transverse Poisson's ratio and longitudinal Poisson's ratio.

Next, the user is asked to input the mass density and viscosity coefficient of the fluid. LS-DYNA requires an equation of state to be specified for the fluid to define its pressure/volume relationship. For this, a Gruneisen equation of state is used. The Gruneisen equation of state for compressed materials is as follows:

$$P = \frac{p_0 C^2 \mu \left[1 + \left(1 - \frac{\gamma}{2}\right)\mu - \frac{a}{2}\mu^2\right]}{\left[1 - (S_1 - 1)\mu - S_2 \frac{\mu^2}{\mu+1} - S_3 \frac{\mu^3}{(\mu+1)^2}\right]^2} + (\gamma + a\mu)E \qquad (1)$$

where **P** is pressure, **C** is the intercept of the shock velocity-particle velocity curve; S_1, S_2 and S_3 are the coefficients of the slope of the velocity-particle velocity curve; γ is the Gruneisen gamma; **a** is the first order volume correction to γ; $\mu = (\rho/\rho_0)-1$; ρ is density and **E** is energy [48]. In accordance with the parameters required by LS-DYNA, the user is asked to input the **C**, S_1, S_2, S_3, γ and **a** parameters of the Gruneisen equation of state for the fluid being considered. While there are Gruneisen equations of state known for common fluids like water, this is not the case for a fluid like bone marrow. For a fluid

like bone marrow, the equation of state must be determined by either calibrating a known equation of state for another fluid to experimental results or by deriving the parameters of the equation of state experimentally.

SECTION 8

```
MAT, 1
TYPE, 1
REAL, 1
*IF, TipType, EQ, 0, THEN
        VSEL, S, VOLU, , 1, , , 1
        LSEL, S, LOC, Z, (-0.03+(Offset))
        LESIZE, ALL, , , 20, , , , , 1
        ALLSEL, ALL
        VSEL, S, VOLU, , 1, , , 1
        LSEL, U, LOC, Z, (-0.03+(Offset))
        LESIZE, ALL, , , 6, , , , , 1
        ALLSEL, ALL
        VMESH, 1
*ELSEIF, TipType, EQ, 1, THEN
        VSEL, S, VOLU, , 2, , , 1
        LSEL, S, LOC, Z, (-0.03+(Offset))
        LESIZE, ALL, , , 20, , , , , 1
        ALLSEL, ALL
        VSEL, S, VOLU, , 1, , , 1
        LSEL, U, LOC, Z, (0+(Offset))
        *IF, Hollow, EQ, 1, THEN
                LSEL, U, LOC, X, (ImplantID/2)
                LSEL, U, LOC, Y, (ImplantID/2)
                *GET, LNum, LINE, 1, NUM, MAX, ,
                LSEL, U, LINE, , LNum
        *ENDIF
        LESIZE, ALL, , , 25, , , , , 1
        ALLSEL, ALL
        *IF, Hollow, EQ, 0, THEN
                VMESH, 1
                VMESH, 2
        *ELSEIF, Hollow, EQ, 1, THEN
                VSWEEP, 1
                VSWEEP, 2
        *ENDIF
*ENDIF
CSWPLA, 11, 1, 1, 1,
*GET, NNum, NODE, 1, NUM, MAX, ,
NGEN, 4, NNum, ALL, , , , 90, , 1,
EGEN, 4, NNum, ALL, , , , , , , , , , ,
NUMMRG, NODE, , , , LOW
NUMCMP, NODE
ALLSEL, ALL
```

In Section 8, the implant is meshed. The elements are rotated three times in 90 degree intervals to generate the complete shape from the quarter volume created earlier in the macro. If a contoured tip has been specified, the implant is given a finer mesh than if a flat tip was specified. This fine mesh allows for a much smoother contour on the tip than a coarse mesh would allow (Figure 8). Because the implant is a rigid body and stresses are not calculated during the solution phase, the mesh density will not have an impact on the accuracy of the results or the solution time.

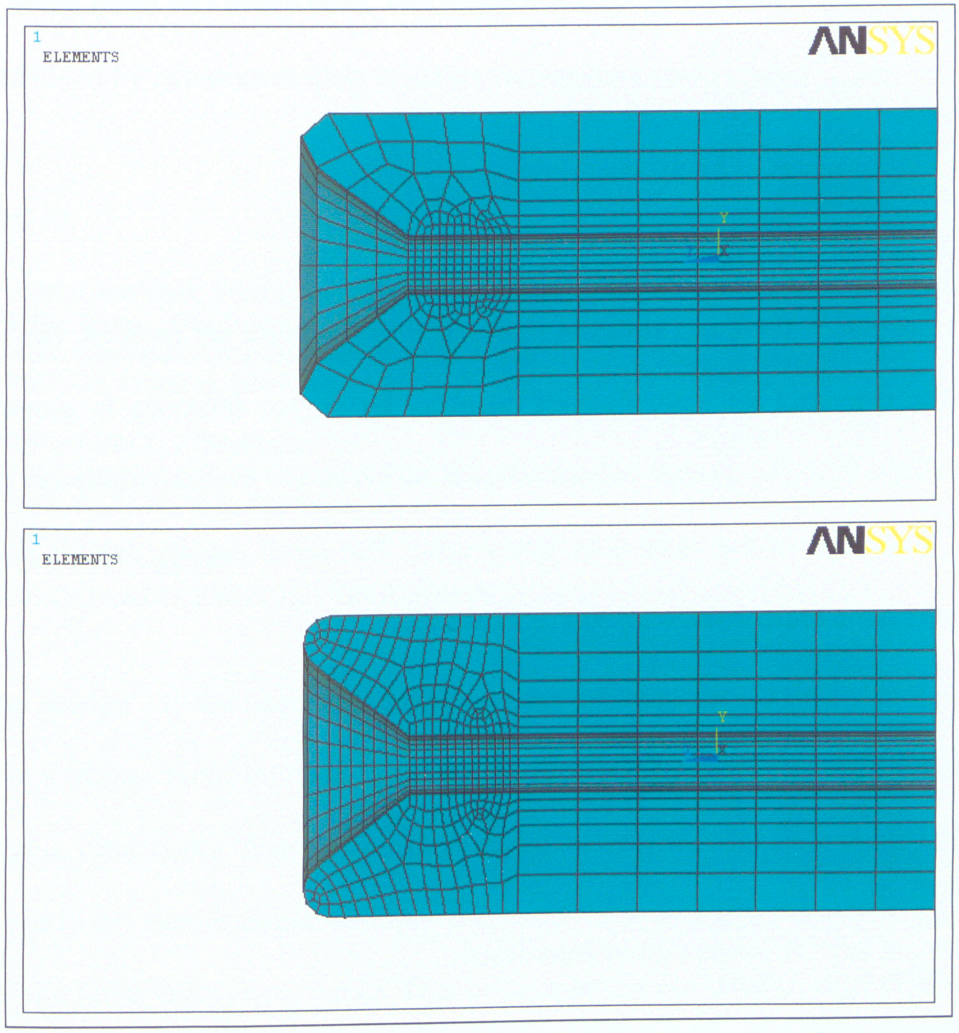

Figure 8: Comparison of Coarse and Fine Implant Tip Meshes

SECTION 9

```
MAT, 2
TYPE, 2
REAL, 2
*GET, VNum, VOLU, 0, NUM, MAX
V1 = VNum-3
V2 = VNum-2
V3 = VNum-1
VSEL, S, VOLU, , V1, V3, , 1
LSEL, S, LOC, Z, (BoneIL/2)
LESIZE, ALL, , , 80, , , , , 1
ALLSEL, ALL
VSEL, S, VOLU, , V1, V3, , 1
LSEL, U, LOC, Z, (BoneIL/2)
LESIZE, ALL, , , 6, , , , , 1
ALLSEL, ALL
VSWEEP, V1
VSWEEP, V2
VSWEEP, V3
VSEL, S, VOLU, , V1, V3, , 1
*GET, NNum, NODE, 1, NUM, MAX, ,
NGEN, 4, NNum, ALL, , , , 90, , 1,
EGEN, 4, NNum, ALL, , , , , , , , , , ,
NUMMRG,NODE, , , ,LOW
NUMCMP,NODE
ALLSEL, ALL
```

In Section 9, the three volumes that make up the bone are meshed. As with the implant, the elements are rotated three times in 90 degree intervals to generate the complete shape from the quarter volume created earlier in the macro. Unlike the implant, the bone is meshed in the same way every time. The mesh density for the bone was determined from a mesh sensitivity test discussed later.

SECTION 10

```
MAT, 3
TYPE, 3
REAL, 3
VSEL, S, VOLU, , VNum, , , 1
LSEL, S, LOC, Z, ((-0.06)+((0.06+BoneOL)/2))
LESIZE, ALL, , , 100, , , , , 1
ALLSEL, ALL
VSEL, S, VOLU, , VNum, , , 1
LSEL, U, LOC, Z, ((-0.06)+((0.06+BoneOL)/2))
LESIZE, ALL, , , 15, , , , , 1
```

```
ALLSEL, ALL
VSWEEP, VNum
VSEL, S, VOLU, , VNum, , , 1
*GET, NNum, NODE, 1, NUM, MAX, ,
NGEN, 4, NNum, ALL, , , ,90, ,1,
EGEN, 4, NNum, ALL, , , , , , , , , , ,
NUMMRG, NODE, , , ,LOW
NUMCMP, NODE
ALLSEL, ALL
```

In Section 10, the fluid volume is meshed. As with the implant and the bone, the elements are rotated three times in 90 degree intervals to generate the complete shape from the quarter volume created earlier in the macro. Like the bone, the fluid volume is meshed in the same way every time. The fluid volume is given a fine mesh whose density was determined by experimentation to keep solution time reasonable.

SECTION 11

```
*ASK, DataPoints, Enter the number of impulse force data points,
*DIM, TIME, , DataPoints,
*ASK, FileName, Enter the name of the time data file,
*VREAD, TIME(1), FileName, txt,,,,
(1F7.5)
*DIM, FORCE, , DataPoints,
*ASK, FileName, Enter the name of the force data file,
*VREAD, FORCE(1), FileName, txt,,,,
(1F4.0)
EDPART, CREATE
EDLOAD, ADD, RBFZ, 0, 1, TIME, FORCE, 0, , , , ,
```

In Section 11, the user is prompted to specify force versus time data to simulate the hammer strike. First, the user is asked to specify the number of data points in the force versus time curve that can be determined experimentally or can be created by design. Next, the user is asked to input the name of a text file that contains the time values of the force versus time curve. This name must be enclosed in single quotes when entered. For example, if the file with the time values is called Time.txt, the user would

input 'Time'. Next, the user is asked to input the name of a text file that contains the force values of the force versus time curve. As with the file for the time values, this name must be enclosed in single quotes when entered. Examples of time and force text files can be found in Appendix B. With the impulse force data specified, the macro creates the impulse force curve in ANSYS (Figure 9) and applies it to the implant. It is advisable to manually alter the force versus time curve so there is sufficient time after the peak force to observe any after effects of the strike. An impulse force curve that includes multiple hammer strikes can also be used with the macro, but the increased analysis time may cause the solution time to become unreasonable.

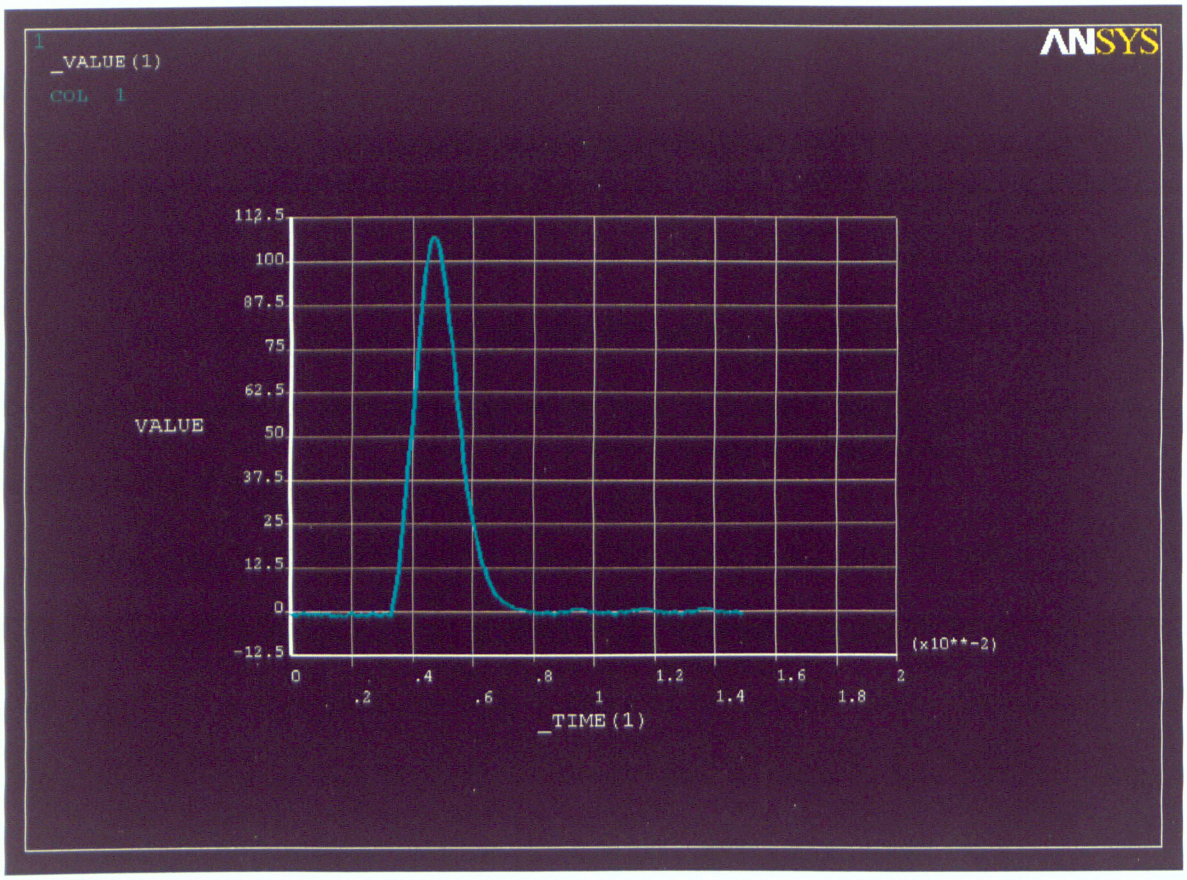

Figure 9: Sample Force versus Time Curve

```
NSEL, S, LOC, Z, 0
NSEL, R, LOC, X, (BoneOD/2)
D, ALL, ,0, , , ,ALL, , , , ,
ALLSEL, ALL
NSEL, S, LOC, Z, BoneOL
NSEL, R, LOC, X, (BoneOD/2)
D, ALL, ,0, , , ,ALL, , , , ,
ALLSEL, ALL
```

In Section 12, boundary conditions are applied to the finite element model. All the nodes along the outer diameter of both ends of the bone are constrained in all degrees of freedom, allowing no translation or rotation about the three global axes (Figure 10).

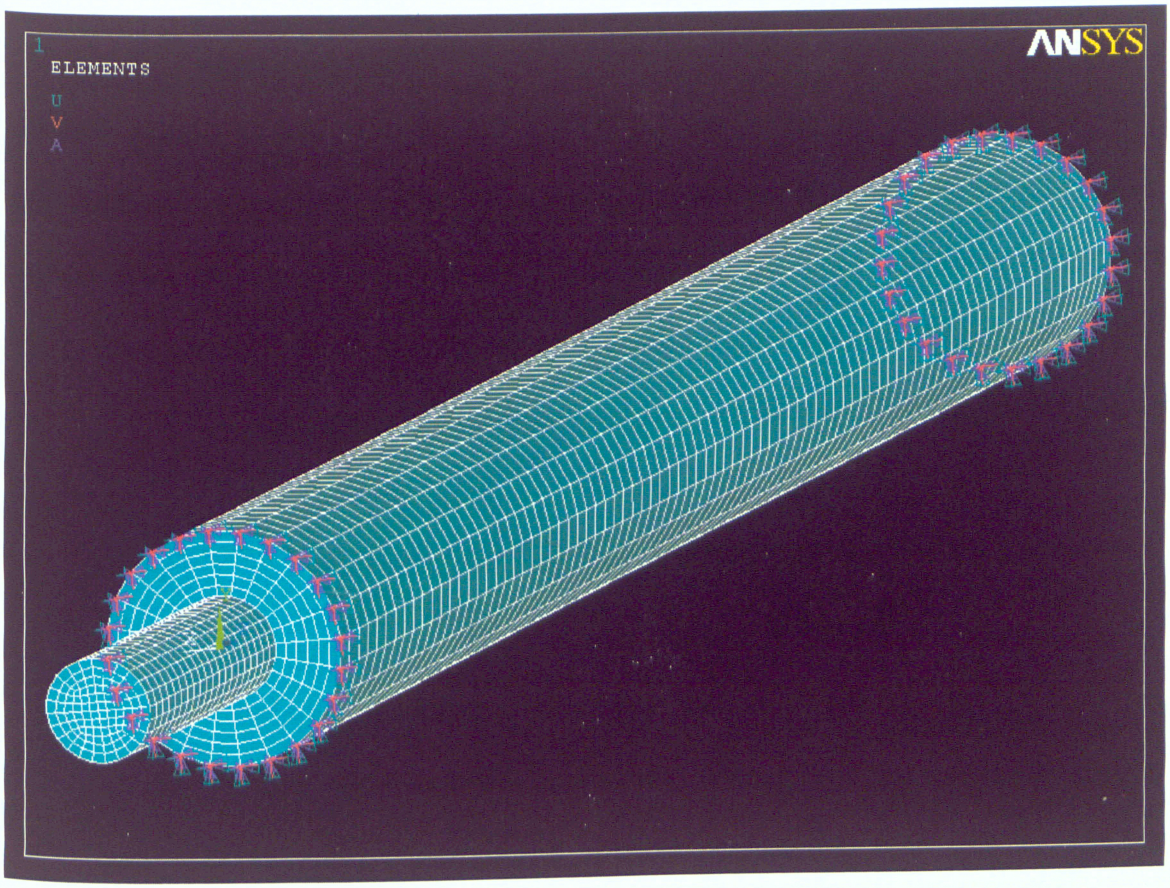

Figure 10: Boundary Conditions Applied to Finite Element Model

SECTION 13

```
*SET, EndTime, TIME(DataPoints)
TIME, EndTime,
EDRST, 100
EDWRITE,BOTH,'InputFile','k',''
```

In Section 13, the macro sets the solution time to the last time value in the force versus time curve defined earlier. This is the reason the force versus time curve should be manually edited to ensure there is sufficient analysis time after the peak force. The number of result file increments is set to 100, and an LS-DYNA input file is created for the solution phase. The LS-DYNA input file will be located in the working directory that was specified when ANSYS was started and will be called 'InputFile.k'.

Unfortunately, not all of the LS-DYNA functionality that is needed for the analysis is accessible through the ANSYS interface. There are a number of functions that the ANSYS translator cannot convert into LS-DYNA keyword commands. As such, the LS-DYNA input file requires some editing before the solution phase. This can be done by opening the input file in a text editor and making the following changes:

1) In the SECTION DEFINITION section, change the lines

```
*SECTION_SOLID
         3       1
```

to the following

```
*SECTION_SOLID
         3      11
```

This changes the element formulation for the fluid to an arbitrary Lagrangian-Eulerian multi-material element. This formulation is used because, when a pure

Lagrangian formulation was tested, the fluid elements that were directly contacted by the implant became severely distorted during the hammering event. This distortion would cause an element to flip inside-out, leading to a negative volume termination of the analysis. The arbitrary Lagrangian-Eulerian formulation allows adaptive meshing of the fluid elements that prevents this from happening.

2) The following lines should be pasted into the input file

```
*PART
Part      4 for Mat      4 and Elem Type      4
         4         4         4         0         0         0
*SECTION_SOLID
         4        11
*MAT_VACUUM
         4
*SET_PART_LIST
         1
         3         4
*CONTROL_ALE
         2         1         1        -1
*ALE_MULTI-MATERIAL_GROUP
         3         1
         4         1
*INITIAL_VOLUME_FRACTION_GEOMETRY
         4         1         1
         4         0         1
         0         0    0.0254         0         0      0.35     0.008     0.008
*CONSTRAINED_LAGRANGE_IN_SOLID
         1         1         1         0         2         4         2         1
         0.01.0E10       0.1       0.0       0.1         0         0       0.1
         0.0                         0       0.1
*CONSTRAINED_LAGRANGE_IN_SOLID
         2         1         1         0         2         4         2         1
         0.01.0E10       0.1       0.0       0.1         0         0       0.1
         0.0                         0       0.1
```

This section can be pasted anywhere in the input file as long as it is not interrupting one of the keyword commands. This section first introduces another part with an ALE multi-material element formulation that will be used in conjunction with the fluid part. This additional part will act as a void space for the fluid to flow into as it is displaced by the implant. This section also includes the

*INITIAL_VOLUME_FRACTION_GEOMETRY command that defines the cylindrical volume the fluid will occupy. This geometry must be defined by the user for each analysis based on the inner diameter of the bone, the inner length of the bone, and the location of the tip of the implant relative to the open end of the bone. This is done in the third line of the command with the following 8 parameters from left to right in the command line:

Parameter 1 - X coordinate of the center of the lower base of the cylinder

Parameter 2 - Y coordinate of the center of the lower base of the cylinder

Parameter 3 - Z coordinate of the center of the lower base of the cylinder

Parameter 4 - X coordinate of the center of the upper base of the cylinder

Parameter 5 - Y coordinate of the center of the upper base of the cylinder

Parameter 6 - Z coordinate of the center of the upper base of the cylinder

Parameter 7 - Radius of the lower base of the cylinder

Parameter 8 - Radius of the upper base of the cylinder

Parameters 1, 2, 4, and 5 will always be zero; and parameters 7 and 8 should always be equal to each other unless a conical fluid volume is desired. Finally, this section also defines the contact between the fluid and the bone as well as the fluid and the implant.

3.3 Mesh Sensitivity

In order to determine the appropriate density of the mesh applied to the bone in the finite element models, a mesh sensitivity analysis was conducted. One test

configuration was considered for this investigation. For this configuration, a force versus time curve with a peak of approximately 107 N and duration of 15 ms was used to strike the implant. The geometry and material properties used for the test configuration are listed in Table 4.

Part	Parameter	Value
Bone	Inner Diameter	15 mm
	Outer Diameter	35 mm
	Inner Length	330 mm
	Outer Length	350 mm
	Density	1950 kg/m^3
	Elastic Modulus	11.5 GPa
	Poisson's Ratio	0.31
Implant	Outer Diameter	15.25 mm
	Tip Type	Flat
	Hollow or Solid	Solid
	Mass	128.5 g
	Elastic Modulus	114.0 GPa
	Poisson's Ratio	0.33
Fluid	Density	1058.1 kg/m^3
	Viscosity	0.035 Ns/m^2
	Equation of State C Parameter	1647 m/s
	Equation of State S_1 Parameter	1.921
	Equation of State S_2 Parameter	-0.096
	Equation of State S_3 Parameter	0.0
	Equation of State γ Parameter	0.35
	Equation of State a Parameter	0.0

Table 4: Geometry and Material Properties of Mesh Sensitivity Model

Using the macro, a number of finite element models were created using the parameters of the test configuration. The only difference between the various finite element models was the mesh density of the bone. Each finite element model was analyzed, and, from the results, the equivalent stress in the bone over the analysis time was plotted. From this plot the maximum equivalent stress was determined and used to decide at what point further refinement to the mesh did not significantly affect the results. The results of the mesh sensitivity analysis are summarized in Table 5.

Test Case	Number of Elements in Bone	Maximum Equivalent Stress (kPa)	Percent Change from Previous
1	5784	255.2	-
2	7224	234.7	8.03%
3	8664	220.6	6.00%
4	10104	214.1	2.95%
5	11544	211.0	1.45%
6	12983	210.1	0.43%

Table 5: Results of Mesh Sensitivity Test

The maximum equivalent stress in the bone for the different bone mesh densities is plotted in Figure 11. The final test case shows a maximum equivalent stress that differs from the previous test case by only 0.43%. For the purpose of this mesh sensitivity analysis, this can be considered to have converged. In addition, in the final test case, the mesh is fine enough along the length of the bone so that stresses at particular locations can be determined more accurately compared to other test cases. For example, computing the stress at a location that falls within an element that is 10 mm wide will give a better

approximation compared to computing the stress at the same location that falls within an element that is 20 mm wide. This will be of particular importance in the next chapter when results from finite element models will be compared to pressures measured at various locations along an experimental bone analogue. For these reasons, the parameters set in the macro were such to generate a mesh density for the bone as per the final test case, namely 12983 elements.

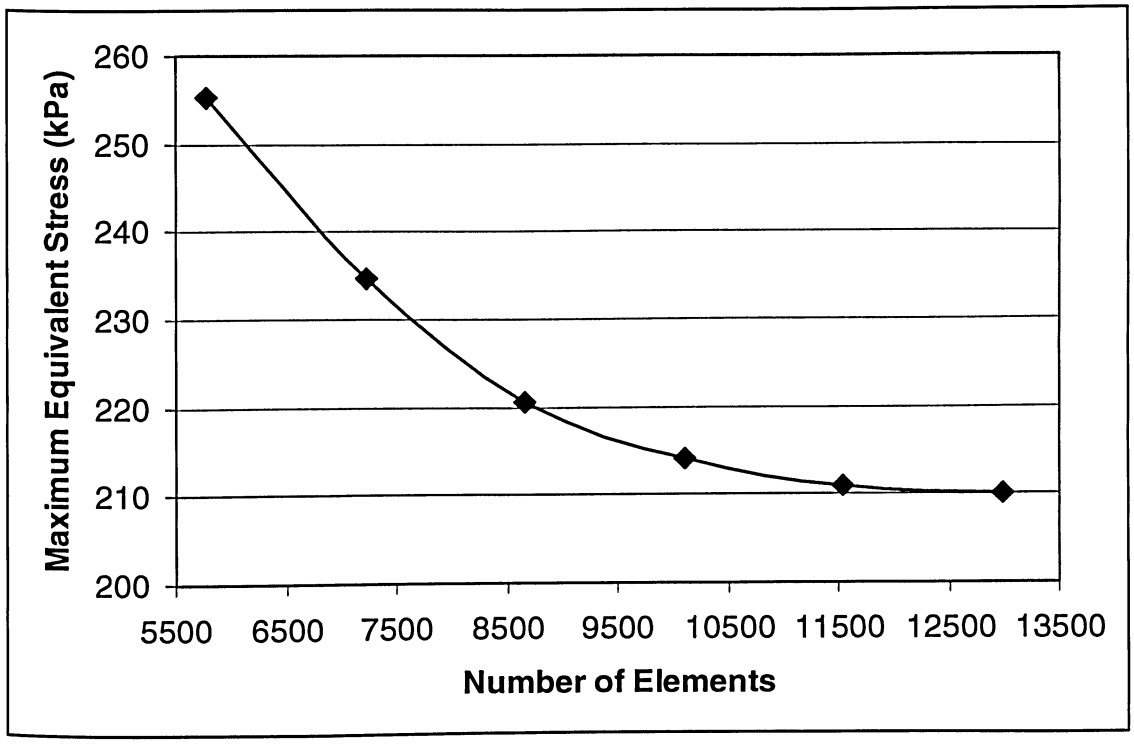

Figure 11: Maximum Equivalent Stress for Different Bone Mesh Densities

CHAPTER 4

FINITE ELEMENT MODEL VALIDATION

4.1 Validation Overview

Although the macro makes it possible to efficiently create finite element models that simulate the bone/fluid/implant system and the hammering event, the accuracy of the results generated are always in question and need to be investigated. To demonstrate that the finite element models produce acceptable results to use for comparative studies, it was necessary to validate the computed results. To do this, another member of the research group built an apparatus to experimentally investigate the bone/fluid/implant system and the surgical event of striking the implant to insert it into the intramedullary canal [49]. During the event of striking the implant, the pressures are measured at various locations in the bone analogue serving as experimental results for comparison. A number of experimental tests are conducted to give more merit to the validation. Finite element models are created using the macro and based on the parameters of the experimental tests. Stress values are determined from the finite element results that the experimental tests are compared to. If the experimental results and the finite element results are comparable to each other, the finite element approach to modeling the bone/fluid/implant system and the hammering event can be deemed acceptable.

4.2 Experimental Testing

To represent the bone, a hollow tube that was open on one end and closed on the other was made. The length, outer diameter, and inner diameter of the tube were 350 mm, 32 mm and 16 mm, respectively. These values were chosen because they roughly match the dimensions of a large human femur. Typically, the first step in the surgical procedure of inserting an intramedullary implant involves preparation of the intramedullary canal to accept the implant. This preparation is done by reaming and/or broaching the intramedullary canal to the proper inner diameter dictated by the outer diameter of the implant that will be used. This process eliminates the cancellous bone from the intramedullary canal. As such, the material of the bone analogue needed only to reproduce the characteristics of cortical bone. In choosing a cortical bone material substitute, the main criteria were to have a similar porosity, density, pore size, and modulus of elasticity to that of human cortical bone (5-30%, 1810kg/m^3, 3-78 microns, and 10-20GPa, respectively). In addition, to accurately simulate the mechanical behavior of human cortical bone, it was important that the material had an open pore structure [50]. A number of materials including Polyurethane foam and open cell ceramics were considered, but ultimately the most suitable cortical bone material substitute was found to be a porous Ultra-High Molecular Weight (UHMW) polyethylene plastic. A porous plastic cylinder was custom manufactured with an open cell structure. The cylinder had a porosity of 15-30% and 40-60 microns pore size, matching the requirements in terms of pore size and porosity. The plastic is not as stiff as human bone but, for the purpose of validating the finite element models, it was deemed to be acceptable. If the finite element

models were able to reasonably predict the intramedullary pressures measured in the experiments, there is no reason to believe that increasing the elastic modulus to that of human cortical bone in future parametric tests would invalidate the finite element models.

The implant consisted of a stainless steel rod with a removable Teflon piston end (Figure 12). The end was made removable so that different pistons could be tested easily. The dimensions of the pistons that were used are summarized in Table 6. Teflon was chosen as the material for the piston to reduce friction between the piston and inner walls of the bone analogue should contact occur during the insertion. A flat tip was chosen for the piston to simplify the finite element model.

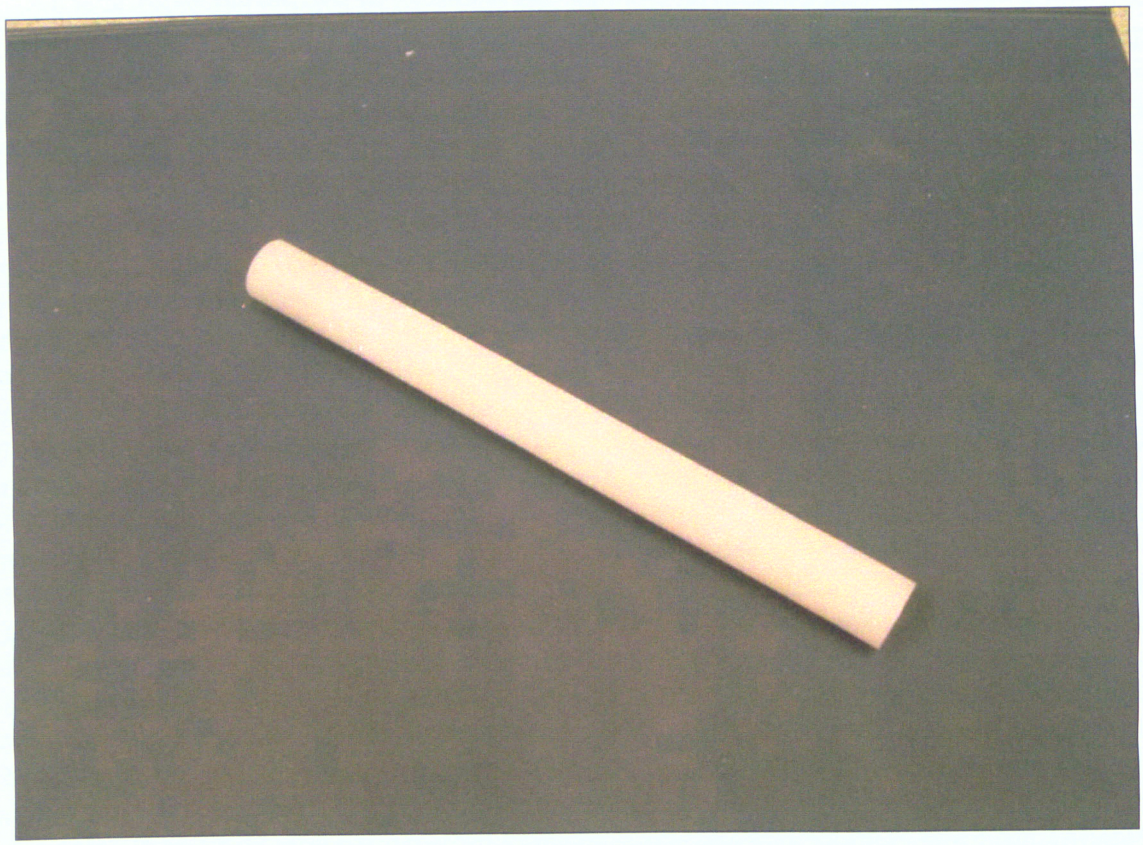

Figure 12: Sample Teflon Piston Used in Experiments [49]

To reproduce the properties of bone marrow, a mixture of petroleum jelly and paraffin was used. The properties of a petroleum jelly and paraffin mixture at 20°C have been shown to be roughly equivalent to those of bone marrow fat at 36°C [51]. The bone analogue was filled with a 45/55 ratio of petroleum jelly/paraffin mixture. The viscosity of this mixture was measured to be a constant 82.6cP using a Gilmont falling ball viscometer. This viscosity is within the range of 50cP to 600cP that represents the variation of viscosity that has been observed between the distal and proximal bone marrow in the femur [52].

In order to measure the pressures resulting from the hammering of an intramedullary device into the bone analogue, an apparatus was built to support and test the bone/fluid/implant system. A swinging pendulum with an adjustable mount was constructed to create controlled impulse forces that simulate a hammer strike (Figure 13). Attached to the mount was a weight which could be changed to control the magnitude of the hammering force. Also attached to the mount was a Dytran 5800B4 impulse hammer that allowed the hammering force to be measured as a function of time. The bone analogue was drilled and tapped at four locations along its span where the pressures were measured. The taps were located approximately 75 mm, 150 mm, 225 mm and 300 mm from the open end of the bone analogue where the implant was inserted (Figure 14). The pressure as a function of time was measured by a Kulite XTM190 miniature pressure transducer that was mounted at each of those locations in the bone analogue.

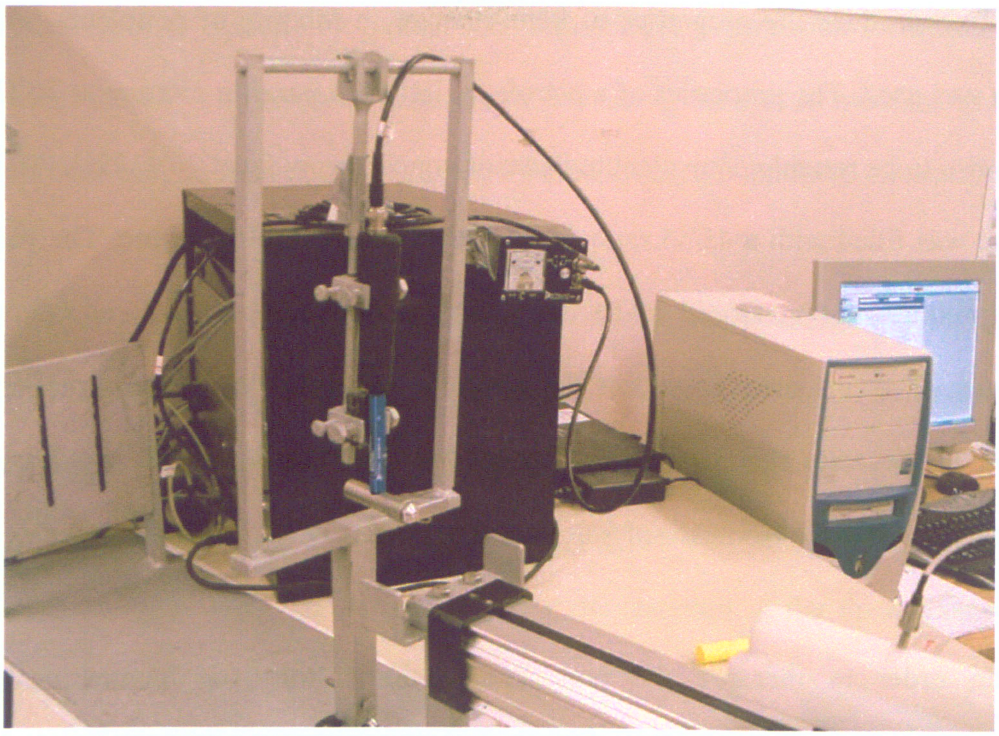

Figure 13: Impulse Hammer Used in Experiments [49]

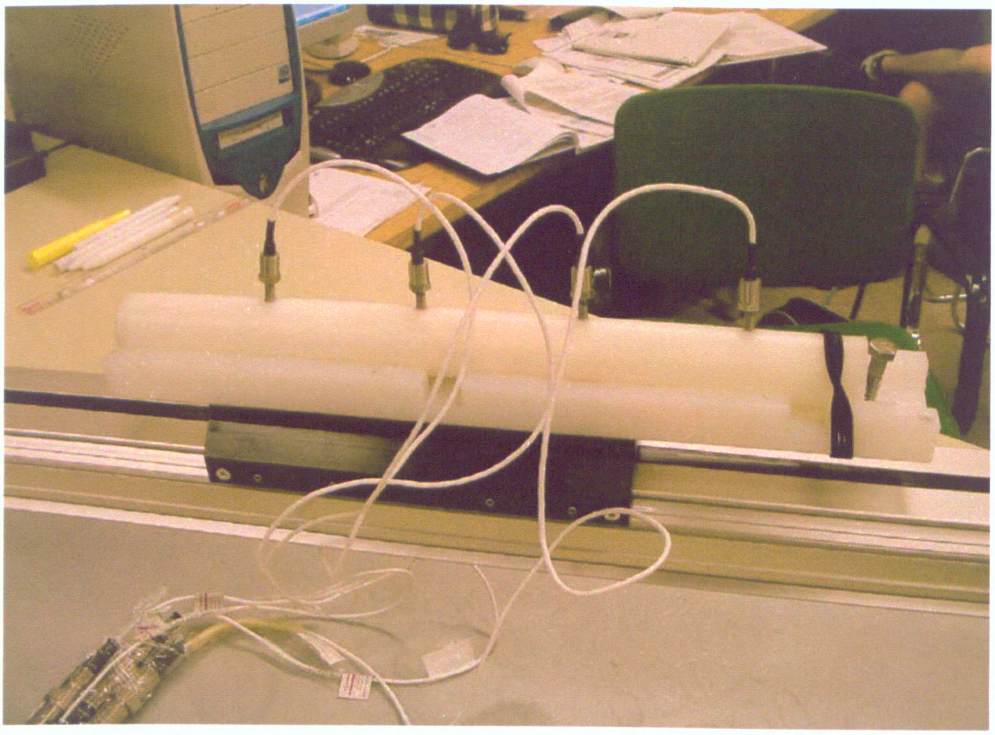

Figure 14: Experimental Bone Analogue and Pressure Transducers [49]

The raw experimental data were recorded with a data acquisition system that was coupled to a Pentium 4-2.6GHz computer. The data acquisition system was capable of collecting 200,000 samples per second from 32 separate channels. This provided excellent resolution for accurately determining the maximum pressures. Experimental results were collected with the use of DaqView 7.13 software and analyzed with Microsoft Excel 2003.

Three experimental test cases were performed for the validation. The parameters that were varied between the test cases were the outer diameter of the implant (and consequentially the gap between the implant and the bone analogue) and the peak force of the hammer strike. A summary of the experimental test cases and the parameters are given in Table 6.

Test Case	Implant Outer Diameter (mm)	Implant Mass (g)	Peak Force Of Hammer Strike (N)
1	14.43	76.7	93.8
2	14.94	79.1	114.5
3	15.49	81.7	144.3

Table 6: Experimental Test Case Parameters [49]

4.3 Finite Element Modeling

Given the parameters of the test cases, the macro was used to build a finite element model of each experimental test case that was conducted. The geometry of the

bone was based on the dimensions of the bone analogue used in the experiments. The implant was specified to have a flat tip and was given the appropriate outer diameter in the finite element models according to the test case. As mentioned in Chapter 3, the implant is always given a length of 60 mm. In addition, the implant in the finite element models did not include the stainless steel rod described above. However, the measured mass of the stainless steel rod with the different Teflon pistons was specified when the macro was used to build the models. The densities were adjusted by the macro so the mass of the implant was equal to that of the Teflon piston and stainless steel rod assembly used in the test cases. The implant was given an initial offset of 25.4 mm into the open end of the bone, as was the case in all the experiments (Figure 15). The fluid was defined as a volume that fills the interior of the bone up to the tip of the implant.

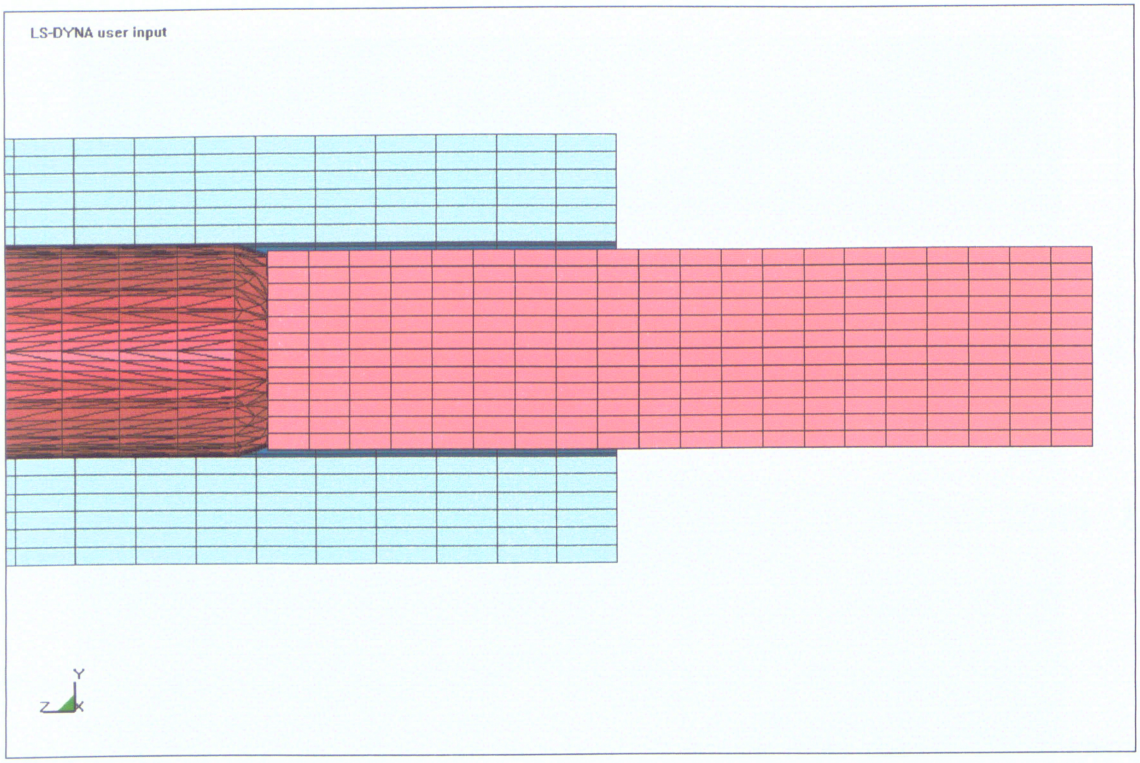

Figure 15: Initial Offset of Implant in Finite Element Models

The material properties of the implant were based on the Teflon material used in the experimental piston. Because the material used in the bone analogue was custom made, the material properties were not readily known. The modulus of elasticity and Poisson's ratio was approximated using a variation of the Gibson-Ashby equation:

$$\left(\frac{E}{E_S}\right)=\left(\frac{(P-P_0)}{(P+P_0)}\right)^M \qquad (2)$$

E is modulus of elasticity of the cellular material that will be used in the finite element model. E_s is the modulus of elasticity of the UHMW polyethylene plastic that makes up the solid skeleton of the cellular material. With a yield stress of 19 MPa and a 13% elongation at yield for the UHMW polyethylene plastic [53], E_s was calculated to be 146.15 MPa. P is the reduced density of the material, which is defined as the density of the cellular material divided by the density of the solid skeleton. The density of the cellular material was calculated to be 720.7 kg/m^3. With a density of 930.0 kg/m^3 for the UHMW polyethylene plastic solid skeleton [53], P was calculated to be 0.775. P_0 and M are constants that depend on the reduced density of the material and are equal to 0.029 and 2.15, respectively.

The material properties for the fluid were based on the properties of the Vaseline/paraffin mixture described previously. Because an equation of state for the Vaseline/paraffin mixture was not available, the equation of state parameters were calibrated using one of the experimental test cases and a number of test trials. This procedure is described in greater detail below. A summary of the geometry and material properties used in the finite element model is given in Table 7.

Part	Material Property	Value
Bone	Inner Diameter	16 mm
	Outer Diameter	32 mm
	Inner Length	350 mm
	Outer Length	370 mm
	Density	720.7 kg/m^3
	Elastic Modulus	124.2 MPa
	Poisson's Ratio	0.36
Implant	Outer Diameter	14.43, 14.94, 15.49 mm
	Tip Type	Flat
	Hollow or Solid	Solid
	Mass	76.7, 79.1, 81.7 g
	Elastic Modulus	193.0 GPa
	Poisson's Ratio	0.30
Fluid	Density	861.5 kg/m^3
	Viscosity	0.0826 Ns/m^2
	Equation of State C Parameter	9000 m/s
	Equation of State S_1 Parameter	1.920
	Equation of State S_2 Parameter	0.0
	Equation of State S_3 Parameter	0.0
	Equation of State γ Parameter	1.5
	Equation of State a Parameter	0.0

Table 7: Geometry and Material Properties of Validation Models

The forces versus time data recorded by the impulse hammer during the experimental test cases were converted to text files as described in Chapter 3. These text files were used with the macro to define the force applied to the implant in the finite element models. The force versus time curves for test cases 1, 2, and 3 are shown in Figure 16, 17, and 18, respectively.

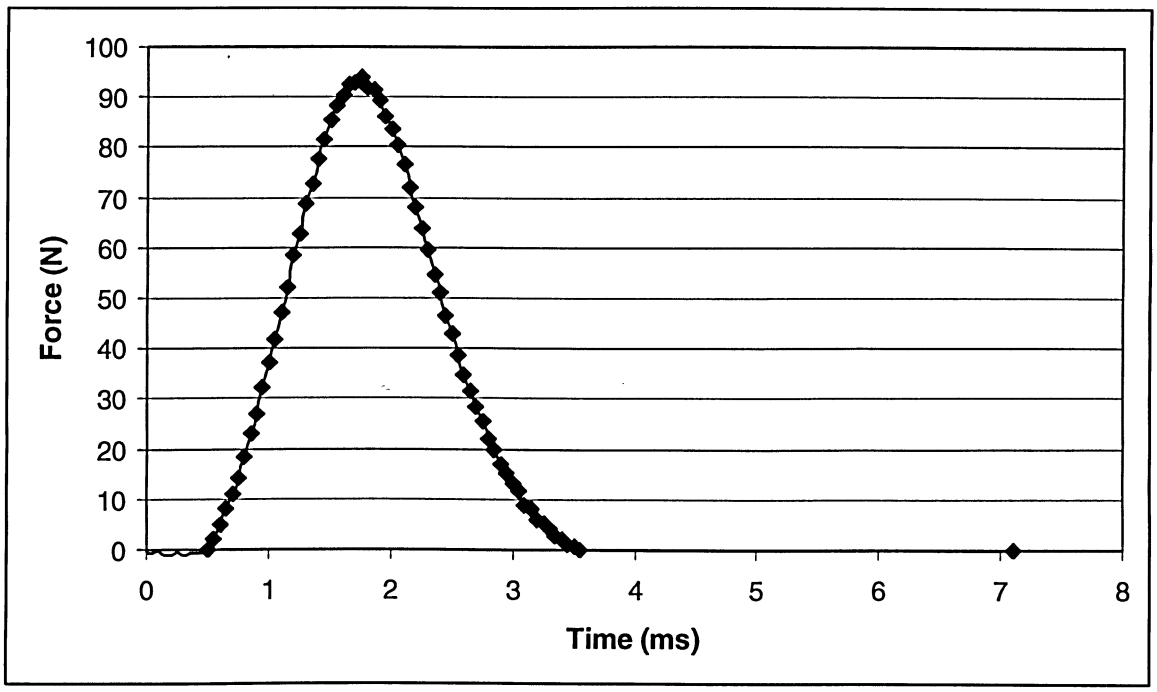

Figure 16: Force versus Time Curve for Test Case 1

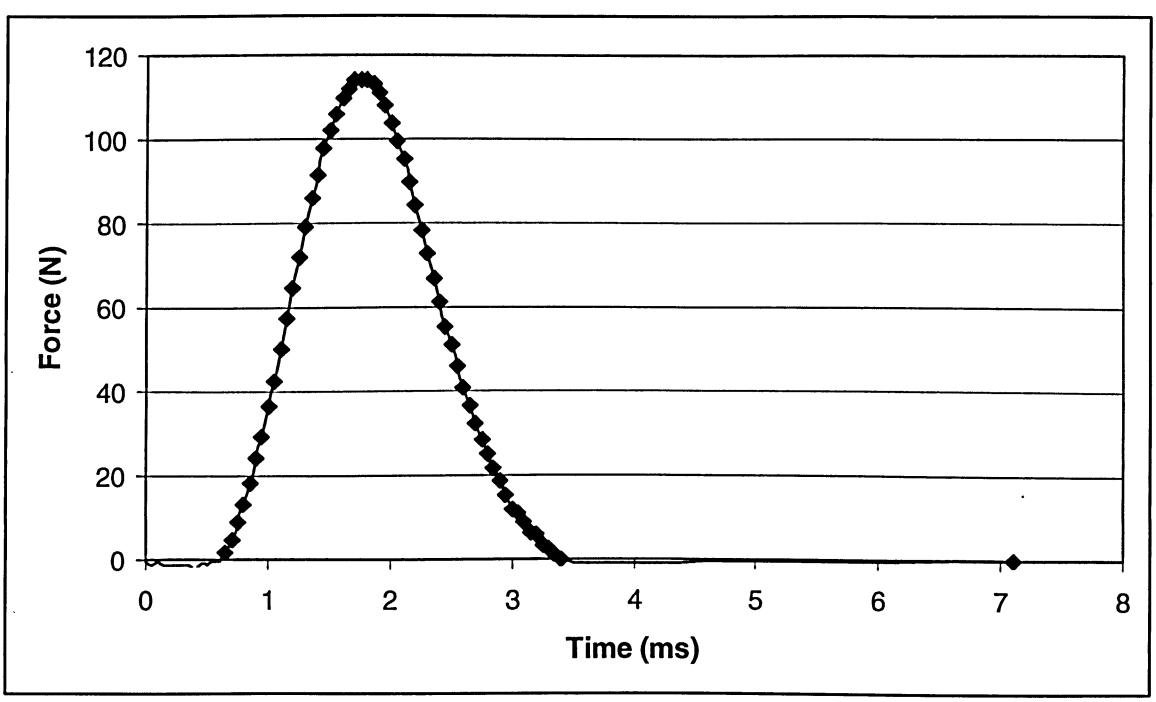

Figure 17: Force versus Time Curve for Test Case 2

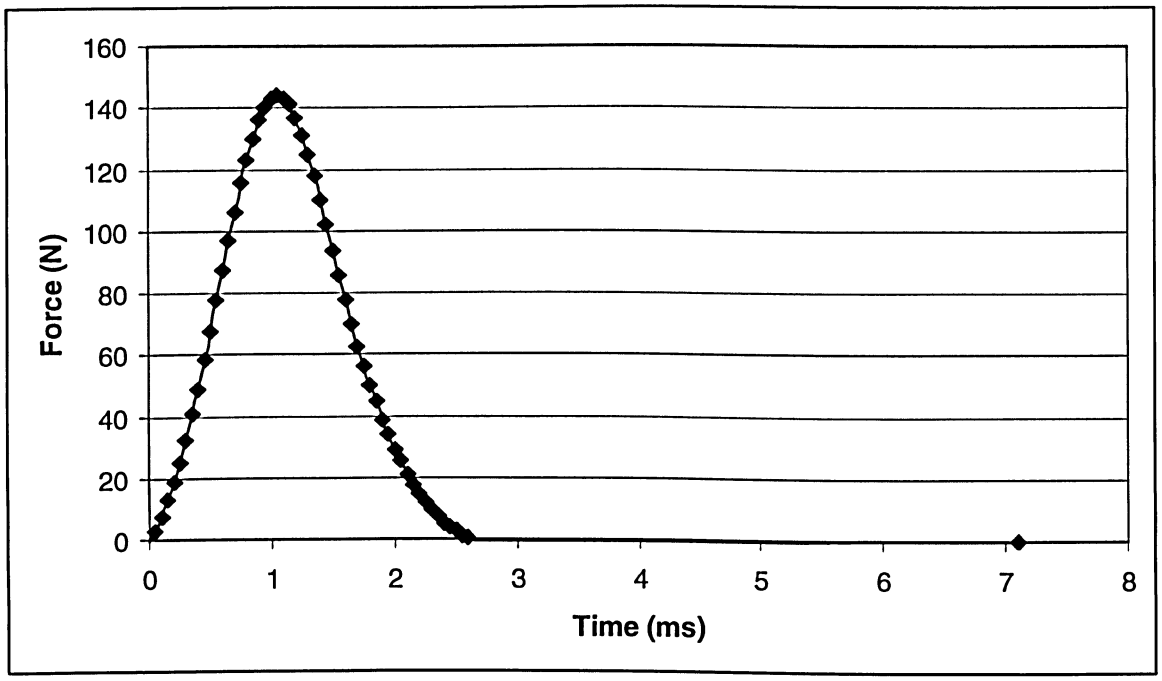

Figure 18: Force versus Time Curve for Test Case 3

Once the finite element models were solved, a slice of elements was isolated at the locations along the length of the bone that corresponded to the locations where the transducers were located on the bone analogue. Because cylindrical coordinate systems cannot be used in LS-PREPOST, only the eight elements on the inner surface of the slice of elements that were aligned with the global X and Y axes were considered (Figure 19). For the elements aligned with the global X axis, the X component of direct stress was plotted over time. Similarly, the Y component of direct stress for the elements aligned with the global Y axis was plotted over time. The normal direct stress on the surface of a solid element is a close representation to an externally applied pressure on the surface of a transducer. From the stress versus time plots, the maximum stress was determined for each of the eight elements. The average of the eight maximum stresses was calculated and considered as a close approximation of the maximum pressure at that location.

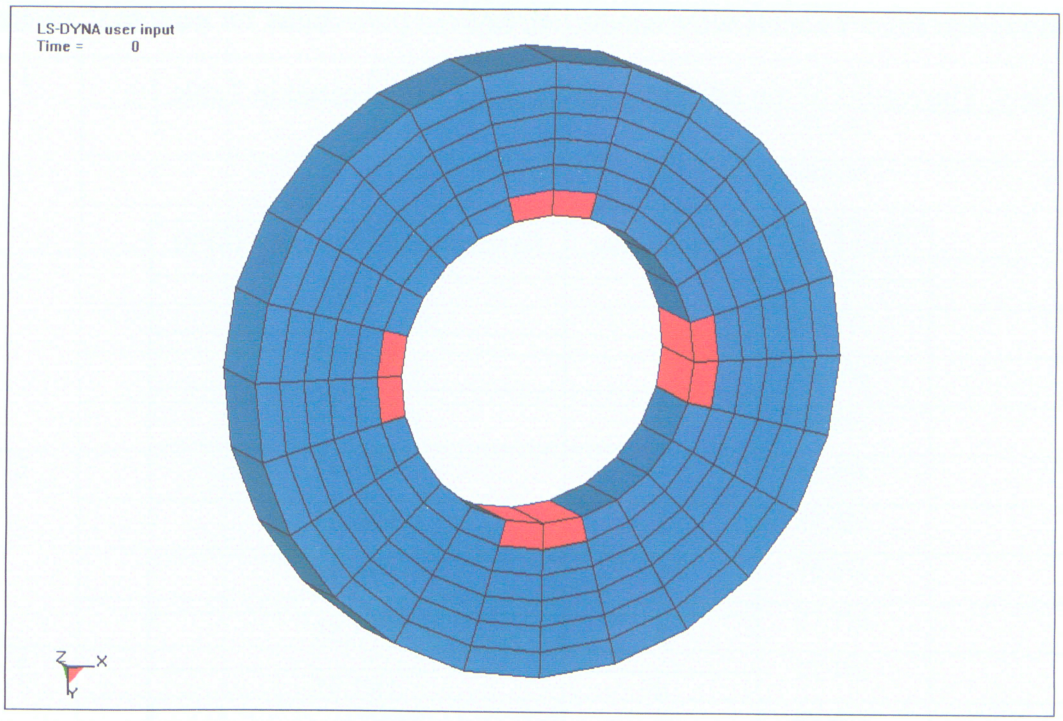

Figure 19: Elements Aligned With Global X and Y Axes

4.4 Validation Results

The maximum pressures recorded in the experimental test cases are shown in Table 8. Transducers 1, 2, 3, and 4 were located 75 mm, 150 mm, 225 mm, and 300 mm from the open end of the bone, respectively. In order to calibrate the equation of state of the fluid, the results of test case 1 were considered. In the finite element model representing the test case 1, the parameters of the equation of state were set to those that have been used to represent water [54]. The model was solved, and the stresses at the four locations were determined and compared to the experimental results. The equation of state parameters were altered until the computed stresses in the finite element model at the four locations were in reasonable agreement with the experimentally measured

pressures. A number of trials were conducted, and the parameters for each trial are listed in Table 9. The results of the calibration process are summarized in Table 10.

Test Case	Transducer	Experimental Pressure (kPa)
1	1	97.67
	2	124.55
	3	137.22
	4	153.35
2	1	126.65
	2	175.38
	3	177.55
	4	187.35
3	1	167.49
	2	194.22
	3	198.77
	4	213.48

Table 8: Experimental Test Case Results [49]

Trial	C Value (m/s)	S_1 Value	S_2 Value	S_3 Value	γ Value	a Value
1	1647	1.921	-0.096	0.0	0.35	0.0
2	164.7	1.921	-0.096	0.0	0.70	0.0
3	1947	1.921	-0.096	0.0	0.30	0.0
4	3947	1.921	-0.096	0.0	0.25	0.0
5	4947	1.921	-0.096	0.0	0.20	0.0
6	6500	1.921	-0.096	0.0	0.15	0.0
7	7500	1.921	-0.096	0.0	0.12	0.0
8	9000	1.920	0.0	0.0	0.15	0.0

Table 9: Equation of State Parameters Used in Calibration Trials

Trial	Location	Calculated Stress (kPa)	Percent Difference From Experimental
1	1	51.13	47.6%
	2	36.13	71.0%
	3	27.24	80.1%
	4	29.04	81.1%
2	1	11.55	88.2%
	2	48.67	96.1%
	3	18.66	98.6%
	4	0.36	99.8%
3	1	55.82	42.8%
	2	40.31	67.6%
	3	32.12	76.6%
	4	34.21	77.7%
4	1	77.03	21.1%
	2	63.03	49.4%
	3	61.68	55.1%
	4	73.17	52.3%
5	1	83.77	14.2%
	2	72.81	41.5%
	3	77.31	43.7%
	4	90.94	40.7%
6	1	92.79	5.0%
	2	91.10	26.9%
	3	94.19	31.4%
	4	104.17	32.1%
7	1	94.98	2.7%
	2	94.21	24.4%
	3	108.58	20.9%
	4	112.53	26.6%
8	1	100.75	3.2%
	2	104.64	16.0%
	3	118.15	13.9%
	4	120.98	21.1%

Table 10: Results of Equation of State Calibration

After the 8th trial, the difference between the calculated stresses and the experimentally measured pressures was deemed acceptable. The equation of state parameters used in the 8th trial were used in the finite element models for test case 2 and test case 3. These two test cases were solved, and, as with the first test case, the calculated stresses were compared to the experimental pressures. The results of all three test cases are summarized in Table 11, and the percent differences between the calculated stresses and experimental pressures for the three test cases are plotted in Figures 20 through 22.

Test Case	Location	Calculated Stress (kPa)	Percent Difference From Experimental
1	1	100.75	3.2%
	2	104.64	16.0%
	3	118.15	13.9%
	4	120.98	21.1%
2	1	121.04	4.4%
	2	130.75	25.5%
	3	140.88	20.7%
	4	159.17	15.0%
3	1	136.81	18.3%
	2	137.54	29.2%
	3	164.44	17.3%
	4	172.74	19.1%

Table 11: Validation Results

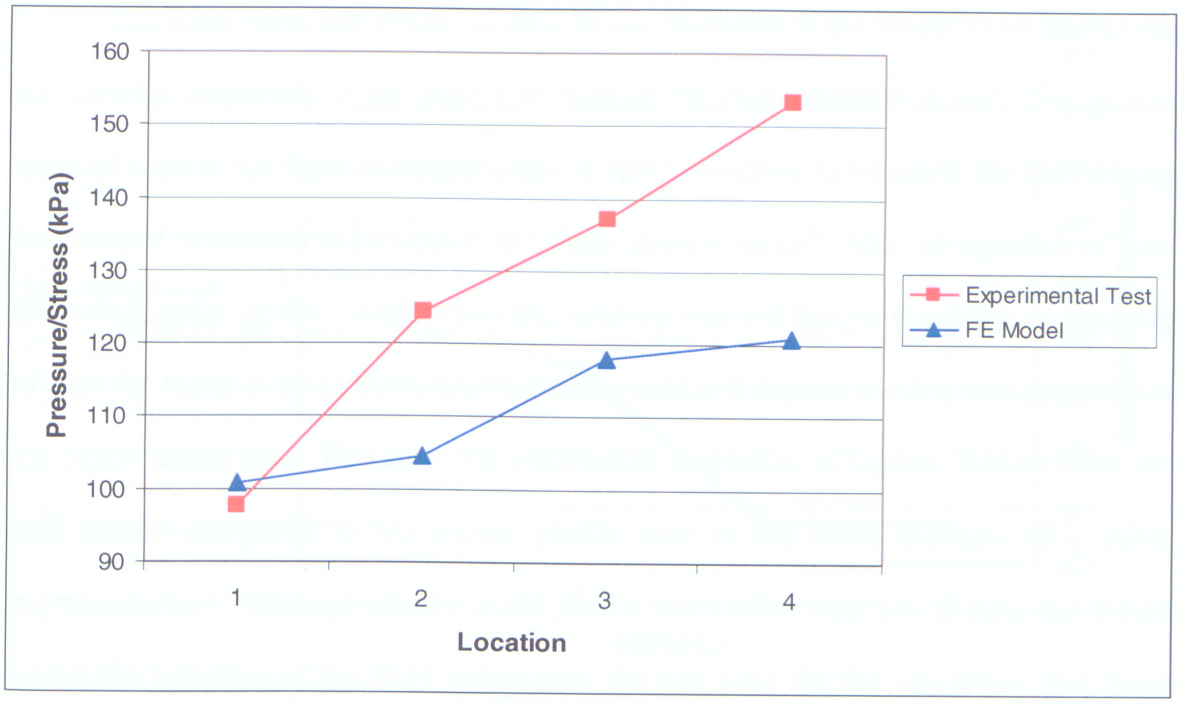

Figure 20: Results of Test Case 1

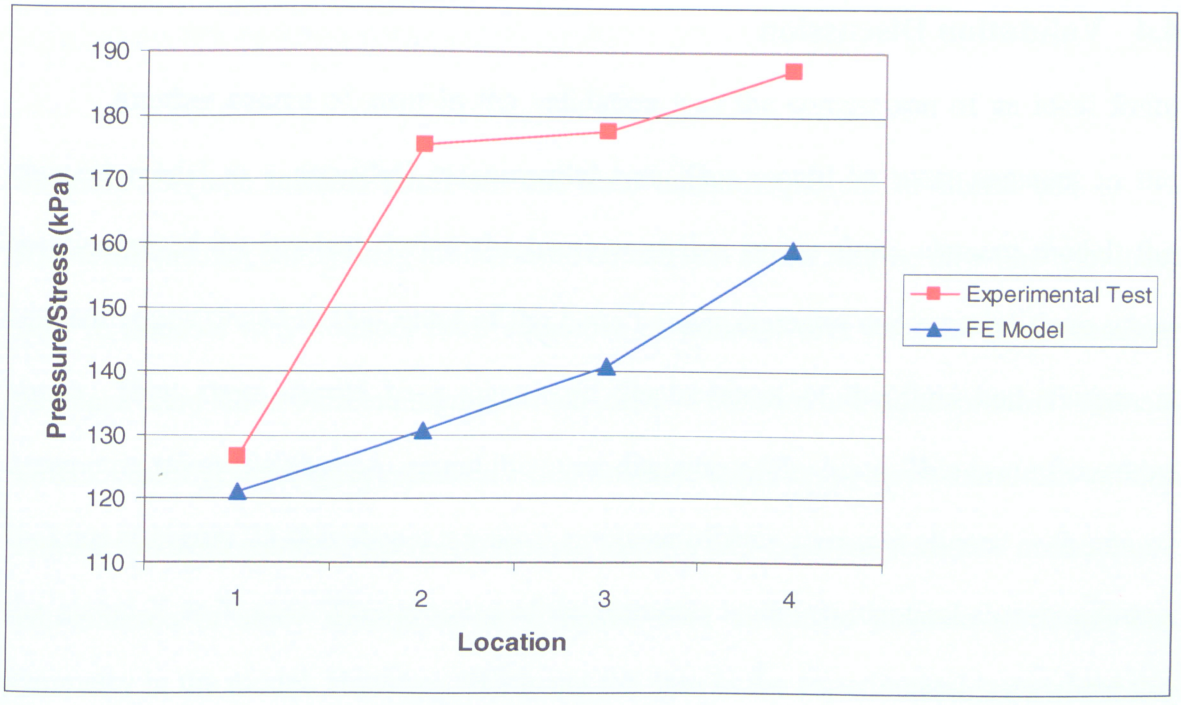

Figure 21: Results of Test Case 2

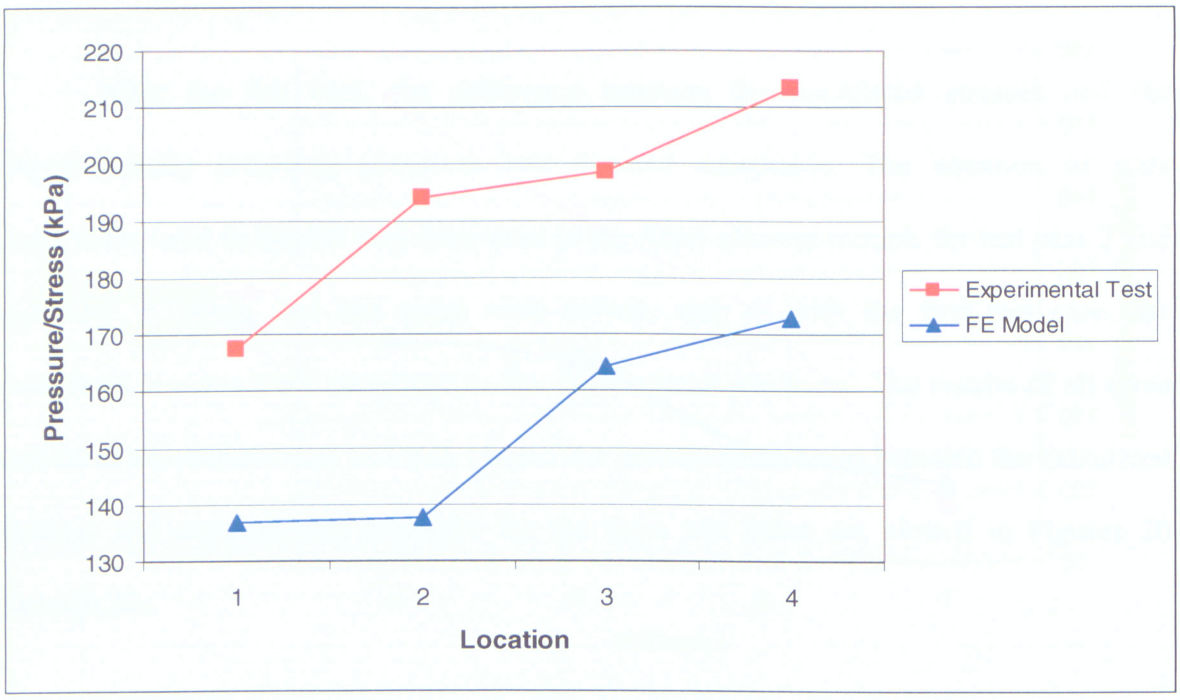

Figure 22: Results of Test Case 3

4.4 Validation Discussion

The results of the experimental tests and the finite element analyses compare relatively well with several trends that can be observed. In general, the percent difference increases from location 1 to location 2, decreases from location 2 to location 3, then increases from location 3 to location 4. Also, the maximum pressure in the bone analogue and the maximum stress in the finite element model increases progressively from location 1 to location 4 in each test case. The average percent difference between the experimental and the finite element results is 17% which is an acceptable value to consider the validation a success.

The most important source of error in the validation is the assumptions made with the material properties of the bone and fluid in the finite element model. The custom material used in the bone analogue required approximations to be made for determining the material properties to be used in the finite element model. Also, an equation of state for bone marrow or the Vaseline/paraffin mixture was not known requiring an equation of state for water to be calibrated until it had a similar behavior to what was observed in the experimental tests. However, the mechanical properties of human cortical bone are well known compared to the porous plastic used in the bone analogue [55]. Also, experimentation with bone marrow could yield a much better equation of state that would model the behavior of the fluid better than the one used for the validation. For these reasons, it is expected that a finite element model would compare well with experimental tests on cadaveric bone and real bone marrow.

Another source of error in the validation was the comparison of an ideal finite element model to a non-ideal experimental test. This would be most apparent in the positioning of the implant during the hammer strike. In the finite element model, the implant is positioned in the center of the bone's inner diameter and remains there when struck. Thus, there should be a symmetric displacement of the fluid and, further, a symmetric stress distribution around the inner diameter of the bone. This is confirmed by looking at Figure 23 that shows a typical response of four elements aligned with one of the global X or Y axes. The response of the elements is almost identical showing strong symmetry in the model. However, this is not the case in the experimental tests where the implant is not centered in the bone analogue's inner diameter when it is struck. This may

have led to an asymmetric pressure distribution around the inner diameter of the bone analogue. Consequently, the pressure recorded by the transducer may not have been the maximum pressure encountered at the particular location in the bone analogue. However, because there was only one pressure transducer at each location in the bone analogue, this cannot be verified or rejected. It should also be noted that the negative stress shown in the elements in Figure 23 is what would be expected for elements under compression.

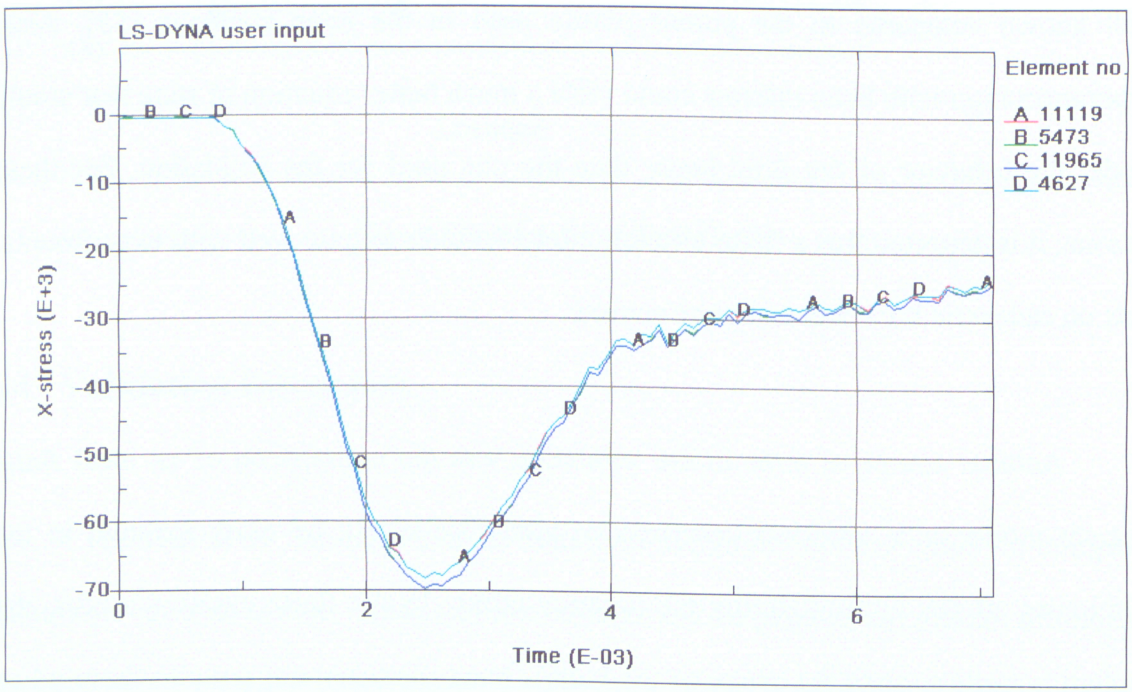

Figure 23: Stress versus Time for 4 Elements Aligned With Global X Axis

CHAPTER 5

PARAMETRIC STUDY

5.1 Parametric Study Overview

When the validation had been completed and the finite element models deemed acceptable to use for comparative tests, a parametric study was conducted on a potential orthopaedic implant design feature. There are a number of studies in the literature that have investigated using hollow instruments during the preparation phase of orthopaedic surgeries in an attempt to decrease intramedullary pressure. Hollow awls, rasps and reamers have been tested and demonstrated to reduce intramedullary pressure compared to solid instruments. However, no studies were found in the literature that investigate the use of hollow implants to reduce the intramedullary pressure when they are hammered into the intramedullary canal. As such, the parametric study will look at the potential of hollow intramedullary implants to reduce intramedullary pressure. With all other factors being held constant, the variable of the study will be the inner diameter of the implant. The study will include tests on implants with a variety of tip geometries that represent hip and knee prostheses rather than intramedullary nails.

5.2 Parametric Study Approach

As was the case with the validation, the macro was used to create a number of finite element models for the parametric study. The dimensions used for the bone were very similar to those used in the validation models. The material model for the bone was specified as isotropic and the material properties of human cortical bone were used [54]. The fluid was given the same material properties that were used in the validation models, including the parameters of the calibrated equation of state.

Four different implant tip shapes were tested in the parametric study. The tip shapes will be referred to as flat, funnel, round, and tapered. Cross-sections of the tip shapes and the meshed geometries are shown in Figures 24 through 27. For each of the four different implant tip shapes that were used in the study, five finite element models were created where the implant was given various inner diameters. The inner diameters that were tested are 0 mm (solid implant), 2 mm, 4 mm, 6 mm and 8 mm. The implants were given an outer diameter that was 0.25 mm larger than the inner diameter of the bone, unlike the validation models where there was a gap between the implant and the bone. This is to simulate the press fit insertion of a prosthetic implant where no fluid would be able to escape between the implant and the bone. Although the outer diameter of the implant is larger than the inner diameter of the bone, there is no contact defined between the two parts and, therefore, no frictional losses when the implant is hammered into the bone.

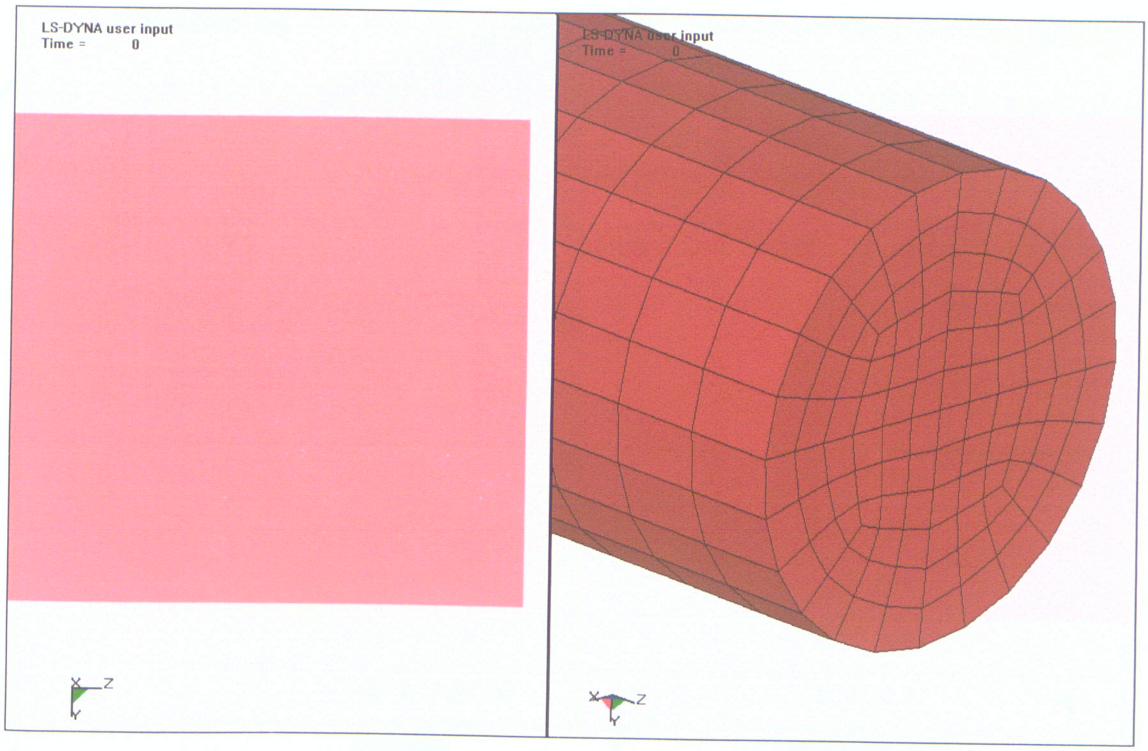

Figure 24: Cross-Section and Meshed View of Flat-Tipped Implant

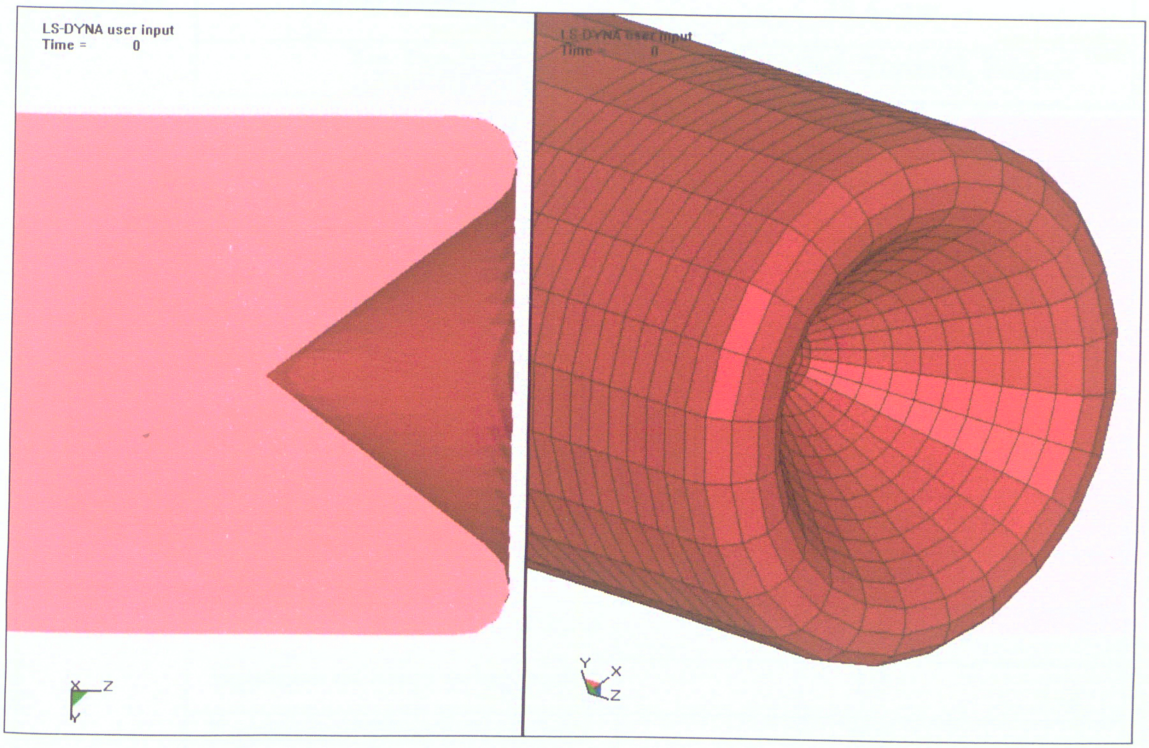

Figure 25: Cross-Section and Meshed View of Funnel-Tipped Implant

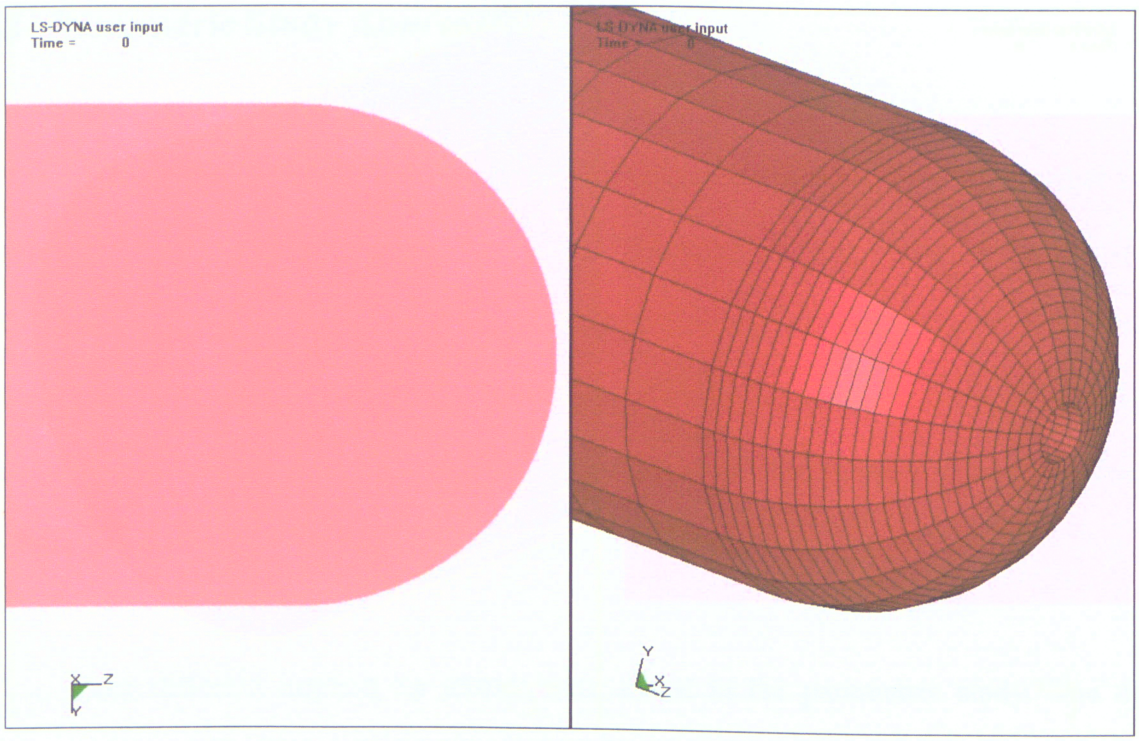

Figure 26: Cross-Section and Meshed View of Round-Tipped Implant

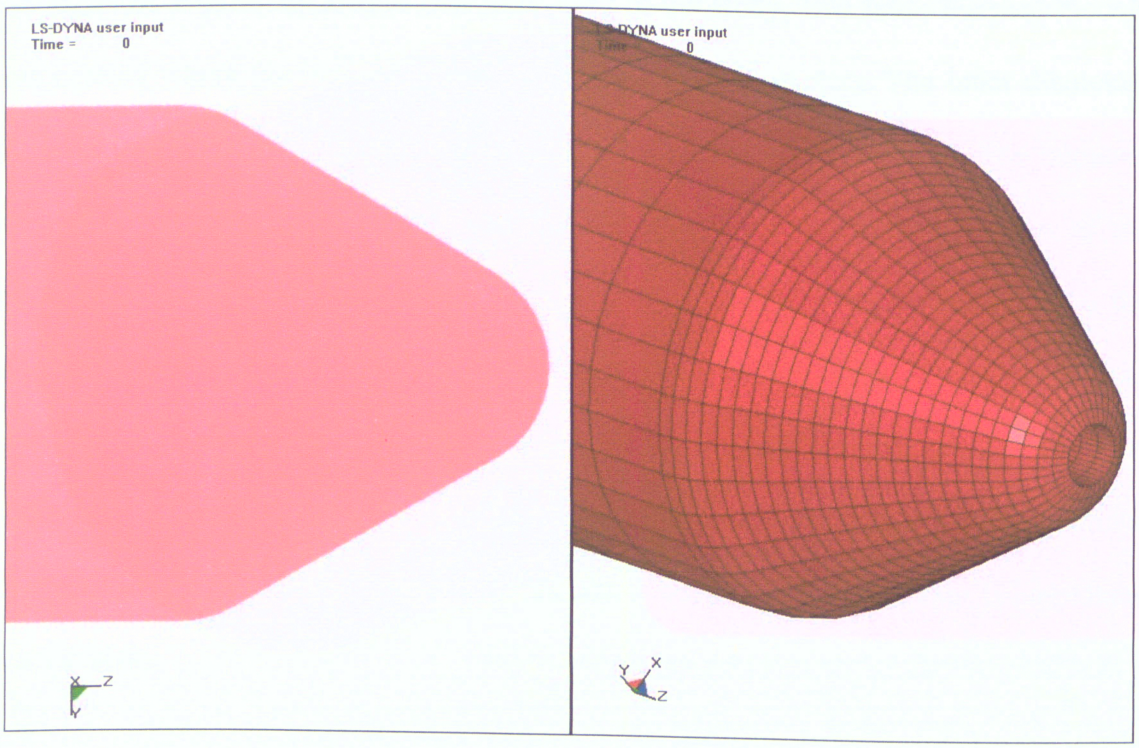

Figure 27: Cross-Section and Meshed View of Tapered-Tipped Implant

In determining the material properties that should be used for the implant, a Zimmer ZMR Hip System Femoral Stem was obtained (Figure 28). The mass of the Zimmer implant was measured and the material properties of the Ti-6Al-4V alloy it was made of were used. A summary of the geometry and material properties used in the parametric study models is given in Table 12.

Part	Material Property	Value
Bone	Inner Diameter	15.25 mm
	Outer Diameter	35 mm
	Inner Length	350 mm
	Outer Length	370 mm
	Density	1950.0 kg/m^3
	Elastic Modulus	11.5 GPa
	Poisson's Ratio	0.31
Implant	Outer Diameter	15.5 mm
	Tip Types	Flat, Round, Tapered, Funnel
	Inner Diameters	0.0, 2.0, 4.0, 6.0, 8.0 mm
	Mass	120.0 g
	Elastic Modulus	114.0 GPa
	Poisson's Ratio	0.33
Fluid	Density	861.5 kg/m^3
	Viscosity	0.0826 Ns/m^2
	Equation of State C Parameter	9000 m/s
	Equation of State S_1 Parameter	1.920
	Equation of State S_2 Parameter	0.0
	Equation of State S_3 Parameter	0.0
	Equation of State γ Parameter	1.5
	Equation of State a Parameter	0.0

Table 12: Geometry and Material Properties of Parametric Study Models

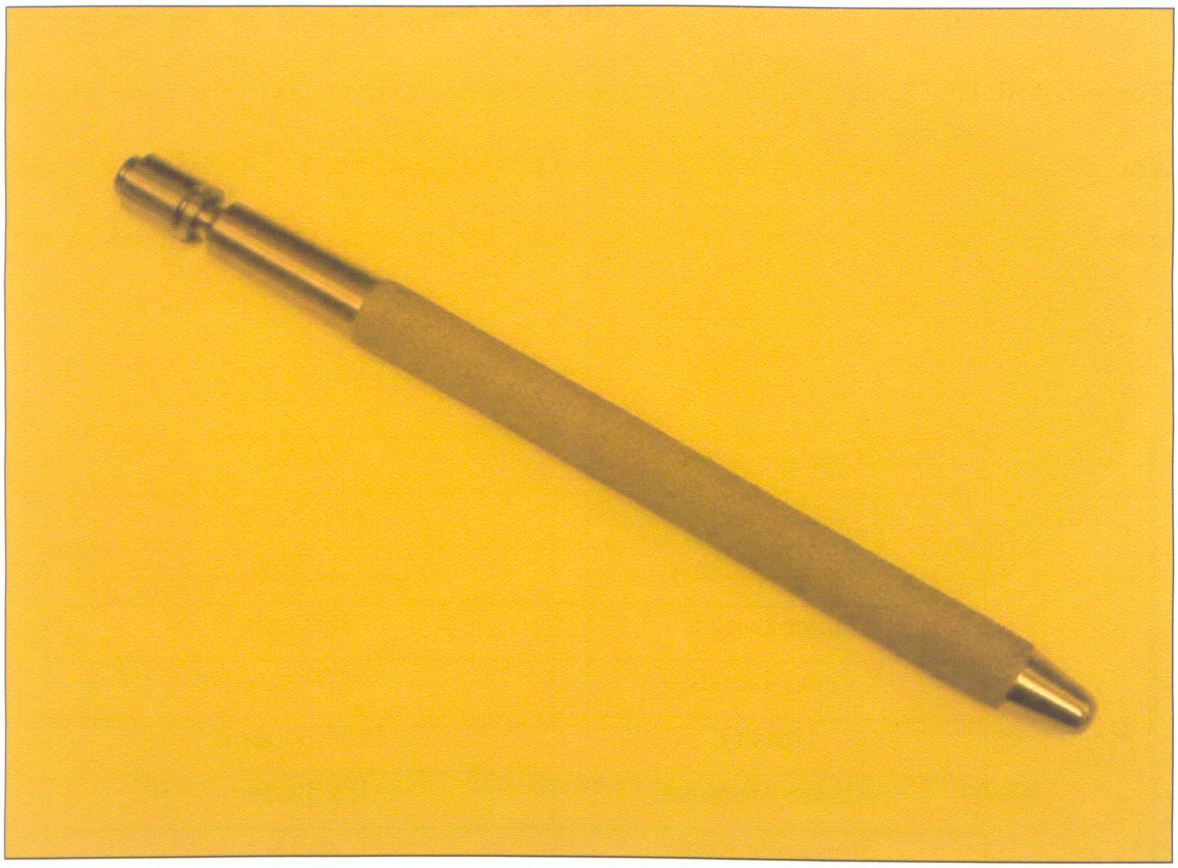

Figure 28: Zimmer ZMR Hip System Femoral Stem

A force versus time curve was applied to the implant with a maximum force of approximately 115 N, similar to one used in the validation models (Figure 29). As with the validation models, the maximum stresses at four locations along the length of the bone were computed and compared between the various models in the parametric study. Locations 1, 2, 3 and 4 where the stress was computed in the bone were 87.5 mm, 175.0 mm, 262.5 mm and 350.0 mm from the open end of the bone, respectively (Figure 30). Also, in common with the validation models, the maximum stresses at the locations were determined by averaging the maximum normal stresses of the eight elements aligned with the global X and Y axes.

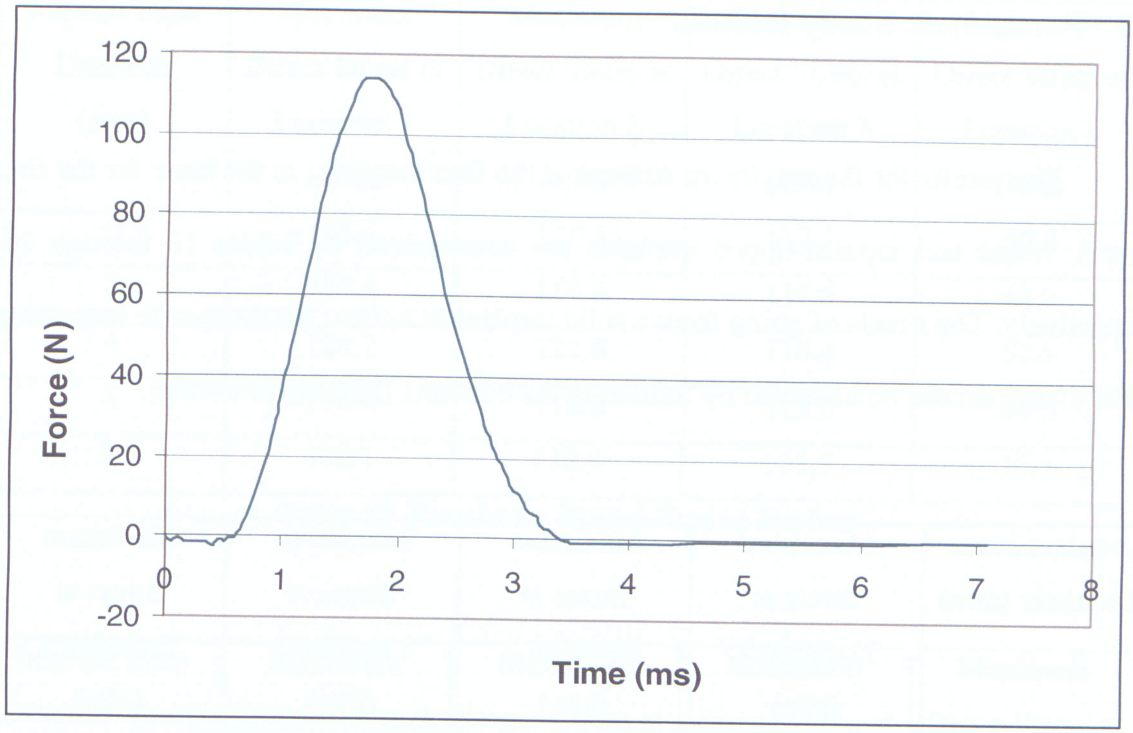

Figure 29: Force versus Time Curve for Parametric Study Models

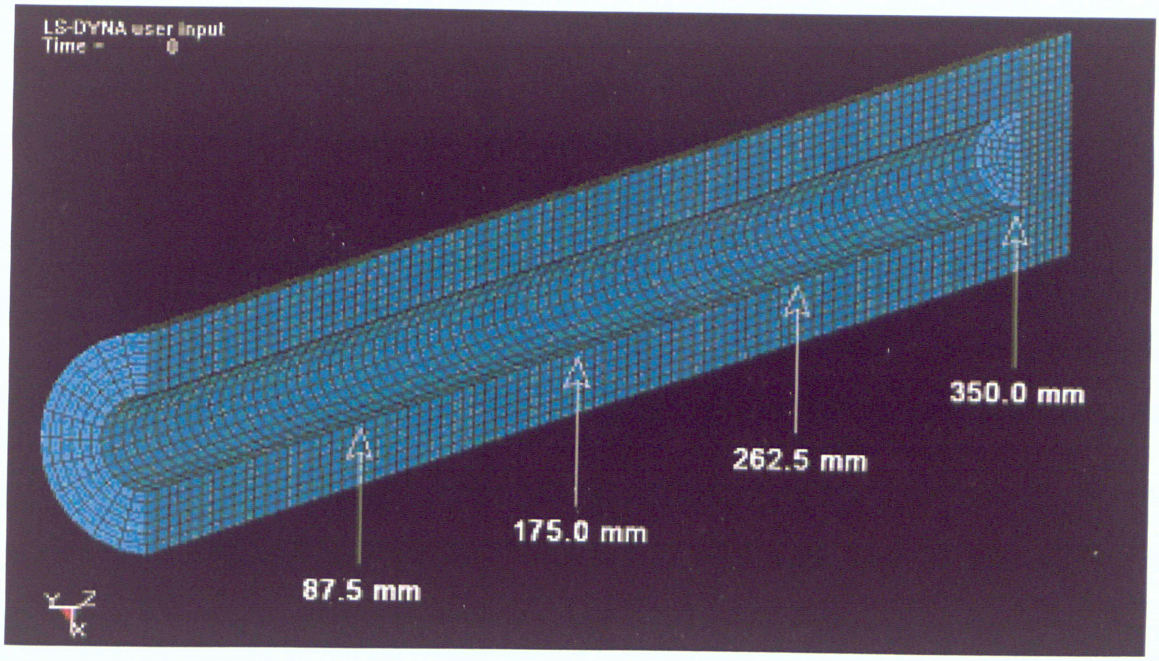

Figure 30: Locations in Bone for Stress Computation

5.3 Parametric Study Results

The results for the maximum stresses at the four locations in the bone for the flat, funnel, round and tapered-tipped implants are summarized in Tables 13 through 16, respectively. The trends of going from a solid implant to hollow implants with increasing inner diameters can be observed by following the columns from top to bottom.

Implant Inner Diameter (mm)	Maximum Stress at Location 1 (kPa)	Maximum Stress at Location 2 (kPa)	Maximum Stress at Location 3 (kPa)	Maximum Stress at Location 4 (kPa)
0	137.9	139.0	127.7	60.4
2	138.6	138.5	126.4	65.9
4	135.6	129.2	124.7	60.6
6	129.7	123.1	118.2	45.2
8	107.9	106.7	101.3	58.1

Table 13: Results for Flat-Tipped Implant

Implant Inner Diameter (mm)	Maximum Stress at Location 1 (kPa)	Maximum Stress at Location 2 (kPa)	Maximum Stress at Location 3 (kPa)	Maximum Direct at Location 4 (kPa)
0	147.4	126.2	122.7	59.6
2	150.2	134.6	132.2	59.4
4	143.2	126.1	122.7	59.6
6	140.5	128.6	123.8	55.7
8	121.9	101.1	96.3	66.2

Table 14: Results for Funnel-Tipped Implant

Implant Inner Diameter (mm)	Maximum Direct Stress at Location 1 (kPa)	Maximum Direct Stress at Location 2 (kPa)	Maximum Direct Stress at Location 3 (kPa)	Maximum Direct Stress at Location 4 (kPa)
0	125.1	120.3	117.1	50.8
2	124.6	119.8	116.5	46.9
4	126.2	122.4	116.4	52.1
6	114.4	116.6	113.0	44.3
8	102.3	110.9	105.5	39.1

Table 15: Results for Round-Tipped Implant

Implant Inner Diameter (mm)	Maximum Direct Stress at Location 1 (kPa)	Maximum Direct Stress at Location 2 (kPa)	Maximum Direct Stress at Location 3 (kPa)	Maximum Direct Stress at Location 4 (kPa)
0	163.5	131.3	127.9	51.5
2	159.7	130.3	129.3	53.7
4	148.3	126.8	122.7	66.0
6	137.3	119.9	114.5	58.6
8	120.4	100.2	103.1	61.2

Table 16: Results for Tapered-Tipped Implant

The maximum stress versus implant inner diameter for the four locations in the flat-tipped implant analysis, funnel-tipped implant analysis, round-tipped implant analysis and tapered-tipped implant analysis is plotted in Figures 31 through 34, 35 through 38, 39 through 42 and 43 through 46, respectively. These plots clearly illustrate the effects of going from a solid implant to hollow implants with progressively larger inner diameters.

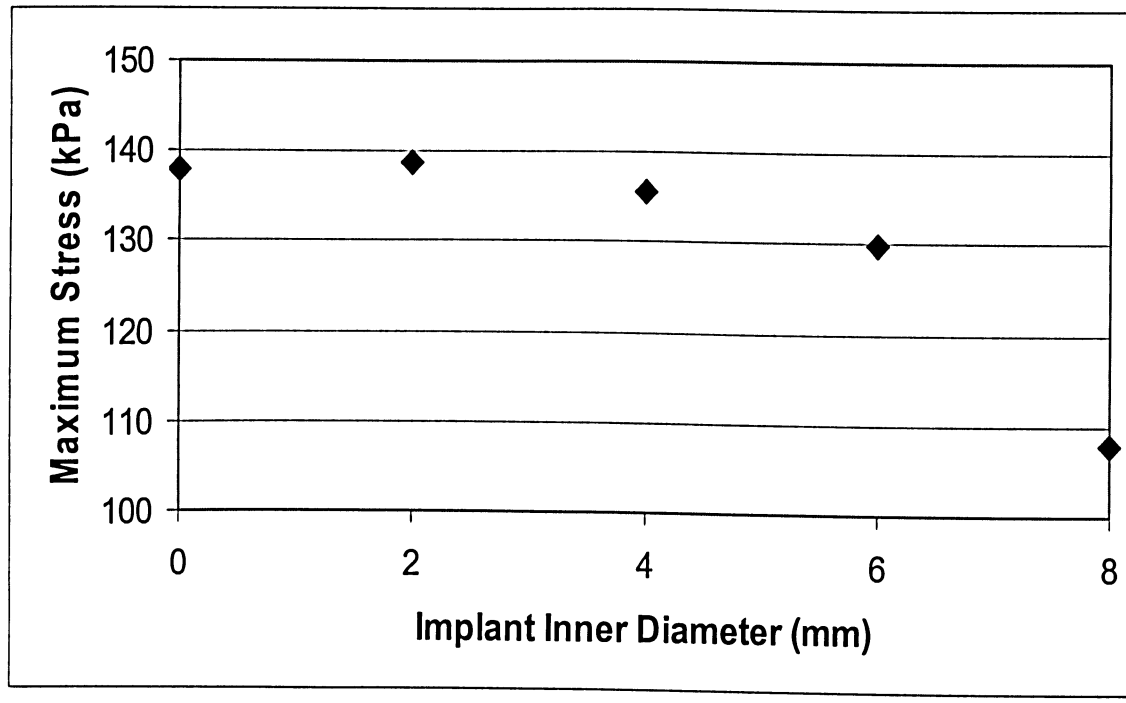

Figure 31: Flat-Tipped Implant, Location 1

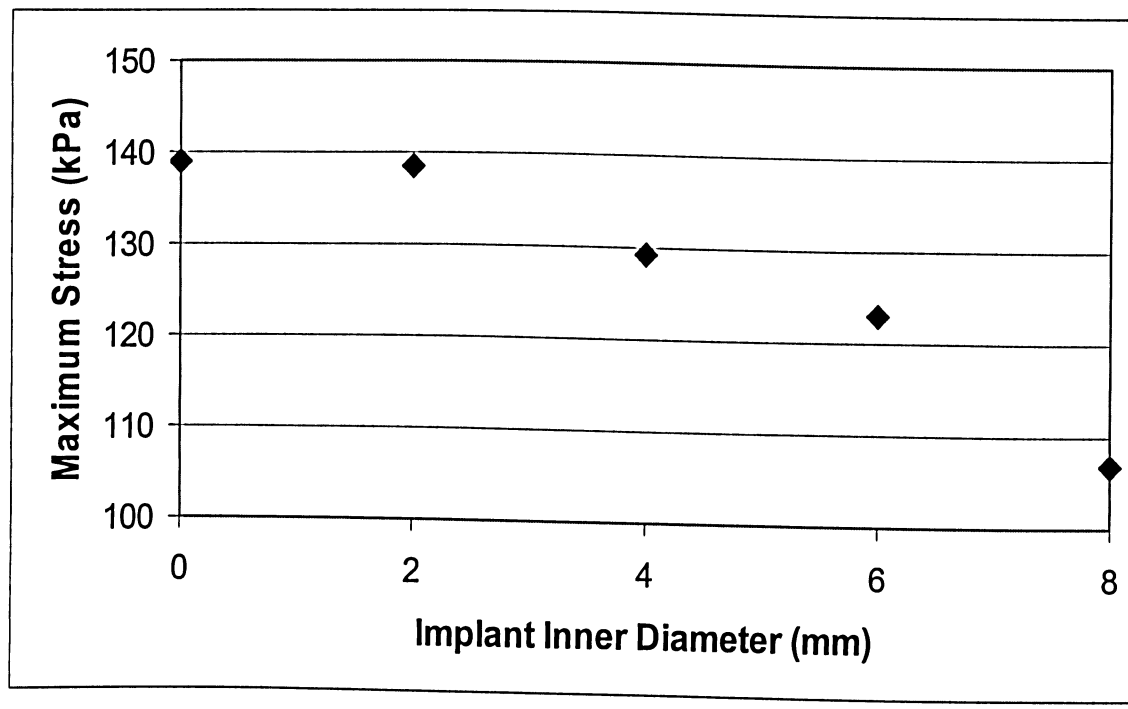

Figure 32: Flat-Tipped Implant, Location 2

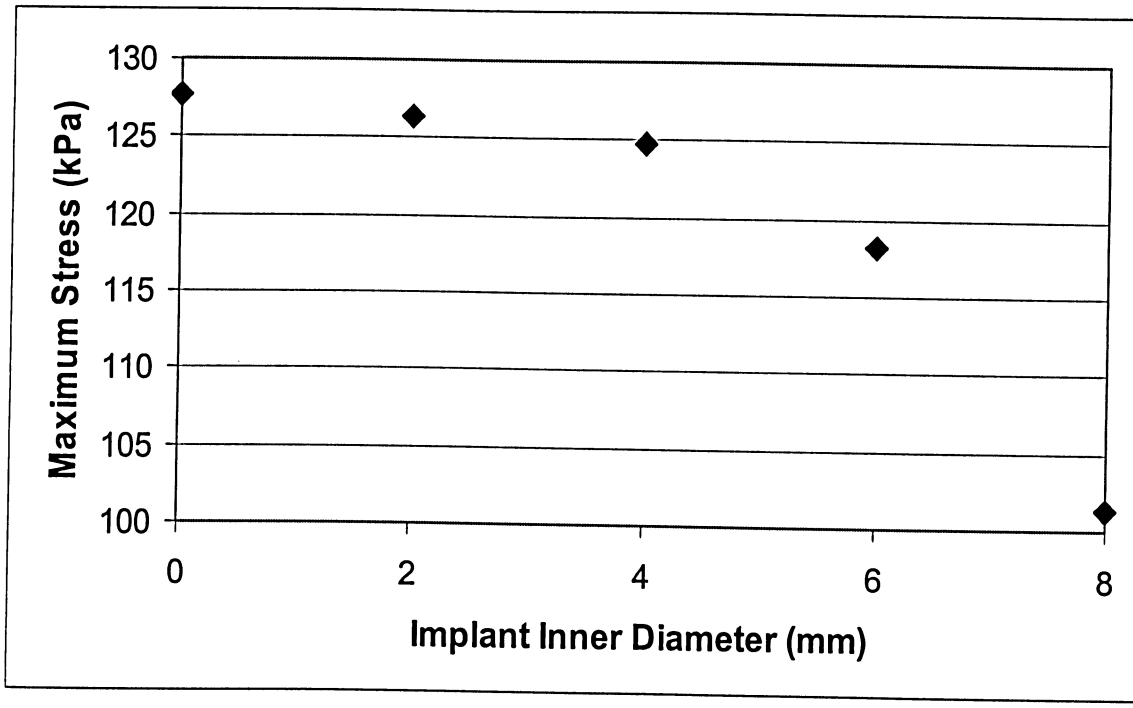

Figure 33: Flat-Tipped Implant, Location 3

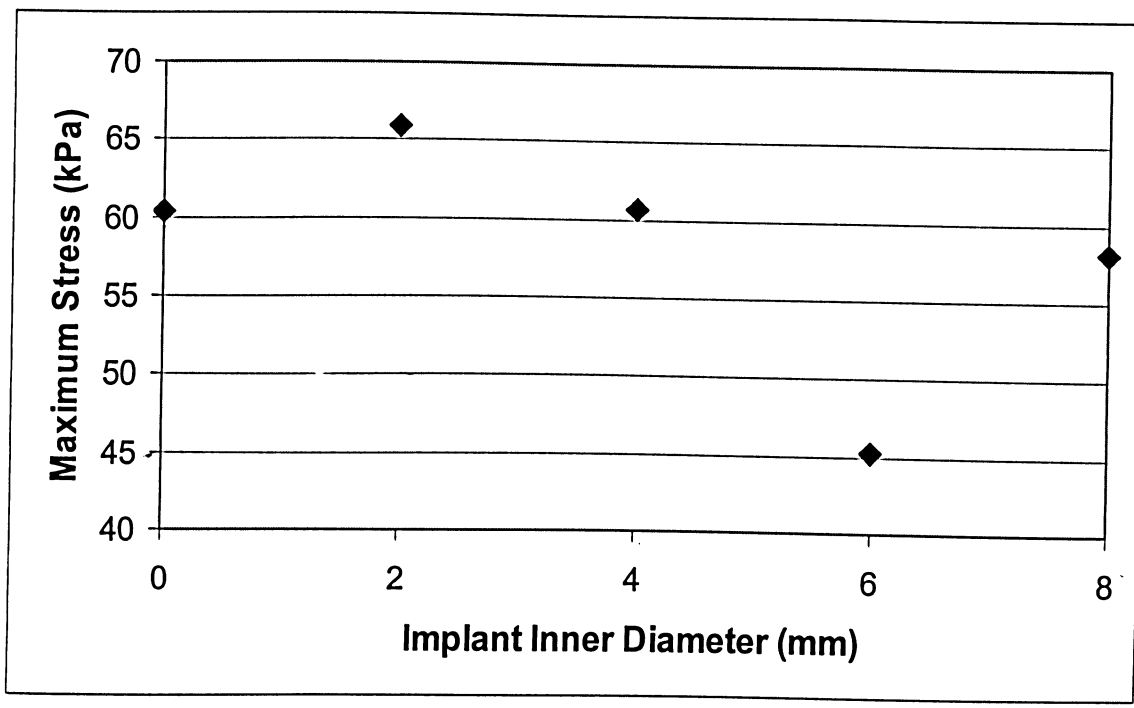

Figure 34: Flat-Tipped Implant, Location 4

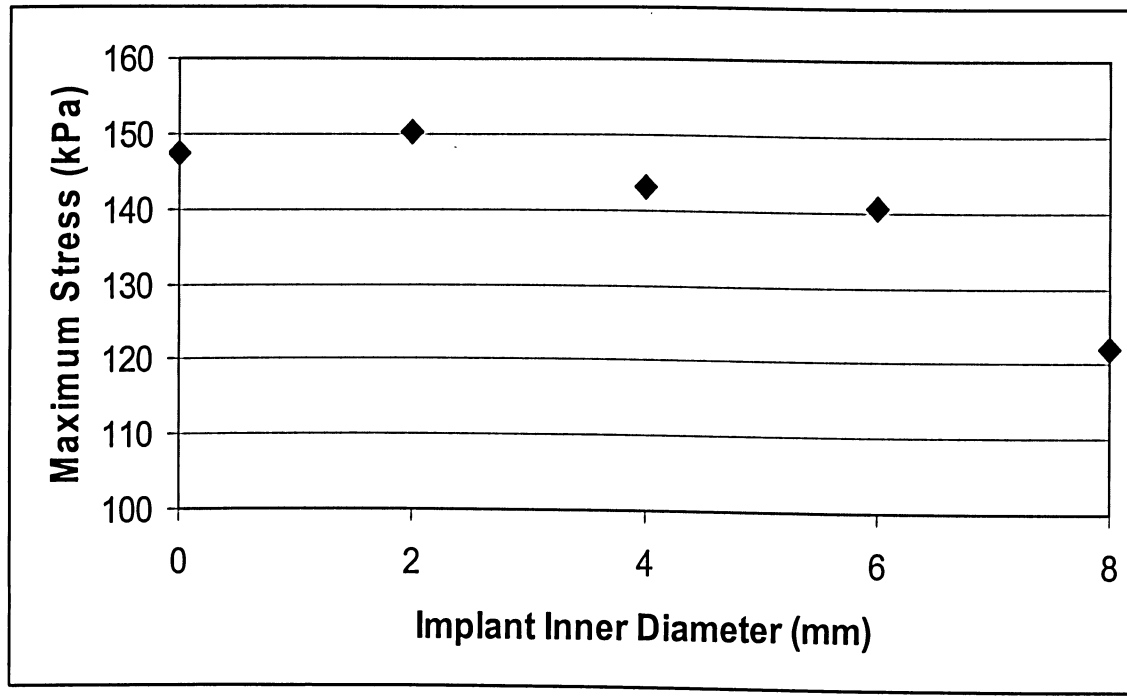

Figure 35: Funnel-Tipped Implant, Location 1

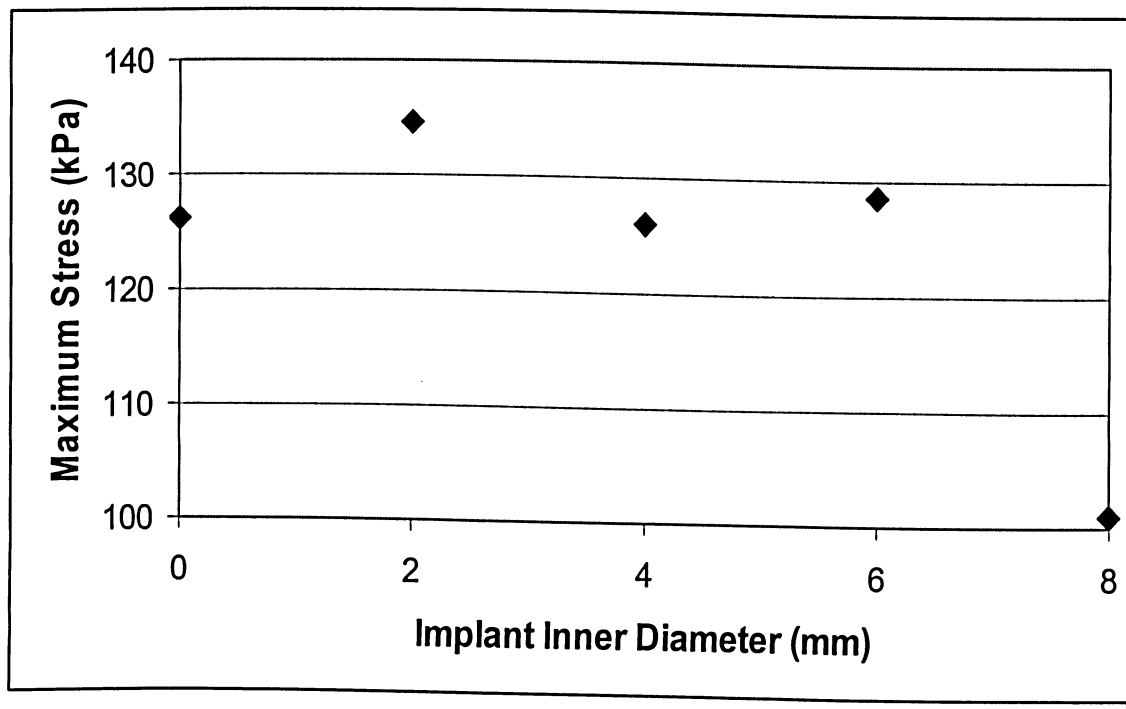

Figure 36: Funnel-Tipped Implant, Location 2

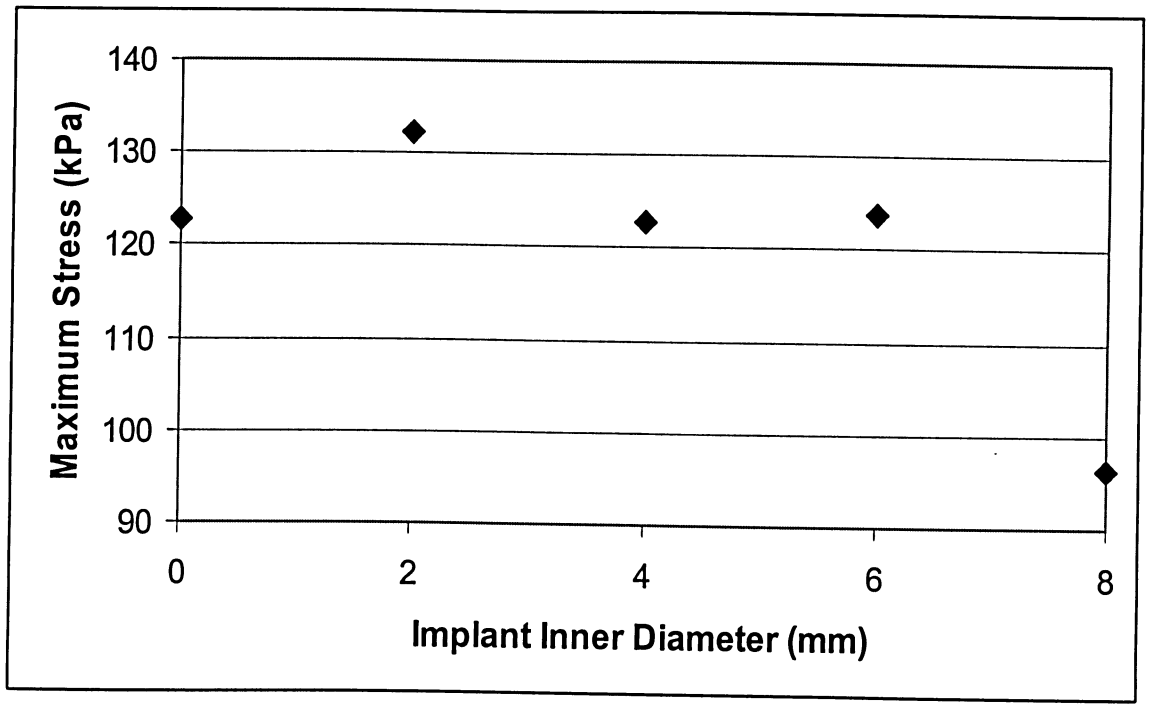

Figure 37: Funnel-Tipped Implant, Location 3

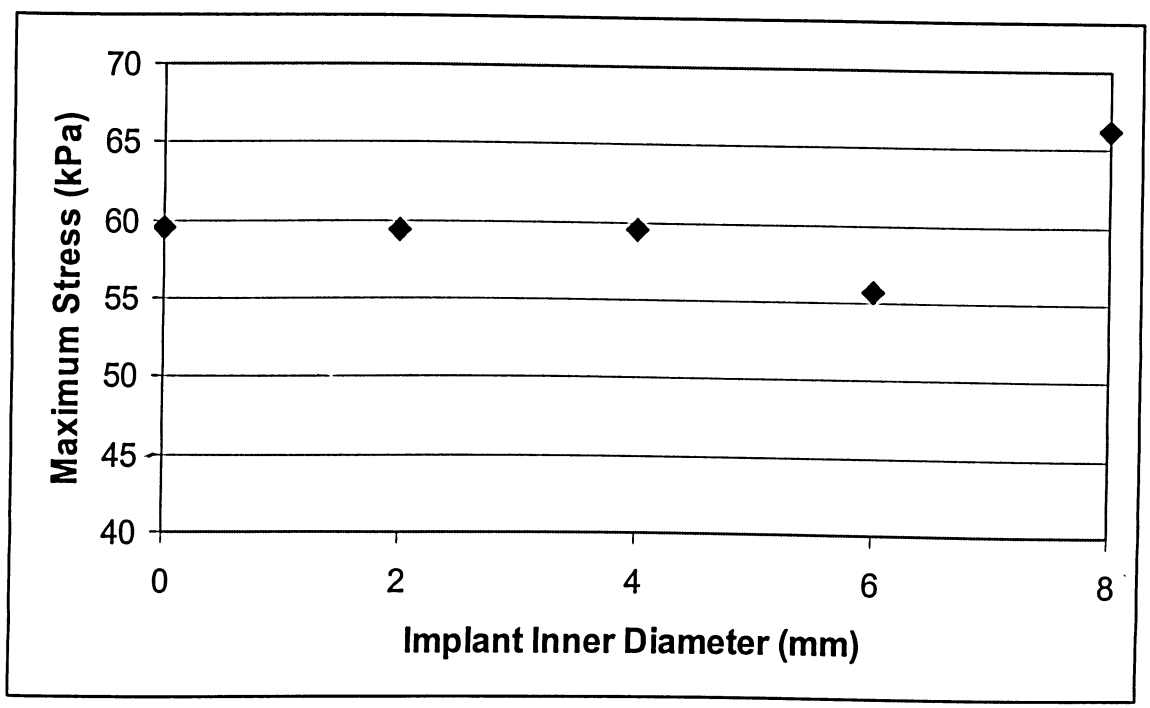

Figure 38: Funnel-Tipped Implant, Location 4

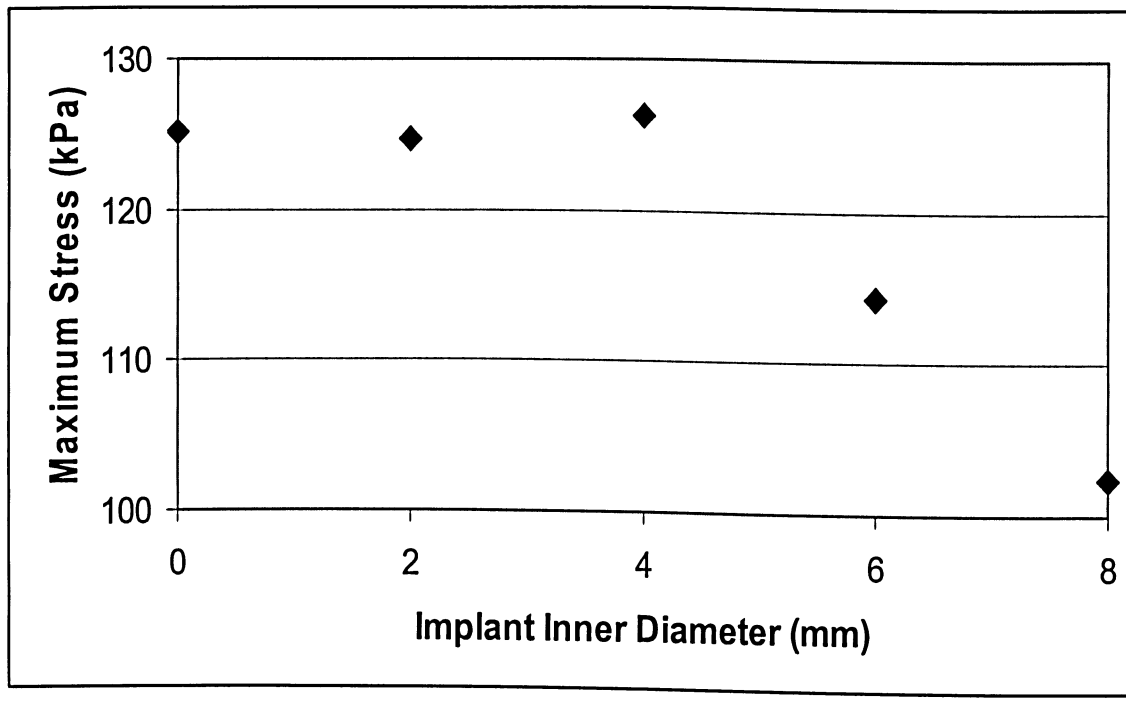

Figure 39: Round-Tipped Implant, Location 1

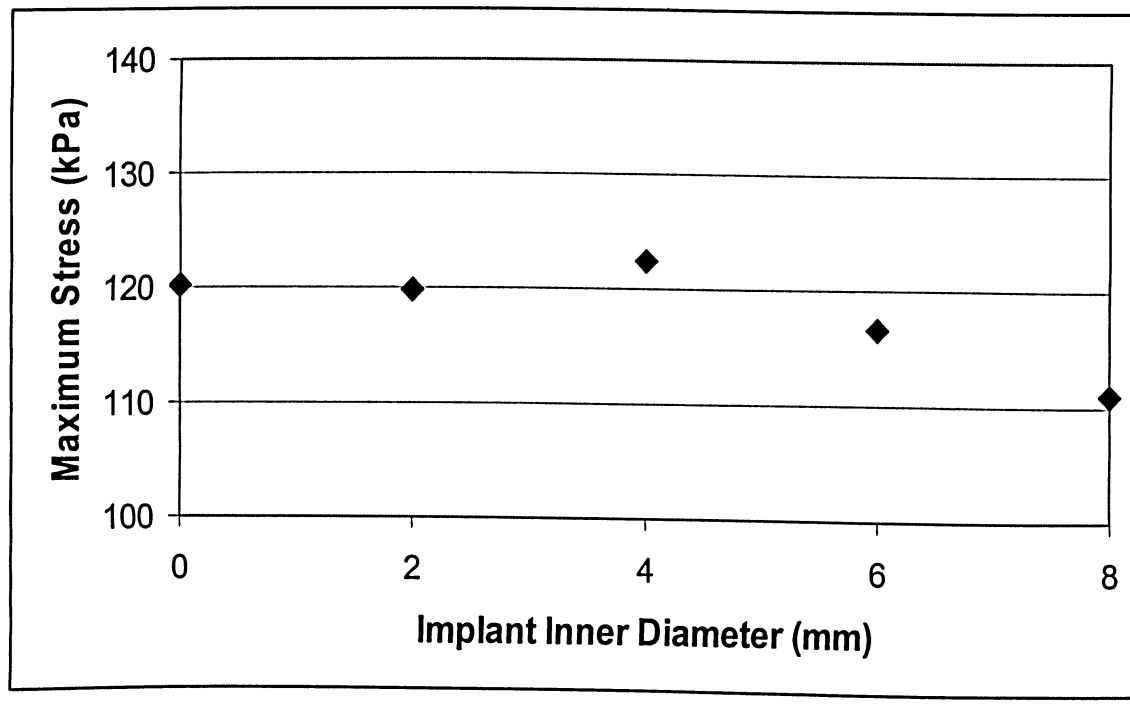

Figure 40: Round-Tipped Implant, Location 2

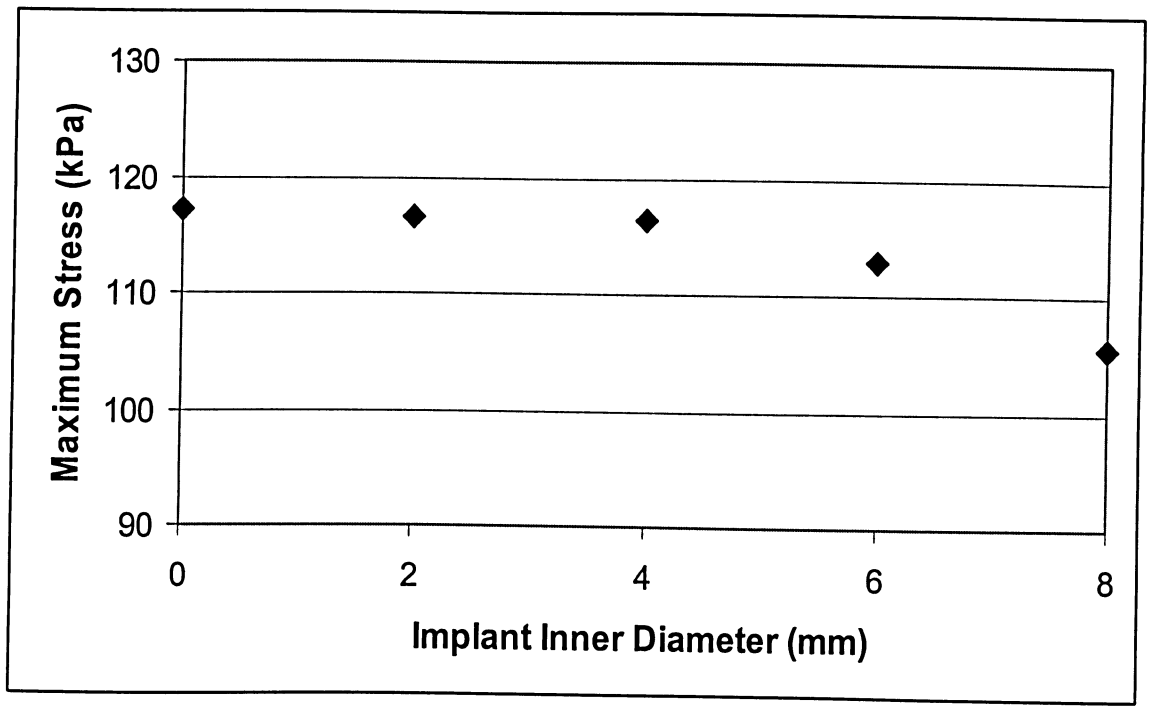

Figure 41: Round-Tipped Implant, Location 3

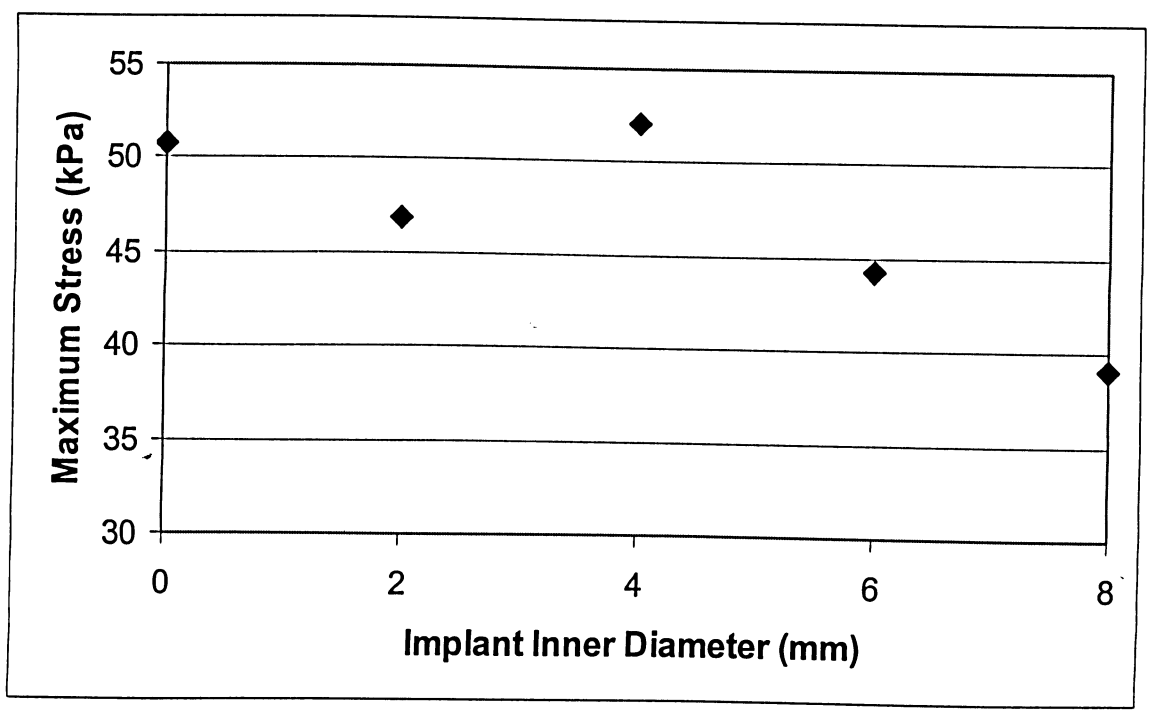

Figure 42: Round-Tipped Implant, Location 4

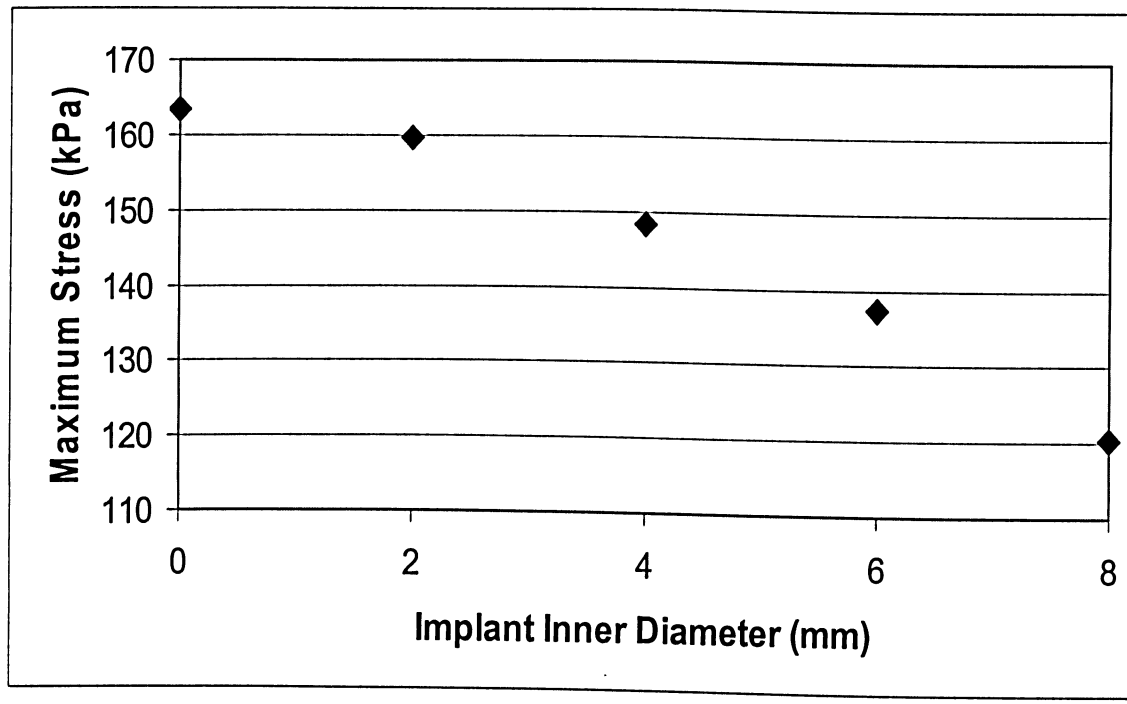

Figure 43: Tapered-Tipped Implant, Location 1

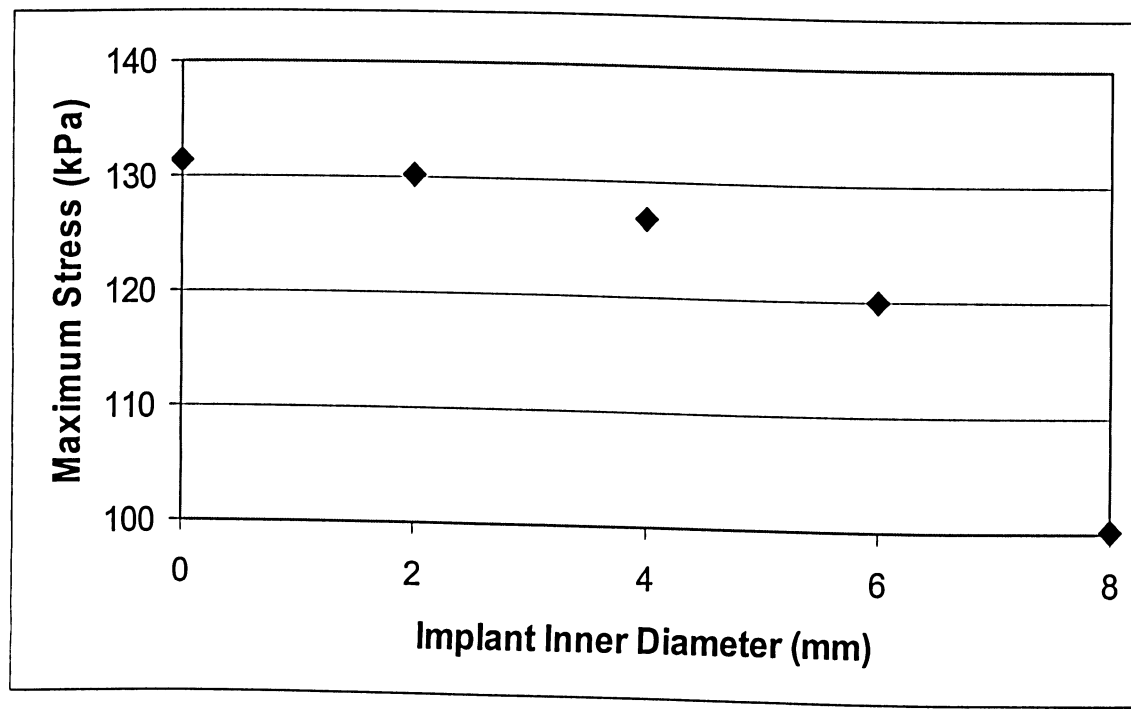

Figure 44: Tapered-Tipped Implant, Location 2

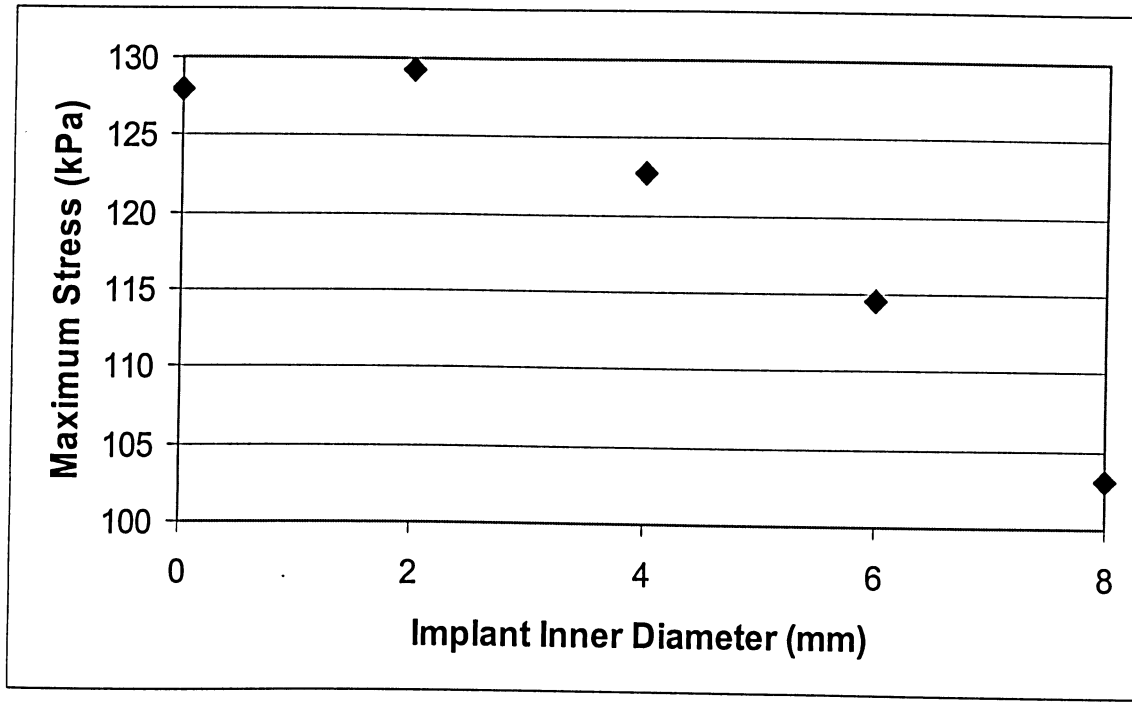

Figure 45: Tapered-Tipped Implant, Location 3

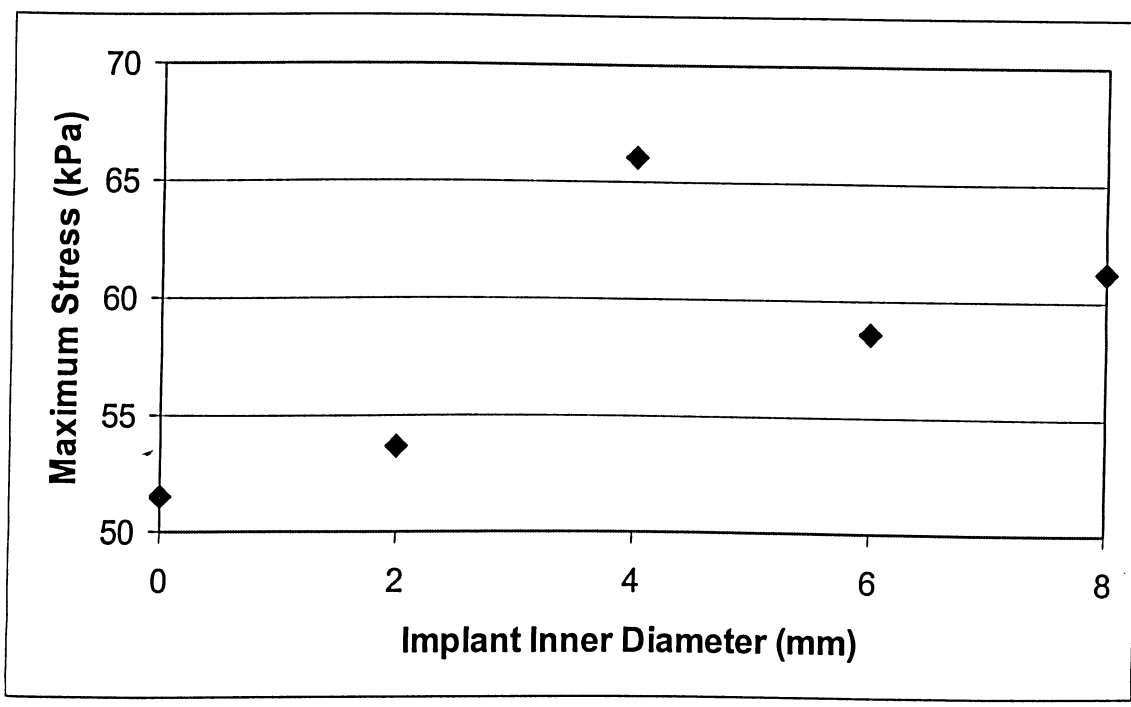

Figure 46: Tapered-Tipped Implant, Location 4

To explain the trends of the results, it is useful to look at how the fluid behaves as a result of the implant being hammered into it. To do this, the models were post processed in LS-PREPOST and all the parts except for the fluid were hidden. The end of the fluid that was impacted by the implant was isolated and the behavior of the fluid at the end of the analysis time was displayed. Examples of the fluid displacement during the analysis for the four different inner diameters of the flat-tipped implant are shown in Figures 47 through 50. The images are clear indications of the effectiveness of the various hollow implants at allowing the fluid to escape. Although not shown, the fluid behavior in the funnel-tipped, round-tipped and tapered-tipped analyses are similar to the behavior of the fluid in the flat-tipped analysis.

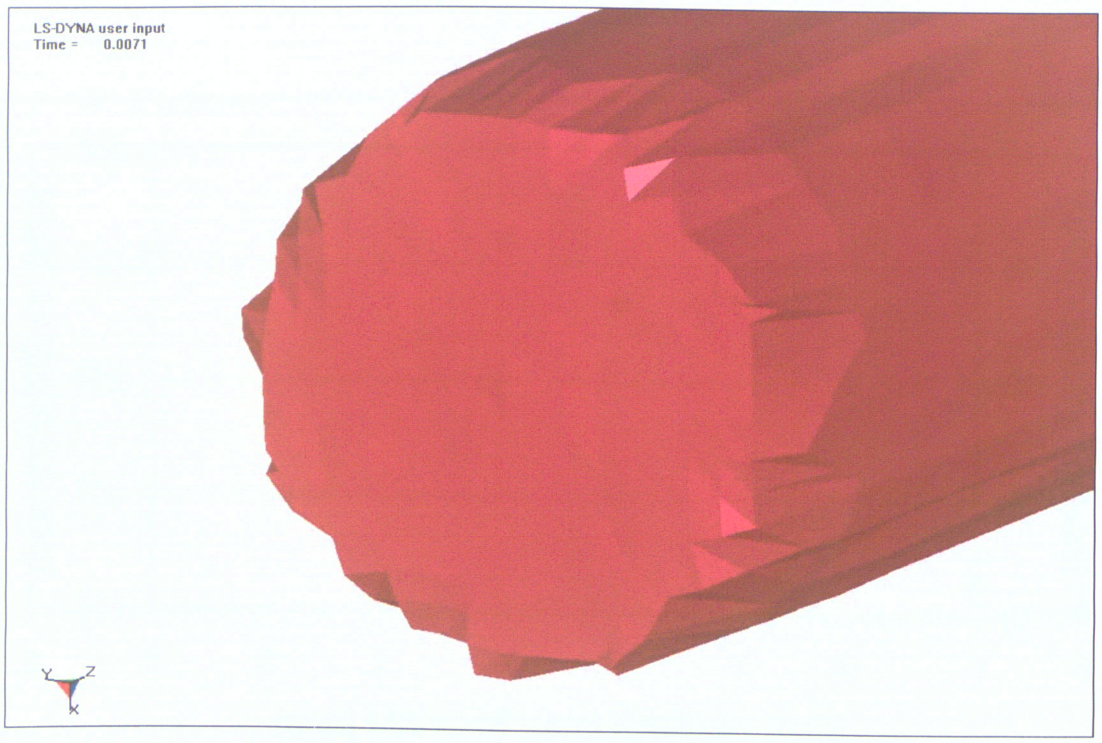

Figure 47: Fluid Displacement, Flat-Tipped Implant, 2 mm Inner Diameter

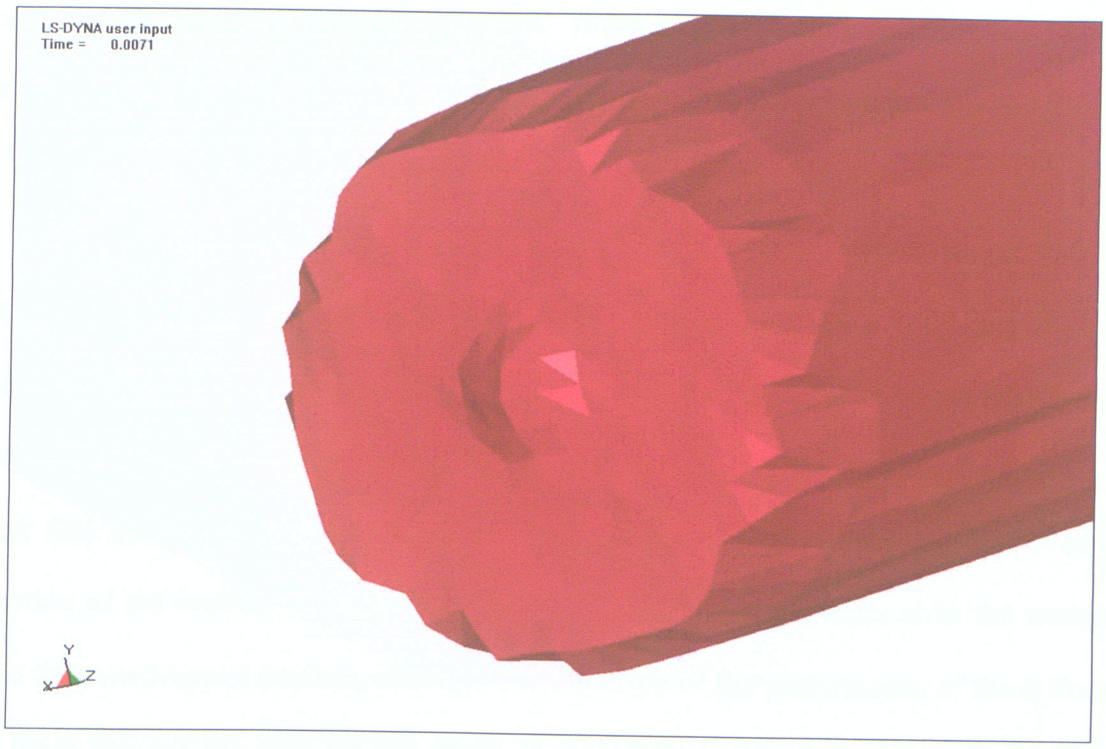

Figure 48: Fluid Displacement, Flat-Tipped Implant, 4 mm Inner Diameter

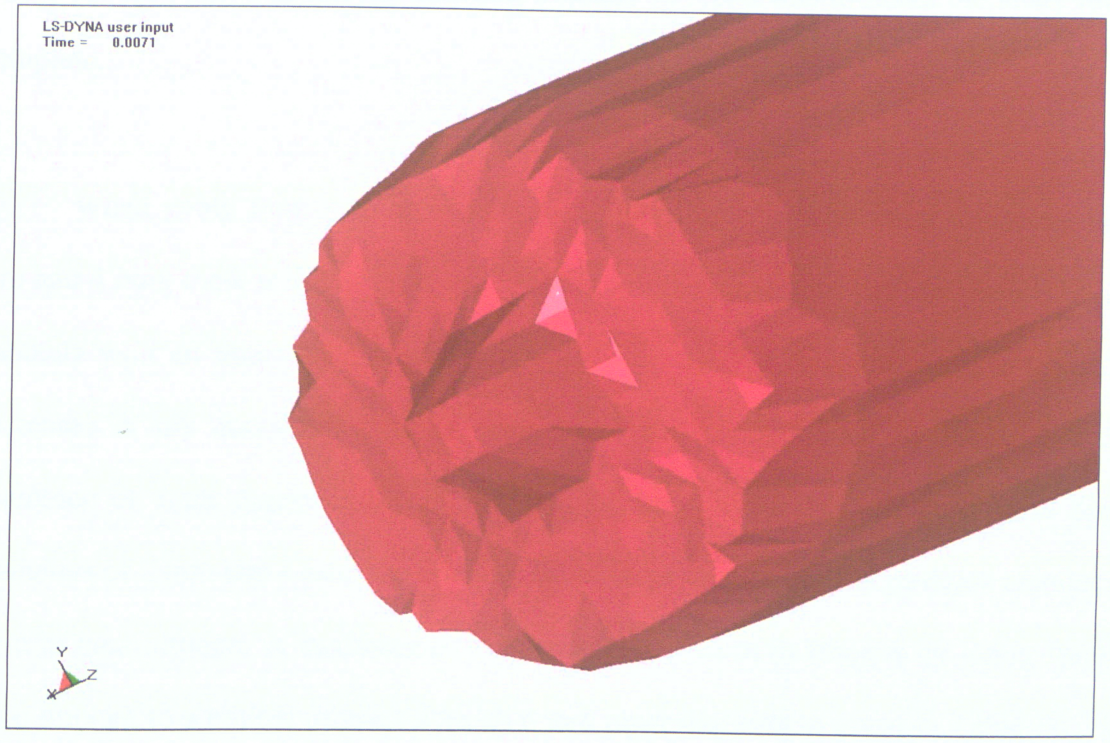

Figure 49: Fluid Displacement, Flat-Tipped Implant, 6 mm Inner Diameter

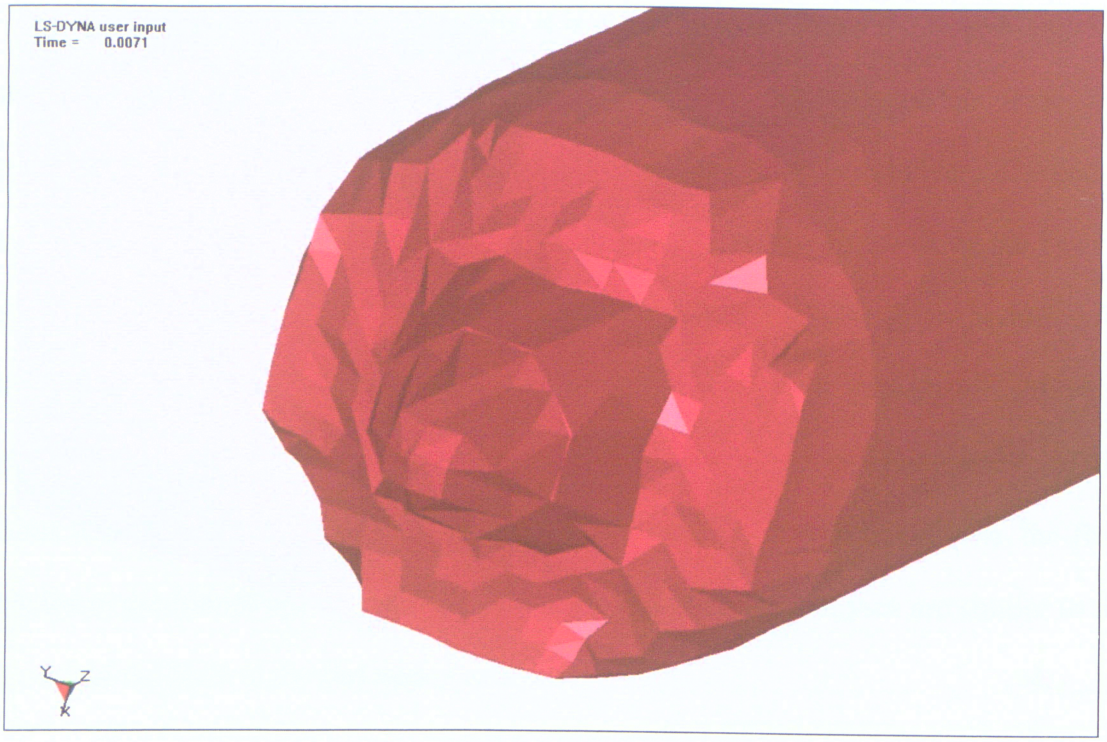

Figure 50: Fluid Displacement, Flat-Tipped Implant, 8 mm Inner Diameter

5.4 Parametric Study Discussion

There are a number of observations that can be made from looking at the results of the parametric study. First, the stresses at location 4 in the bone do not follow any kind of trend. Using hollow implants of various inner diameters does not have any consistent effect, for better or worse, on the stress at this location. Further, the magnitude of the maximum stress at this location is significantly lower than the magnitude of the maximum stress at the other three locations. The most probable explanation for this discrepancy is due to the local geometry. The fourth location is at a corner, where the shaft meets the closed end of the bone, and the stress measure used to represent pressure

could be affected by neighboring elements. Because of this, the results from the fourth location will not be included in the observation of trends in the parametric study.

For the first three locations in the bone, there is a clear trend. In general, the magnitude of the maximum stresses decreases when going from a solid implant to a hollow implant with progressively larger inner diameters. Because the macro adjusted the density of the implant so that its mass was the same regardless of its inner diameter, it is clear that this observation is an isolated effect of using hollow implant and is not a function of the implant being lighter. This trend is the least pronounced in the analyses with the round-tipped implant, although a comparison of the performance of the different tip types was not the goal for this study. It should be reiterated that the purpose of the parametric study was only to look at the effect of using hollow implants on stresses in the bone, and the reason for testing different implant tip types was to make the study more complete.

When going from a solid implant to hollow implants with inner diameters of 2 mm and 4 mm, there is not a significant decrease in the maximum stresses. However, for implants with an inner diameter of 6 mm and especially 8 mm, there are noteworthy decreases in the maximum stresses. This trend can be explained by looking at the examples of fluid displacement in Figures 47 through 50. For implants with inner diameters of 2 mm and 4 mm, the opening is not large enough for a significant amount of fluid to pass through. A summary of the percent reductions in stresses by going from a solid implant to a hollow implant with an 8 mm inner diameter is given in Table 17. The

average percent reduction in stress obtained by going from a solid implant to a hollow implant with an 8 mm inner diameter is 19.1%.

Implant Tip Type	Percent Stress Reduction, Location 1	Percent Stress Reduction, Location 2	Percent Stress Reduction, Location 3
Flat	21.7%	23.2%	20.7%
Funnel	17.3%	19.9%	21.5%
Round	18.2%	7.8%	9.9%
Tapered	26.4%	23.7%	19.4%

Table 17: Percent Stress Reductions for Parametric Study

CHAPTER 6

CONCLUSIONS

6.1 Implications of Current Work

The macro was used to create a total of 23 finite element models through the course of this thesis for the validation and parametric study. Had these finite element models been developed from scratch, the amount of time spent for pre-processing would have been significantly greater. As such, the macro that was developed has been proven to be an effective and efficient tool to create finite element models of the bone/fluid/implant system for comparative studies. Further, there is flexibility in terms of what can be done with the macro. Because the macro is created as a regular text file and written using APDL, it can easily be updated to include any additional functionality that is required by potential future users.

Although finite element analysis makes it easy to model situations like the bone/implant/fluid system, it is never a given that the results of the analysis will be meaningful without a comparison to real-world data. The validation that was performed has shown that the results of the finite element models have reasonable correlation with

experimental results, and using finite element analysis to model the bone/fluid/implant system is an acceptable approach. The fact that the validation was performed with an acceptable outcome gives merit to the parametric study that was conducted.

Finally, the results of the parametric study have shown that using hollow intramedullary implants has the potential to decrease the intramedullary pressure during its insertion into the bone. With the amount of variation in the literature regarding intramedullary pressure and fat extravasation, it cannot be said with certainty that the use of hollow intramedullary implants will decrease the degree of fat embolism unless clinical tests are performed. However, the results of the parametric study justify the creation of some physical hollow intramedullary implant prototypes for real-world testing in the field. A hollow intramedullary implant can be designed to be as structurally efficient as a solid implant, with the additional benefit of being lighter in weight for the patient who will be fitted with it.

6.2 Recommendations for Future Work

There are several things that could be done to further build upon the work performed in this thesis.

1) The macro could be expanded to include some features of the physical hammering event that would make the finite element model more realistic. The most notable feature would be contact and consequently friction between the implant and the bone when

modeling press-fit insertions of intramedullary implants. Another feature would be the ability to apply boundary conditions to the bone that allow a small amount of displacement in the axial direction in response to the hammering event. In reality, during an orthopaedic surgery, the bone is not rigidly fixed in the same way that the macro defines the boundary conditions.

2) Several things could be done to improve on the results of the validation. Most notably, more accurate material properties could be used in the finite element models. For the bone, this can be accomplished by using cadaveric bone for which the material properties are well known, or by performing the appropriate mechanical testing on the synthetic bone material so that its mechanical properties do not have to be approximated. For the fluid, the appropriate experimental testing could be performed so that the parameters of the equation of state can be determined more accurately than by calibration. In addition to improving the material properties in the finite element model, more pressure transducers along the length of the bone and multiple pressure transducers at each location along the length of the bone could be used in the experimental tests to provide more points of comparison.

3) Parametric studies on other aspects of the hammering the event could be conducted to see what effect they have on reducing intramedullary pressure. Examples of other aspects that could be tested are the profile of the force versus time curve applied to the implant, the shape of the implant tip, and the amount of implant oversize in press-fit insertions or implant undersize in cemented insertions.

APPENDIX A

MACRO

```
/PREP7
*ASK, BoneOD, Enter the outer diameter of the bone (mm),
*ASK, BoneID, Enter the inner diameter of the bone (mm),
*ASK, BoneOL, Enter the outer length of the bone (mm),
*ASK, BoneIL, Enter the inner length of the bone (mm),
*ASK, TipType, Implant tip? (0 for Flat, 1 for Contoured),
*IF, TipType, EQ, 0, THEN
        *ASK, ImplantOD, Enter the outer diameter of the implant (mm),
*ELSEIF, TipType, EQ, 1, THEN
        *ASK, FileName, Enter the name of the implant profile file,
*ENDIF
*ASK, Hollow, Hollow implant? (0 for No, 1 for Yes),
*IF, Hollow, EQ, 1, THEN
        *ASK, ImplantID, Enter the inner diameter of the implant (mm),
*ENDIF
*ASK, Offset, Enter the initial implant offset (mm),

BoneOD = BoneOD/1000
BoneID = BoneID/1000
BoneOL = BoneOL/1000
BoneIL = BoneIL/1000
*IF, TipType, EQ, 0, THEN
        ImplantOD = ImplantOD/1000
*ENDIF
*IF, Hollow, EQ, 1, THEN
        ImplantID = ImplantID/1000
*ENDIF
Offset = Offset/1000

*IF, TipType, EQ, 0, THEN
        CYL4, 0, 0, (ImplantOD/2), 90, , , -0.06
        *IF, Hollow, EQ, 1, THEN
```

```
            CYL4, 0, 0, (ImplantID/2), 90, , , -0.06
            VSBV, 1, 2
            NUMCMP, KP
            NUMCMP, LINE
            NUMCMP, AREA
            NUMCMP, VOLU
        *ENDIF
        VGEN, ,ALL, , , , ,Offset, , ,1
*ELSEIF, TipType, EQ, 1, THEN
        /UIS, MSGPOP, 3
        NREAD, FileName, txt,
        KNODE, 0, ALL
        BSPLIN, ALL,
        NDELE, ALL
        KSEL, S, LOC, Z, 0
        *GET, KPNum, KP, , NUM, MAX, ,
        *GET, YLOC, KP, KPNum, LOC, Y
        K, , 0, YLOC, -0.06,
        KSEL, S, LOC, Z, 0
        *GET, KP1, KP, , NUM, MAX, ,
        KSEL, S, LOC, Z, -0.06
        *GET, KP2, KP, , NUM, MAX, ,
        ALLSEL, ALL
        LSTR, KP1, KP2
        K, , 0, 0, -0.06,
        KSEL, S, LOC, Y, 0
        KSEL, U, LOC, Z, -0.06
        *GET, KP1, KP, , NUM, MAX, ,
        KSEL, S, LOC, Y, 0
        KSEL, R, LOC, Z, -0.06
        *GET, KP2, KP, , NUM, MAX, ,
        ALLSEL, ALL
        AROTAT, 1, 2, , , , , KP1, KP2, 90, ,
        LSTR, KP1, KP2
        KSEL, S, LOC, Z, -0.06
        KSEL, R, LOC, X, YLOC
        *GET, KP1, KP, , NUM, MAX, ,
        ALLSEL, ALL
        LSTR, KP1, KP2
        KSEL, S, LOC, Z, -0.06
        KSEL, R, LOC, Y, YLOC
        *GET, KP1, KP, , NUM, MAX, ,
        ALLSEL, ALL
        LSTR, KP1, KP2
```

```
        LSEL, S, LOC, Z, -0.06
        AL, ALL
        LSEL, S, LOC, X, 0
        AL, ALL
        LSEL, S, LOC, Y, 0
        AL, ALL
        ALLSEL, ALL
        VA, ALL
        *IF, Hollow, EQ, 1, THEN
                WPOFFS, 0, 0, (-0.06+(Offset))
                CYL4, 0, 0, (ImplantID/2), 90, 0, 0, 0.1
                VSBV, 1, 2
                WPCSYS,-1,0
                NUMCMP, VOLU
        *ENDIF
        VSBW, 1
        NUMCMP, KP
        NUMCMP, LINE
        NUMCMP, AREA
        NUMCMP, VOLU
        VGEN, ,ALL, , , , ,Offset, , ,1
        /UIS, MSGPOP, 2
*ENDIF

*IF, TipType, EQ, 0, THEN
        VSUM, DEFAULT
        *GET, ImplantVolume, VOLU, 1, VOLU, , ,
        ImplantVolume = (ImplantVolume*4)
*ELSEIF, TipType, EQ, 1, THEN
        VSUM, DEFAULT
        *GET, V1, VOLU, 1, VOLU, , ,
        *GET, V2, VOLU, 2, VOLU, , ,
        ImplantVolume = V1+V2
        ImplantVolume = (ImplantVolume*4)
*ENDIF

CYL4, 0, 0, (BoneOD/2), 90, , , BoneOL
CYL4, 0, 0, (BoneID/2), 90, , , BoneIL
*GET, V2, VOLU, 0, NUM, MAX
V1 = V2-1
VSBV, V1, V2, , ,DELETE
WPOFFS, 0, 0, BoneIL
*GET, V1, VOLU, 0, NUM, MAX
VSBW, V1
WPCSYS, -1, 0
LSEL, S, LOC, Z, BoneIL
```

```
LSEL, R, RADIUS, , (BoneID/2)
*GET, LNum1, LINE, 0, NUM, MAX
ALLSEL, ALL
LSEL, S, LOC, Z, (((BoneOL-BoneIL)/2)+BoneIL)
LSEL, R, LOC, X, 0
LSEL, R, LOC, Y, 0
*GET, LNum2, LINE, 0, NUM, MAX
ALLSEL, ALL
ADRAG, LNum1, , , , , , LNum2
ALLSEL, ALL
LSEL, S, LOC, Z, BoneIL
LSEL, A, LOC, Z, BoneOL
LSEL, R, RADIUS, , (BoneID/2)
LSEL, A, LOC, Z, (((BoneOL-BoneIL)/2)+BoneIL)
LSEL, U, LOC, X, (BoneOD/2)
LSEL, U, LOC, Y, (BoneOD/2)
ASLL, S, 1
*GET, ANum, AREA, 0, NUM, MAX
ALLSEL, ALL
ASEL, S, LOC, Z, BoneOL
VSLA, S, 0
*GET, VNum, VOLU, 0, NUM, MAX
ALLSEL, ALL
VSBA, VNum, ANum, , , KEEP
ALLSEL, ALL
NUMCMP, KP
NUMCMP, LINE
NUMCMP, AREA
NUMCMP, VOLU

WPOFFS, 0, 0, -0.06
CYL4, 0, 0, ((((BoneOD/2)-(BoneID/2))/2)+(BoneID/2)), 90, , , (0.06+BoneOL)
WPCSYS, -1, 0

KEYW, LSDYNA, 1
ET, 1, SOLID164
ET, 2, SOLID164
ET, 3, SOLID164
EDMP, RIGID, 1
KEYOPT, 2, 1, 2
*ASK, ImplantMass, Enter the mass of the implant (g),
*ASK, ImplantEX, Enter the elastic modulus of the implant (Pa),
*ASK, ImplantNUXY, Enter the Poisson's ratio of the implant (),
ImplantMass = ImplantMass/1000
ImplantDens = ImplantMass/ImplantVolume
MP, DENS, 1, ImplantDens
```

```
MP, EX, 1, ImplantEX
MP, NUXY, 1, ImplantNUXY
*ASK, Isotropic, Bone material isotropic? (0 for No, 1 for Yes),
*IF, Isotropic, EQ, 0, THEN
        *ASK, BoneDens, Enter the density of the bone (kg/m3),
        *ASK, BoneEX, Enter the transverse elastic modulus of the bone (Pa),
        *ASK, BoneEZ, Enter the longitudinal elastic modulus of the bone (Pa),
        *ASK, BoneGXY, Enter the transverse shear modulus of the bone (Pa),
        *ASK, BoneGXZ, Enter the longitudinal shear modulus of the bone (Pa),
        *ASK, BoneNUXY, Enter the transverse Poisson's ratio of the bone,
        *ASK, BoneNUXZ, Enter the longitudinal Poisson's ratio of the bone,
*ELSEIF, Isotropic, EQ, 1, THEN
        *ASK, BoneDens, Enter the density of the bone (kg/m3),
        *ASK, BoneEX, Enter the elastic modulus of the bone (Pa),
        *ASK, BoneNUXY, Enter the Poisson's ratio of the bone (),
*ENDIF
*IF, Isotropic, EQ, 0, THEN
        EDMP, ORTHO, 2, 100
        MP, DENS, 2, BoneDens
MP, EX, 2, BoneEX
        MP, EY, 2, BoneEX
        MP, EZ, 2, BoneEZ
        MP, GXY, 2, BoneGXY
        MP, GYZ, 2, BoneGXY
        MP, GXZ, 2, BoneGXZ
MP, NUXY, 2, BoneNUXY
        MP, NUYZ, 2, BoneNUXY
        MP, NUXZ, 2, BoneNUXZ
*ELSEIF, Isotropic, EQ, 1, THEN
        MP, DENS, 2, BoneDens
        MP, EX, 2, BoneEX
        MP, NUXY, 2, BoneNUXY
*ENDIF
*ASK, FluidDens, Enter the mass density of the fluid (kg/m3),
*ASK, FluidVisc, Enter the viscosity coefficient of the fluid (Ns/m2),
*ASK, FluidC, Enter the C parameter of the fluid EOS (m/s),
*ASK, FluidS1, Enter the S1 parameter of the fluid EOS,
*ASK, FluidS2, Enter the S2 parameter of the fluid EOS,
*ASK, FluidS3, Enter the S3 parameter of the fluid EOS,
*ASK, FluidGamma, Enter the Gamma parameter of the fluid EOS,
*ASK, FluidA, Enter the A parameter of the fluid EOS,
MP, DENS, 3, FluidDens
MP, EX, 3, 0
MP, NUXY, 3, 0
TB, EOS, 3, , , 2, 2
TBDATA, 2, FluidVisc
```

```
TBDATA, 16, FluidC
TBDATA, 17, FluidS1
TBDATA, 18, FluidS2
TBDATA, 19, FluidS3
TBDATA, 20, FluidGamma
TBDATA, 21, FluidA

MAT, 1
TYPE, 1
REAL, 1
*IF, TipType, EQ, 0, THEN
        VSEL, S, VOLU, , 1, , , 1
        LSEL, S, LOC, Z, (-0.03+(Offset))
        LESIZE, ALL, , , 20, , , , , 1
        ALLSEL, ALL
        VSEL, S, VOLU, , 1, , , 1
        LSEL, U, LOC, Z, (-0.03+(Offset))
        LESIZE, ALL, , , 6, , , , , 1
        ALLSEL, ALL
        VMESH, 1
*ELSEIF, TipType, EQ, 1, THEN
        VSEL, S, VOLU, , 2, , , 1
        LSEL, S, LOC, Z, (-0.03+(Offset))
        LESIZE, ALL, , , 20, , , , , 1
        ALLSEL, ALL
        VSEL, S, VOLU, , 1, , , 1
        LSEL, U, LOC, Z, (0+(Offset))
        *IF, Hollow, EQ, 1, THEN
                LSEL, U, LOC, X, (ImplantID/2)
                LSEL, U, LOC, Y, (ImplantID/2)
                *GET, LNum, LINE, 1, NUM, MAX, ,
                LSEL, U, LINE, , LNum
        *ENDIF
        LESIZE, ALL, , , 25, , , , , 1
        ALLSEL, ALL
        *IF, Hollow, EQ, 0, THEN
            VMESH, 1
            VMESH, 2
        *ELSEIF, Hollow, EQ, 1, THEN
                VSWEEP, 1
                VSWEEP, 2
        *ENDIF
*ENDIF
CSWPLA, 11, 1, 1, 1,
*GET, NNum, NODE, 1, NUM, MAX, ,
NGEN, 4, NNum, ALL, , , , 90, , 1,
```

```
EGEN, 4, NNum, ALL, , , , , , , , , ,
NUMMRG, NODE, , , , LOW
NUMCMP, NODE
ALLSEL, ALL

MAT, 2
TYPE, 2
REAL, 2
*GET, VNum, VOLU, 0, NUM, MAX
V1 = VNum-3
V2 = VNum-2
V3 = VNum-1
VSEL, S, VOLU, , V1, V3, , 1
LSEL, S, LOC, Z, (BoneIL/2)
LESIZE, ALL, , , 80, , , , , 1
ALLSEL, ALL
VSEL, S, VOLU, , V1, V3, , 1
LSEL, U, LOC, Z, (BoneIL/2)
LESIZE, ALL, , , 6, , , , , 1
ALLSEL, ALL
VSWEEP, V1
VSWEEP, V2
VSWEEP, V3
VSEL, S, VOLU, , V1, V3, , 1
*GET, NNum, NODE, 1, NUM, MAX, ,
NGEN, 4, NNum, ALL, , , , 90, , 1,
EGEN, 4, NNum, ALL, , , , , , , , , , ,
NUMMRG,NODE, , , ,LOW
NUMCMP,NODE
ALLSEL, ALL

MAT, 3
TYPE, 3
REAL, 3
VSEL, S, VOLU, , VNum, , , 1
LSEL, S, LOC, Z, ((-0.06)+((0.06+BoneOL)/2))
LESIZE, ALL, , , 100, , , , , 1
ALLSEL, ALL
VSEL, S, VOLU, , VNum, , , 1
LSEL, U, LOC, Z, ((-0.06)+((0.06+BoneOL)/2))
LESIZE, ALL, , , 15, , , , , 1
ALLSEL, ALL
VSWEEP, VNum
VSEL, S, VOLU, , VNum, , , 1
*GET, NNum, NODE, 1, NUM, MAX, ,
NGEN, 4, NNum, ALL, , , ,90, ,1,
```

```
EGEN, 4, NNum, ALL, , , , , , , , , ,
NUMMRG, NODE, , , ,LOW
NUMCMP, NODE
ALLSEL, ALL

*ASK, DataPoints, Enter the number of impulse force data points,
*DIM, TIME, , DataPoints,
*ASK, FileName, Enter the name of the time data file,
*VREAD, TIME(1), FileName, txt,,,,
(1F7.5)
*DIM, FORCE, , DataPoints,
*ASK, FileName, Enter the name of the force data file,
*VREAD, FORCE(1), FileName, txt,,,,
(1F4.0)
EDPART, CREATE
EDLOAD, ADD, RBFZ, 0, 1, TIME, FORCE, 0, , , , ,

NSEL, S, LOC, Z, 0
NSEL, R, LOC, X, (BoneOD/2)
D, ALL, ,0, , , ,ALL, , , , ,
ALLSEL, ALL
NSEL, S, LOC, Z, BoneOL
NSEL, R, LOC, X, (BoneOD/2)
D, ALL, ,0, , , ,ALL, , , , ,
ALLSEL, ALL

*SET, EndTime, TIME(DataPoints)
TIME, EndTime,
EDRST, 100
EDWRITE, BOTH, 'InputFile' ,'k', ' '
```

APPENDIX B

SAMPLE INPUT FILES

The following is an example of the input for a contoured tip implant:

1	0.0000000000000	10.816821650e-3
2	0.0000000000000	0.3098982200e-3 10.801898000e-3
3	0.0000000000000	0.5989853300e-3 10.760709350e-3
4	0.0000000000000	0.8734819300e-3 10.696281470e-3
5	0.0000000000000	1.1566216900e-3 10.602283500e-3
6	0.0000000000000	1.4380802100e-3 10.478445370e-3
7	0.0000000000000	1.6409859700e-3 10.368123370e-3
8	0.0000000000000	1.8920478000e-3 10.203500000e-3
9	0.0000000000000	2.1085126400e-3 10.032089360e-3
10	0.0000000000000	2.2947558300e-3 9.8578427300e-3
11	0.0000000000000	2.4635075600e-3 9.6731461100e-3
12	0.0000000000000	2.6175193700e-3 9.4758068600e-3
13	0.0000000000000	2.9050427400e-3 9.0005824400e-3
14	0.0000000000000	3.2854370100e-3 8.3595752200e-3
15	0.0000000000000	3.6518182000e-3 7.7421815900e-3
16	0.0000000000000	4.0280032000e-3 7.1082674500e-3
17	0.0000000000000	4.8139306800e-3 5.7838910300e-3
18	0.0000000000000	5.6432510300e-3 4.3863927200e-3
19	0.0000000000000	6.5113321200e-3 2.9235782100e-3
20	0.0000000000000	6.9694592900e-3 2.1515822600e-3
21	0.0000000000000	7.3879666100e-3 1.4463502400e-3
22	0.0000000000000	7.5214489800e-3 1.1706189000e-3
23	0.0000000000000	7.5705802800e-3 1.0414325500e-3
24	0.0000000000000	7.6193440300e-3 0.8922886400e-3
25	0.0000000000000	7.6604122200e-3 0.7413506300e-3
26	0.0000000000000	7.6927101400e-3 0.5943994200e-3
27	0.0000000000000	7.7180933400e-3 0.4445003500e-3
28	0.0000000000000	7.7373929800e-3 0.2798422600e-3
29	0.0000000000000	7.7484451800e-3 0.0983634400e-3
30	0.0000000000000	7.7500000000e-3

This input should be saved in a text file with the extension '.txt'. ANSYS reads this data in fixed format; therefore, the spacing between the columns should be as in the above example when generating an implant tip input file. The format of the input file for the implant tip is: spline point reference number followed by the X, Y and Z coordinates of this point in meters. The profile is defined in the YZ plane, so the X coordinates will always be zero. The coordinate system used to define the implant is shown in Figure 51. The more reference points used to define the spline profile, the smoother the shape will be when created in ANSYS.

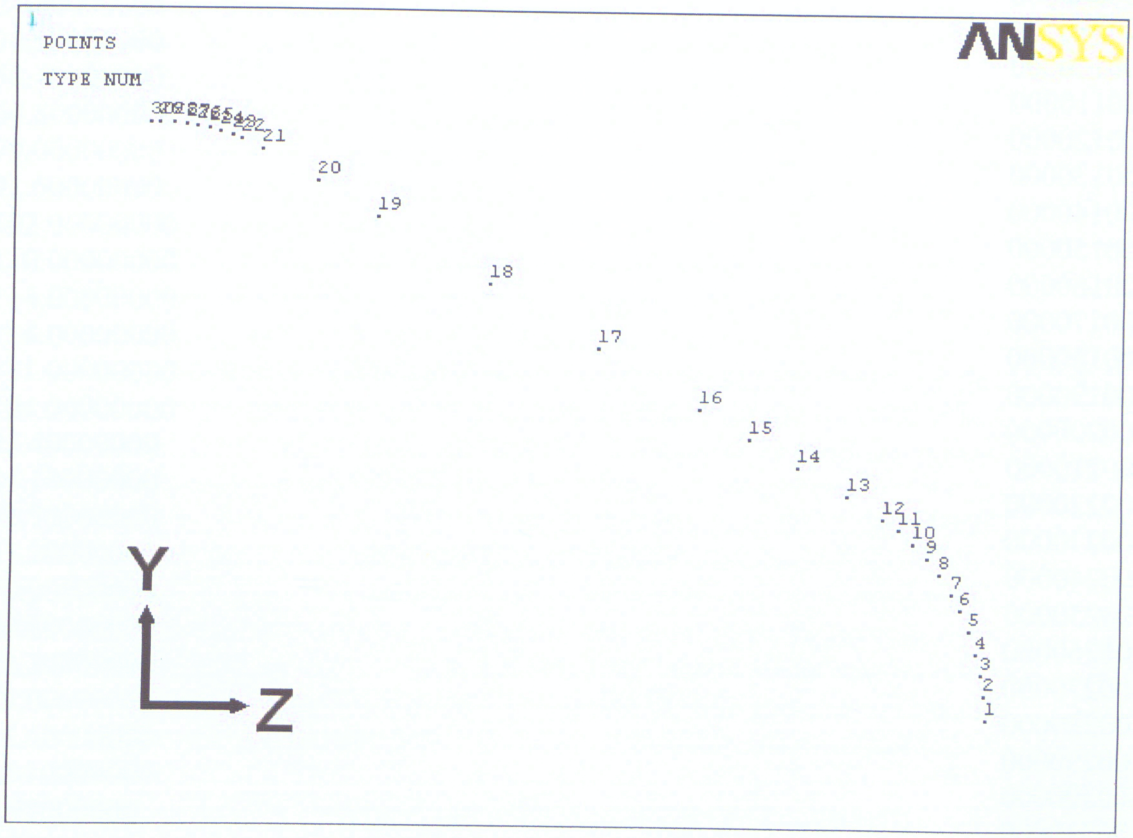

Figure 51: Coordinate System for Contoured Implant Tip

The following is an example of the input for the time data of a force versus time curve applied to the implant. The time input is in seconds; therefore, the time data below represents a force function duration of 7 milliseconds. The file should be saved in a text file with the extension '.txt'.

0.00000000
0.00010000
0.00020000
0.00030000
0.00040000
0.00050000
0.00060000
0.00070000
0.00080000
0.00090000
0.00100000
0.00110000
0.00120000
0.00130000
0.00140000
0.00150000
0.00160000
0.00170000
0.00180000
0.00190000
0.00200000
0.00210000
0.00220000
0.00230000
0.00240000
0.00250000
0.00260000
0.00270000
0.00280000
0.00290000
0.00300000
0.00310000
0.00320000
0.00330000
0.00340000
0.00350000
0.00700000

The following is an example of the input for the force data of a force versus time curve applied to the implant. The force input is in Newtons; therefore, the force data below represents a force function with a peak of 114 Newtons. The file should be saved in a text file with the extension '.txt'.

-0.40000000
-0.30000000
-1.40000000
-1.10000000
-2.10000000
-1.10000000
-0.40000000
4.83000000
13.20000000
24.40000000
36.50000000
50.40000000
64.80000000
79.00000000
91.60000000
102.00000000
110.00000000
114.00000000
114.00000000
111.00000000
104.00000000
95.40000000
84.10000000
72.70000000
61.20000000
50.90000000
40.80000000
32.30000000
25.00000000
18.60000000
12.10000000
8.98000000
5.79000000
2.47000000
0.00000000
-0.90000000
0.00000000

REFERENCES

[1] - Evenleigh RJ. A review of biomechanical studies of intramedullary nails. *Med. Eng. Phys.* 1995; 17(5):323-331

[2] - Inadome T, Wall MC, Smith CL, Whiteside LA. Femoral intramedullary pressure during in vitro cemented and cementless total hip arthroplasty. *Orthopaedic Trans.* 1999; 22:154-155

[3] - Bren, L. Joint replacement: An inside look. FDA Consumer Magazine. 2004, Vol. 38, No. 2

[4] - Fulde G, Harrison P. Fat Embolism: A review. *Archives of Emergency Medicine.* 1991; 8:233-239

[5] - Zenker FA. Beitrage zur Anatomie und Physiologie der Lunge. *Dresden: J Braunsdorf.* 1861

[6] - Bergmann EB. Ein Fall todlicher Fettembolie. *Klin Wochenschr.* 1873; 10:385-387

[7] - Czerny V. Uber die klinische Bedeutung der Fettemboli. *Klin Wochenschr.* 1875; 12:604-607

[8] - Wartin AS. Traumaticl lipaemia and fatty embolism. *Int Clin.* 1913; 4:171-227

[9] - Gauss H. Studies in cerebral fat embolism: with reference to the pathology of delirium and coma. *Arch Intern Med.* 1916; 18:76-102

[10] - Maatz R. Die Bedeutung der Fettembolie bei der Marknagelung nach Kuntscher. *Zbl Chir.* 1943; 70:383

[11] - Peltier LF. Fat embolism following intramedullary nailing. Report of a fatality. *Surgery.* 1952; 10:719-722

[12] - Modig J, Malmberg P. Pulmonary and circulatory reactions during total hip replacement. *Acta Anaesthesiol Scand.* 1975; 19:219-237

[13] - Lachiewicz PF, Renawat CS. Fat embolism syndrome following bilateral total knee replacement with total condylar prosthesis. Report of two cases. *Clin Orthop.* 1981; 160(10):106-108

[14] - Shergill G, Parmar H. Fat Embolism and The Fat Embolism Syndrome. Online posting. *Orthopaedics.* 1 June 2004 <www.orthopaedics.com>

[15] - Baker PL, Pazzeo JA, Peltier LF. Free fatty acids, catecholamines, and arterial hypoxemia in patients with fat embolism. *J Trauma.* 1971; 11:1026-1030

[16] - Peltier LF. Fat embolism, III. The toxic properties of neutral fat and free fatty acids. *Surgery.* 1956; 40:665

[17] - King KG, Wagner WW, Ashbaugh DG, Latham LP, Halsey DR. Alterations in pulmonary microanatomy after fat embolism. *Chest*. 1971; 59:524-530
[18] - Hager CA, Brncick N. Fat embolism syndrome: A complication of orthopaedic trauma. *Orthopaedic Nursing*. 1998; 17:41-46
[19] - Johnson MJ, Lucas GL. Fat embolism syndrome. *Orthopaedics*. 1996; 19(1):41-48
[20] - Pellegrini VD, Reid S, Evarts CM. Fractures in adults. 4th ed. Philadelphia: Lippincott-Raven; 1996. p. 425-512
[21] - Gurd AR, Wilson RI. The fat embolism syndrome. *J Bone Joint Surg [Br]*. 1974; 56:408-416
[22] - Lindeque BGP, Schoeman HS, Dommisse GF, Boeyens MC, Blok AL. Fat embolism and the fat embolism syndrome. A double-blind therapeutic study. *J Bone Joint Surg [Br]*. 1987; 69:128-131
[23] - Shier MR, Wilson RF. Fat embolism syndrome: Traumatic coagulopathy with respiratory distress. *Surg Annu*. 1980; 12:139
[24] - Christie J, Robinson CM, Pell ACH. Transcardiac echocardiography during invasive intramedullary procedures. *J Bone Joint Surg [Br]*. 1995; 77:450
[25] - Magerl F, Tscherne H. Zur Diagnose, Therapie und Prophylaxe der Fettembolie. Langenbecks *Arch klin Chir*. 1966; 314:292
[26] - Peltier LF. Fat embolism. A current concept. *Clin Orthop*. 1969; 66: 241-253
[27] - Pelzl H. Klinik und Prophylaxe der Fettembolie. *Med Klinik*. 1969; 64:1107
[28] - Peltier LF, Collins JA, Evarts CM. Fat embolism. *Arch Surg*. 1974; 109:12-16
[29] - Kim YH. Incidence of fat embolism syndrome after cemented or cementless bilateral simultaneous and unilateral total knee arthroplasty. *J Arthroplasty*. 2001; 16(6):730-739
[30] - Dorr LD, Merkel C, Mellman MF, Klein L. Fat emboli in bilateral total knee arthroplasty. *Clin Orthop*. 1989; 248:112-118
[31] - Pell AC, Christie J, Keating JF, Sutherland GR. The detection of fat embolism by transoesophageal echocardiography during reamed intramedullary nailing. A study of 24 patients with femoral and tibial fractures. *J Bone Joint Surg [Br]*. 1993; 75(6):921-925
[32] - Sturmer KM, Schuchardt W. New aspects of closed intramedullary nailing and marrow cavity reaming in animal experiments. II: intramedullary pressure in marrow cavity reaming. *Unfallheilkunde*. 1980; 83:346
[33] - Wenda K, Runkel M, Rudig L. Influence of bone marrow embolization on the choice of procedure in the stabilization of femur fractures. *Orthopade*. 1995; 24:151
[34] - Kropfl A, Davies J, Berger U, Hertz H, Schlag G. Intramedullary pressure and bone marrow fat extravasation in reamed and unreamed femoral nailing. *J Orthop Res*. 1999; 17(2):261-268
[35] - Wozasek GE, Simon P, Redl H. Intramedullary pressure changes and fat intravasation during intramedullary nailing: an experimental study in sheep. *J Trauma*. 1994; 36:202
[36] - Hopf T, Gleitz M, Hess T. Intramedullary pressure during reaming and nailing of the femur with modern compression interlocking nails: a potential cause of fat embolism? *Unfallchirurg*. 1994; 97:458
[37] - Tronzo RG, Kallos T, Wyche MQ. Elevation of intramedullary pressure when methylmethacrylate is inserted in total hip arthroplasty. *J Bone Joint Surg*. 1974; 56A:714-718

[38] - Beck A, Strecker W, Gebhard F. The influence of prosthesis design in intramedullary femoral pressure during the implantation of femoral stem prosthesis. *Unfallchirurg*. 2001; 104:1140-1144
[39] - Schmidt J, Sulk C, Weigand K, LaRosee K. Reduction of fat embolic risks in total hip arthroplasty using cannulated awls and rasps for the preparation of the femoral canal. *Arch Orthop Trauma Surg*. 2000; 120:100-102
[40] - Martin R, Leighton RK, Petrie D, Ikejiani C, Smyth B. Effect of proximal and distal venting during intramedullary nailing. *Clin Orthop*. 1996; 332:80-89
[41] - Pitto RP, Schramm M, Hohmann D, Kobler M. Relevance of the drainage along the linea aspera for the reduction of fat embolism during cemented total hip arthroplasty. *Arch Orthop Trauma Surg*. 1999; 119:146-150
[42] - Pitto RP, Koessler M, Kuehle JW. Comparison of fixation of the femoral component without cement and fixation with use of a bone-vacuum cementing technique for the prevention of fat embolism during total hip arthroplasty. *J Bone Joint Surg*. 1999; 81A:831-843
[43] - Muller C, McIff T, Rahn BA, Pfister U, Weller S. Intramedullary pressure, strain on the diaphysis and increase in cortical temperature when reaming the femoral medullary cavity. *Injury*. 1993; 24:22-30
[44] - Muller C, McIff T, Rahn BA, Pfister U, Perren SM, Weller S. Influence of the compression force on the intramedullary pressure development in reaming of the femoral medullary cavity. *Injury*. 1993; 24:36-39
[45] - Johnson JA, Berkshire A, Leighton RK, Gross M, Chess DG, Petrie D. Some basic biomechanical characteristics of medullary pressure generation during reaming of the femur. *Injury* 1995; 26:451-454
[46] - Muller C, Frigg R, Pfister U. Effect of flexible drive diameter and reamer design on increase of pressure in the medullary cavity during reaming. *Injury*. 1993; 24:40-47.
[47] - Parvizi J, Holiday AD, Ereth MH, Lewallen DG. Sudden death during primary hip arthroplasty. *Clin Orthop*. 1999; 369:39-48
[48] - Hallquist, JO. LS-DYNA Keyword User's Manual, Version 970, Livermore Software Technology Corporation, Livermore, 2003
[49] - Dobrjanski D (2005). *Experimental Parametric Study of the Factors Leading to Elevated Femoral Intramedullary Pressure and Fat Embolus Syndrome in Orthopaedic Procedures*. M.A.Sc. thesis. Ryerson University, Toronto, Canada.
[50] - Wang X, Ni Q. Determination of cortical bone porosity and pore size distribution using a low field pulsed NMR approach. *J Orthop Res*. 2003; 21:312-319
[51] - Production, viscosity, and shear force measurements of the Vaseline/paraffin mixture were performaed by C. Meier, Rhevisco Co. Ltd., Wislikofen, Switzerland.
[52] - Bryant JD, David T, Gaskell PH, King S, Lond G. Rheology of bovine bone marrow. *Proc Instn Mech Engrs*.1989; 203:71-75
[53] - Online Material Data Sheet: Montell Type 1900 UHMW Polyethylene. MatWeb. 10/14/2004 <http://matweb.com/search/SpecificMaterial.asp?bassnum=PMO567>.
[54] - Lu JP, Dorsett, H. Simulation of aquarium tests for PBXW-115(Aust). 12th International Detonation Symposium. San Diego, CA.
[55] - Reilly DT, Burstein AH. The elastic and ultimate properties of compact bone tissue. *Journal of Biomechanics*. 1975; 8:393-405

GLOSSARY OF MEDICAL TERMS

Arthroplasty – A surgery to relieve pain and restore range of motion by realigning or reconstructing a joint.

Capillary - One of the tiny blood vessels that connect the smallest divisions of the arteries and the smallest divisions of the veins.

Diaphysis - The shaft of a long bone.

Distal - Anatomically located far from a point of reference.

Etiology - The study of the causes of disease.

In Vivo - Studies carried out in living organisms.

Intramedullary - Within the marrow cavity of bone.

Linea Aspera - The elevated line that extends down the posterior surface of the femoral shaft.

Metaphysis - The portion of a developing long bone that is between the diaphysis and the epiphysis.

Otrhopaedics - The branch of surgery broadly concerned with bones.

Petechiae - Small, pinpoint red or brown spots that represent escape of blood from the vessels into the surrounding skin.

Proximal - Anatomically located near from a point of reference.

Pulmonary - To do with the lungs.

Transesophageal Echocardiography - A diagnostic test using an ultrasound device that is passed into the esophagus of the patient, to create a clear image of the heart muscle and the contents of the heart.

Vena Cava Inferior - A large vein that receives blood from the lower extremities, pelvis and abdomen and empties it into the right atrium of the heart.

Venous - Referring to veins and the flow of blood to the heart.